IMPLEMENTATION AND COMPARISON OF TURBULENCE MODELS ON A FLAT PLATE PROBLEM USING A NAVIER-STOKES SOLVER

A THESIS SUBMITTED TO
THE GRADUATE SCHOOL OF NATURAL AND APPLIED SCIENCE
OF
THE MIDDLE EAST TECHNICAL UNIVERSITY

BY
BALKAN ZİYA GENÇ

IN PARTIAL FULFILMENT OF THE REQUIREMENTS FOR THE DEGREE
OF
MASTER OF SCIENCE
IN
THE DEPARTMENT OF MECHANICAL ENGINEERING

DECEMBER 2003

Approval of the Graduate School of Natural and Applied Sciences

_____

Prof. Dr. Canan ÖZGEN
Director

I certify that this thesis satisfies all the requirement as a thesis for the degree of Master of Science.

_____

Prof. Dr. Kemal İDER
Head of Department

This is to certify that we have read this thesis and that in our opinion it is fully adequate, in scope and quality, as a thesis for the degree of Master of Science.

_____

Prof. Dr. M. Haluk AKSEL
Supervisor

Examining Committee Members

Prof. Dr. Kahraman ALBAYRAK _____

Prof. Dr. M. Haluk AKSEL _____

Prof. Dr. Nafiz ALEMDAROĞLU _____

Asst. Prof. Dr. Tahsin ÇETİNKAYA _____

Dr. Cüneyt SERT _____

ABSTRACT

IMPLEMENTATION AND COMPARISON OF TURBULENCE MODELS ON A FLAT PLATE PROBLEM USING A NAVIER-STOKES SOLVER

GENÇ, Balkan Ziya
M.Sc., Department of Mechanical Engineering
Supervisor: Prof. Dr. M. Haluk Aksel

December 2003, 102 pages

For turbulent flow calculations, some of the well-known turbulence models in the literature are applied on a previously developed Navier-Stokes solver designed to handle laminar flows. A finite volume formulation, which is cell-based for inviscid terms and cell-vertex for viscous terms, is used for numerical discretization of the Navier-Stokes equations in conservative form. This formulation is combined with one-step, explicit time marching Lax-Wendroff numerical scheme that is second order accurate in space. To minimize non-physical oscillations resulting from the numerical scheme, second and fourth order artificial smoothing terms are added. To increase the convergence rate of the solver, local time stepping technique is applied.

Before applying turbulence models, Navier-Stokes solver is tested for a case of subsonic, laminar flow over a flat plate. The results are in close agreement with Blasius similarity solutions.

To calculate turbulent flows, Boussinesq eddy-viscosity approach is utilized. The eddy viscosity (also called turbulent viscosity), which arises as a consequence of this approach, is calculated using Cebeci-Smith, Michel et. al., Baldwin-Lomax, Chien's k-ε and Wilcox's k-ω turbulence models. To evaluate the performances of these turbulence models and to compare them with each other, the solver has been tested for a case of subsonic, laminar - transition fixed - turbulent flow over a flat plate. The results are verified by analytical solutions and empirical correlations.

Keywords: Navier-Stokes equations, finite volume method, Lax-Wendroff method, Cebeci-Smith turbulence model, Michel et. al. turbulence model, Baldwin-Lomax turbulence model, k-ε turbulence model, k-ω turbulence model.

ÖZ

BİR NAVIER-STOKES ÇÖZÜCÜSÜ KULLANARAK TÜRBÜLANS MODELLERİNİN BİR DÜZ PLAKA PROBLEMİ ÜZERİNDE UYGULANMASI VE KARŞILAŞTIRILMASI

GENÇ, Balkan Ziya
Yüksek Lisans, Makina Mühendisliği Bölümü
Tez Yöneticisi: Prof. Dr. M. Haluk Aksel

Aralık 2003, 102 sayfa

Türbülanslı akışları hesaplamak için, daha önceden laminar akışlar için geliştirilen hazır durumda bir Navier-Stokes çözücüsüne, literatürde iyi bilinen bazı türbülans modelleri eklenmiştir. Korunum biçimindeki Navier-Stokes denklemlerinin sayısal olarak ayrıştırılması için, viskoz olmayan terimlerde hücre köşeli, viskoz terimlerde ise hücre merkezli olan bir sonlu hacim yöntemi kullanılmıştır. Bu formülasyon, uzayda ikinci dereceden hassas, tek adımlı ve zaman ilerlemeli Lax-Wendroff sayısal şeması ile birleştirilmiştir. Sayısal yöntemden kaynaklanan fiziksel olmayan dalgalanmaları önlemek için ikinci ve dördüncü dereceden yapay yumuşatma terimleri eklenmiştir. Çözücünün yakınsama hızını artırmak için yerel zaman adımlama tekniği uygulanmıştır.

Türbülans modellerini uygulamadan önce, Navier-Stokes çözücüsü, bir düz plaka üzerindeki sesten düşük hızlı, laminar bir akış durumu için denenmiştir. Sonuçlar Blasius benzerlik çözümleriyle yakın uyum içerisindedir.

Türbülanslı akışları hesaplamak için, Boussinesq edi-viskozite yaklaşımı kullanılmıştır. Bu yaklaşımın sonucu olarak ortaya çıkan edi viskozitesi (türbülans viskositesi de denilir), Cebeci-Smith, Michel, Baldwin-Lomax, Chien'in k-ε ve Wilcox'un k-ω türbülans modelleri kullanılarak hesaplanmıştır. Türbülans modellerinin performanslarını değerlendirmek ve birbirleriyle karşılaştırmak için çözücü düz bir plaka üzerindeki sesten düşük hızlı, laminar - sabit geçişli - türbülanslı bir akış durumu için test edilmiştir. Sonuçlar, analitik çözümler ve deneysel korelasyonlar kullanılarak doğrulanmıştır.

Anahtar Kelimeler: Navier-Stokes denklemleri, sonlu hacim yöntemi, Lax-Wendroff yöntemi, Cebeci-Smith türbülans modeli, Michel ve arkadaşlarının türbülans modeli, Baldwin-Lomax türbülans modeli, k-ε türbülans modeli, k-ω türbülans modeli.

ACKNOWLEDGMENTS

I would like to thank Prof. Dr. Haluk Aksel for supplying me with the research grant and the computer facilities, which were of vital importance for the completion of the thesis work.

I would like to express my gratitude to my family, for their loving care and efforts. I especially like to thank my brother Volkan, for his accompany while writing the thesis, sharing my stress and emotions, and for the respect he showed to me.

I want to thank all the colleagues in the CFD group, for their friendship and for sharing their ideas about many issues, giving me the inspiration to complete this work.

Finally, I am also thankful to Dr. Cüneyt Sert for his invaluable suggestions and corrections on the thesis.

TABLE OF CONTENTS

LIST OF FIGURES

LIST OF SYMBOLS

$\vec{A}$	Surface Vector
A^+	Closure coefficient for a zero-equation turbulence model
c	Speed of sound
C_μ	Closure coefficient for a two-equation turbulence model
$C_{\varepsilon 1}$	Closure coefficient for a two-equation turbulence model
$C_{\varepsilon 2}$	Closure coefficient for a two-equation turbulence model
C_{cp}	Closure coefficient for a zero-equation turbulence model
C_{kleb}	Closure coefficient for a zero-equation turbulence model
C_{wk}	Closure coefficient for a zero-equation turbulence model
E	Total energy per unit volume
F	Inviscid Flux vector in x-direction
G	Inviscid Flux vector in y-direction
H	Inviscid Flux vector in z-direction
h	Total enthalpy
$\vec{i}$	Unit vector in x-direction
$\vec{j}$	Unit vector in y-direction
J	Jacobian
k	Turbulent kinetic energy
$\vec{k}$	Unit vector in z-direction
k_R	Average height of a sand-grain
l_{mix}	Mixing length
L	Similarity Matrix
M	Mach number
$\vec{n}$	Unit normal vector
p	Static pressure
Pr	Prandtl number
Q	Conservative variable, space coordinate
q	Heat flux
$\vec{r}$	Position vector
R	Universal Gas Constant
R_β	Closure coefficient for a two-equation turbulence model

R_ω	Closure coefficient for a two-equation turbulence model
R_k	Closure coefficient for a two-equation turbulence model
Re_T	Turbulent Reynolds number
Re	Reynolds number
$\vec{S}$	Surface vector
t	Time
T	Temperature
u	Velocity component in x-direction
U	Conservative variable vector
U_e	Boundary layer edge velocity
v	Velocity component in y-direction
$\vec{V}$	Velocity vector
w	Velocity component in z-direction
W	Characteristic variable vector
x	Spatial variable in physical domain
y	Spatial variable in physical domain
z	Spatial variable in physical domain

Greek Symbols

α	Closure coefficient for a two-equation and a zero-equation turbulence models
α^*	Closure coefficient for a two-equation turbulence model
β	Closure coefficient for a two-equation turbulence model
β^*	Closure coefficient for a two-equation turbulence model
γ	Ratio of specific heats
δ	Correction operator, boundary layer thickness
δ_v^*	Velocity thickness
Δ^2	Second-order change operator
Δt	Time step
$\Delta\forall$	Cell volume
ζ	Local coordinate in computational domain
ε	Dissipation rate of turbulent kinetic energy
η	Local coordinate in computational domain, Blasius similarity variable
κ	Thermal conductivity, closure coefficient for a zero-equation model
λ	Eigenvalues of the diagnolized Jacobian matrix
Λ	Diagonalized jacobian matrix
μ	Absolute viscosity

ξ	Local coordinate in computational domain
ρ	Density
σ	Artificial smoothing coefficient
σ_k	Closure coefficient for a two-equation turbulence model
σ_ε	Closure coefficient for a two-equation turbulence model
σ_ω	Closure coefficient for a two-equation turbulence model
τ	Shear stress
ϕ	Dummy variable
$\vec{\omega}$	Vorticity vector
∇	Gradient operator
∂	Partial derivative operator

Subscripts

b	Binormal
corrected	Corrected value
far	Far-field value
i	Node index
inviscid	Inviscid
lam	Laminar
n	Normal direction
predicted	Predicted value
s	Tangential direction
total	Total (Stagnation) value, Total effective value
tur	Turbulent
v	Viscous component of flux vector
viscous	Viscous
wall	Property calculated on the wall
∞	Free stream value

Superscripts

n	Time level
thermal	Thermal conductivity
-	Value known from the previous time step
~	Primitive form
+	Non-dimensional variable

CHAPTER 1

INTRODUCTION

1.1 WHY COMPUTATIONAL FLUID DYNAMICS (CFD)?

The science of modern fluid dynamics, the subject of which is the understanding and modeling of fluid flow phenomena, has three major approaches to solve the problems of fluid flow: Experimental, theoretical, and computational, as stated in the order of their historical outcome and significance.

Each of these three approaches has different methods to obtain solutions, but serve for the same objective: To obtain the most realistic solution, compromising cost and accuracy. So to achieve this, they interact with each other synergistically, as can be shown in the figure below:

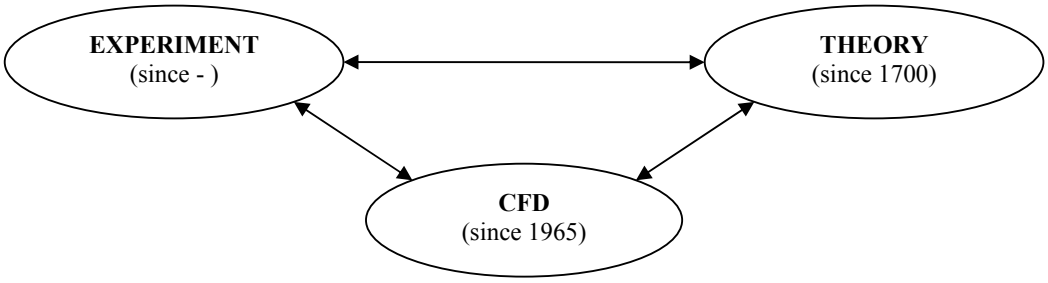

Figure 1.1 Interaction of major approaches in CFD, Gerritsma [1].

Especially in aerodynamics, this interaction brings a very useful teamwork, resulting in superior designs of flow fields. In this teamwork, the role of these basic

three approaches, with their advantages and disadvantages can briefly be stated as follows:

1.1.1 Experimental Approach:

Experiments are efficient means of measuring global parameters like drag, lift, pressure drop, heat transfer coefficients, etc… with the advantage of containing the correct physics [2]. However, for example, if the experiments are carried out in a wind tunnel, scale effects may become important. Therefore, setting the correct Mach number, Reynolds number and other similarity parameters appropriately may not be possible. What's more, there is always the influence of the wind tunnel walls and the support of the model. As another option, if a field test with the actual prototype has to be carried out, then the disadvantages will consist of the difficulties in instrumentation, the inability to provide controlled flow conditions and lack of safety.

Thus, where possible, experiments offer the ultimate test, but the restricting factors are [1]:

i. Object or model modification may be extremely difficult or expensive
ii. Model test is not always possible due to high temperature and real gas effects
iii. The cost and availability of equipment

1.1.2 Theoretical (Analytical) Approach:

Theoretical approaches, on the other hand, have the advantage of providing solutions in closed forms. Thus one can immediately identify the fundamental parameters and study the effect of varying a certain parameter on the answers to problems. Even so, to obtain this much of a "mathematical comfort", either a simple flow should be chosen or approximations (i.e. boundary layer hypothesis) to the full flow problem should be engaged.

Having briefly stated the above drawbacks for experimental and theoretical approaches, one can easily see the need for a reasonable complementary alternative to flow problems. Hence computational approaches come into the picture:

1.1.3 Computational (Numerical) Approach:

The fundamental principles governing fluid flow, can be expressed in terms of mathematical equations, which in their most general form, are usually partial differential equations. CFD is, in part, the art of replacing the governing partial differential (or integral) equations of fluid flow with numbers and advancing these numbers in space and time to obtain a final numerical description of the complete flow field of interest [3]. In this regard, computational problems involve the manipulation of, and the solution for numbers. It can be said that the end product of CFD is a collection of numbers presented with their detailed analysis and discussion.

CFD has become an indispensable tool in aerodynamics for both designing and analyzing flows which have no analytical solutions. Indeed, from late 1950's - from the time when aerodynamicists were seeking for the solution of the famous bow-shock problem - up to now, CFD has been the subject of continuous increase in popularity. Moreover, the increase in the performance to cost ratios of computer speeds - which shows no sign of slowing down - draws the interest towards numerical techniques, and brings the opportunities for more realistic simulations at a lower cost. Here, it is worth mentioning that many of the key ideas for numerical solution methods of partial differential equations were established more than a century ago, but they were of little use before computers appeared [2]. So today, it is well appreciated that computers make the study of fluid flow easier and more effective.

This trend for CFD would well be understood, when its important advantages are considered [4]:

i. Substantial reduction of lead times and costs of new designs

ii. Ability to study systems where controlled experiments are difficult or impossible to perform (e.g. very large systems)
iii. Ability to study systems under hazardous conditions at and beyond their normal performance limits (e.g. safety studies and accident scenarios)
iv. Practically unlimited level of detail of results

Despite all its advantages, there are limitations and restrictions for CFD: Flow predictions are as superior as the level of physics that goes into the formulations. That is to say, the quality of the computational results will always depend on our ability to model the physics appropriately (interaction with the theory). Here, one should keep in mind that numerical results are always approximate. Furthermore, the solution will not only depend on the physical parameters but also on the numerical parameters such as time step, relaxation parameters, the mesh, etc... Thus, in order to make sure that the problem is really solved and there are no misconceptions, comparison of the results with experiments is necessary (interaction with experiment). This process is called "validation".

1.2 WHAT DOES CFD ENCOMPASS?

1.2.1 Mathematical Modeling:

CFD is interested in fluid flows for which the equations describing their behavior are known but no analytical solution exists. Thus, in CFD, an approximate solution is sought. To accomplish this, a mathematical model is needed, which will describe the flow with enough detail and reduce the complexity of the original equations.

The motion of an heat conducting, viscous fluid is governed by a set of non-linear partial differential equations, known as Navier-Stokes equations, derived from the conservation laws for mass, momentum and energy. Expressed in different forms, Navier-Stokes equations are the most comprehensive models for problems of fluid flow. However, they are highly non-linear and have complex solutions: To simplify

the solutions, for example, one can consider "inviscid flow" assumption to get rid of viscous terms in these equations, but then the chances of obtaining a detailed flow analysis near solid boundaries and predicting frictional effects will be impossible. Alternatively, a two-dimensional approximation for the flow field can be employed, but this time, the inherent three-dimensional structure of turbulence will be overseen: Unfortunately, two-dimensional flow models are unable to account for the three-dimensional mechanism of "vortex stretching", the major source of turbulence structures. As it can be seen from these examples, solutions to fluid flow problems, can be obtained by various levels of approximation, like spatial level, steadiness level or dynamical level, as covered by Hirsch [5]. Such approximations, assumptions and their effects should always be kept in mind, to understand and comment on the character of solutions.

1.2.2 Grid Generation:

In a numerical solution, the flow properties are defined on a numerical grid, which is basically a discrete representation of the problem domain. The grid is bounded by the object and the peripherals of the domain considered, and the process of rendering such a grid is called grid generation. Grid generation makes the problem manageable for computer simulations.

There are various ways to define a grid around an object, which one to choose depends on the following facts:

i. Geometric complexity of the object around or inside which the fluid flows
ii. Mathematical model chosen to solve the problem (i.e. Euler or N-S equations)
iii. Qualitative shape of the flow field solution (i.e. where large gradients occur, like shock waves, boundary layers, etc…)

Among the above stated considerations, the latter is rather intuitive, and depends on the previous experiences of the grid designer. With careful consideration

of the above facts about grid generation, different kinds of algorithms can be employed to produce grids, like structured ones of O-type, C-type, H-type, etc … or unstructured ones.

1.3.3 Discretization of the Governing Equations:

It is the recipe by which the continuous partial differential equations, governing the fluid flow, are converted into their discrete algebraic counterpart, to be handled by the computer. Well known discretization methods are [1,2]:

Finite Difference Method (FDM): This method approximates the governing equations by Taylor series expansions. It is believed to have been introduced by Euler in the 18^{th} century. Disadvantages are restriction to simple geometries and conservation principle is not enforced unless special care is taken.

Finite Element Method (FEM): It is similar to FVM in many ways. The domain is broken into a set of discrete volumes or finite elements that are generally unstructured. The distinguishing feature is that the equations are multiplied by a weight function, before they are integrated over the entire domain. It has the advantage of ability to deal with arbitrary geometries.

Finite Volume Method (FVM): This method takes the integral form of the conservation equations as the starting point, and divides the domain into finite number of contiguous control volumes. It uses discrete approximations to surface integrals appearing in the integral formulation. This approach is perhaps the simplest to understand and to program. All approximated terms have physical meaning which is why it is popular among engineers. Disadvantage is that methods of order higher than two are more difficult to develop in three-dimensional space. That's because finite volume approach involves three stages of approximation which are interpolation, differentiation and integration. This is also the kind of approach implemented in this study.

Spectral Element Method (SEM): This is a fairly new method, similar to FEM. One of its differences with FEM is that in SEM, the basis functions are chosen perpendicular to each other.

It should be noted that there is no method optimal to every problem of fluid flow.

1.3 MATHEMATICAL MODELING OF TURBULENCE FOR CFD

1.3.1 Definition and Characteristics of Turbulence:

In 1937, Taylor and Von Kármán proposed the following definition of turbulence: "Turbulence is an irregular motion in general makes its appearance in fluids, gaseous or liquid, when they flow past solid surfaces or even when neighboring streams of the same fluid flow past over one another" [6]. Most flows occurring in nature and in engineering applications are turbulent. The irregularity of turbulent motion is due the inherent nonlinear nature of Navier-Stokes equations, when the Reynolds number is beyond a critical value. Thus, contrary to laminar flow, which is regular and deterministic, turbulent flow is stochastic and chaotic [7]. Luckily, for engineers, rather than instantaneous properties, average behavior of turbulence is generally sufficient for which mathematical models are established. Before plunging into these mathematical models it will be useful to take a look at characteristics of turbulence, as briefly stated below [8]:

i. Turbulence is **irregular or random**, which makes deterministic approaches impossible; instead, one relies on several statistical methods to handle fluctuating properties over time.
ii. Turbulence is **diffusive**, which causes rapid mixing and increased rates of momentum, heat and mass transfer. This property is useful for some applications.
iii. Turbulence arises at **large Reynolds numbers,** due to the instability of laminar flows, when the nonlinear convective term in Navier-Stokes

equations gets increasing importance compared with the viscous term. Thus the tendency to instability, which is damped by viscosity, increases.

iv. Turbulence is intrinsically **three dimensional**, characterized by high levels of vorticity fluctuations produced by the vortex stretching mechanism. This mechanism is absent in two dimensional flows.

v. Turbulence **dissipates energy**. Viscous shear stresses perform deformation work, which increases the internal energy of the fluid at the expense of kinetic energy of the turbulence.

vi. Turbulence is a **continuum phenomenon** governed by equations of fluid mechanics. This is because even the smallest scales of turbulence are far larger than any molecular length scale (i.e. mean free path of molecules).

vii. Turbulence is **flow dependent**, not a feature of fluids but of fluid flows.

1.3.2 A Brief History of Turbulence Modeling:

Modern turbulence modeling efforts go back to the time when Osbourne Reynolds proposed one of the most popular averaging techniques in 1895 and established the famous Reynolds averaged Navier-Stokes equations (RANS). His approach can be taken as the origin of modern turbulence research. This technique is also adopted in this work and will be discussed in Chapter 2.

But, before Reynolds, in 1877, Boussinesq introduced the eddy viscosity concept, which is an analog of molecular counterpart in Navier-Stokes equations established for laminar viscous flows [9]. This approach has greatly influenced turbulence research on the coming years such that few authors find a need to refer to Boussinesq's original paper.

No one until Prandtl's discovery of boundary layer concept in 1904 had ever attempted to solve RANS equations [6]. After further research, in 1925, Prandtl introduced the mixing length concept (from an analogy to the kinetic theory of gases) by which he could propose an algebraic expression for eddy viscosity.

In 1935, a different approach was proposed by G. I. Taylor in his pioneering work. Prior to this time, there had been no clear recognition and acceptance of the fact that the velocity of the fluid in turbulent motion is a random continuous function of position and time, and the theories of the turbulence were only based on mixing length hypothesis [10]. His work has statistical importance, where he introduced the correlation between the velocities at two points as one of the quantities needed to describe turbulence. He could realize that "statistical homogeneity" would greatly simplify the analysis leading to the concept of "isotropic turbulence". After Taylor's work, T. Von Karman (1937) perceived that the mean values of the products of the velocities at two (or more) points were tensors which immediately enabled the analysis to be expressed more concisely and greatly facilitated the deductions from the assumption of isotropy [10].

In 1941, Kolmogoroff has come up with the hypothesis that the small scale components of the turbulence are approximately in statistical equilibrium. Together with an equation for k, the turbulence kinetic energy, he modeled an equation for a second parameter ω, which he referred to as "the rate of dissipation turbulence kinetic energy in unit volume and time. This model is known as k-ω model and it is the first proposed model of two equation type.

In 1945, Prandtl postulated a model, in which the eddy viscosity were depending upon the kinetic energy of the turbulent fluctuations, k. Conceptually, this took into account the fact that the eddy viscosity were depending on flow history. This has given rise to one equation model of turbulence.

In 1951, Rotta has laid the foundation for turbulence models that eliminates the use of Boussinesq approximation. He devised a differential equation governing the evolution of the Reynolds stress tensor. This approach is called second order closure.

So in taking an average of the Navier-Stokes equations for turbulent flow, detailed information about the fluid motion is lost. In order to recover the information lost, a turbulence model must be introduced.

Computational efforts based on these turbulence models started in early 60's. A classification of turbulence models which have been subjected to computational use since then can be made as follows:

i. algebraic (zero) equation models,
ii. one-equation models,
iii. two equation models and
iv. second order closure models.

The evolution of these models can briefly be described as follows [6]:

Algebraic models: Van Driest (1956), Cebeci and Smith (1974), Baldwin and Lomax (1978) have contributed to the mixing length model in different ways and their models are the most popular ones among other algebraic models.

One equation models: Bradshaw, Ferriss and Atwell (1967) have formulated the first popular model of this type. Further contributions came from Baldwin and Barth (1990), Goldberg (1991) and Spalart and Allmaras (1992). There has recently been an interest in one equation models of turbulence, due to their accuracy, simplicity of implementation and less demanding computational requirements as reported by El Khoury [11].

Two equation models: After Kolmogoroff (1941), Launder et. al. (1972) has made the first significant contribution by introducing famous k-ε model. Wilcox et. al. have pursued further development and presented successful applications of k-ω model.

Second order closure models: After sufficient computer resources became available by 1970's, most notable improvements to the model were done by Donaldson and Rosenbaum (1968), Daly and Harlow (1970) and Lounder et. al (1975). These models are advantageous in the sense that they automatically accommodate complicating effects such as streamline curvature, rigid body rotation and body forces. However because of large number of extra partial differential equations, complexity and computational cost, these models have found relatively small number of applications.

Apart from the above mentioned models, the tremendous increase in the speed of computers in the last two decades has given the opportunity for the introduction of new techniques to the field of computational turbulence research: These techniques are, namely, Large Eddy Simulation (LES) and Direct Numerical Simulation (DNS). These techniques have become the two popular topics of interest for turbulence researchers of today. They can briefly be explained as follows:

DNS directly include the physics of turbulence. No turbulence model is imposed on the Navier-Stokes equations; thereby no closure approximations are utilized. However, it has some major drawbacks: DNS is limited to relatively low Reynolds numbers in practice and it is currently very expensive to conduct a DNS calculation at even moderately high Reynolds number. It can be said that DNS is still under development stage and needs further increase in CPU speeds.

On the other hand, as its name suggests, LES has the less ambitious goal of describing the larger scales of the flow by numerical simulation, approximating the smaller ones. This in turn allows higher Reynolds numbers to be achieved [12]. Consequently, LES technique constitutes a good compromise for accuracy and cost in between DNS and two equation models.

1.4 PRESENT STUDY

In the present study, a previously developed Navier-Stokes solver is used to implement some well known turbulence models, those of which employ eddy viscosity approximation. To evaluate the effects of turbulence transport equations (namely k-ε and k-ω models) on the solutions, the solver is tested for a turbulent flow case over a flat plate.

The one step, second order accurate Lax-Wendroff scheme is used in the study. The Lax-Wendroff technique is first introduced in 1960, and Ni [13] combined it with a finite volume technique and applied it to Euler equations in 1982. He later improved it to solve for Navier-Stokes equations and his work forms the basis of this study.

Pertaining to Ni's technique, the discretization is hybrid in the sense that it is cell-vertex for the inviscid terms and cell-centered for viscous terms. The same technique is used for the discretization of turbulence closure equations and a cell based approach is used to calculate the source term.

To damp the numerical oscillations, artificial viscosity terms are added to the formulations. For the discretized turbulence transport equations, artificial viscosity coefficient is chosen considerably higher than the one chosen for Navier-Stokes equations, which rendered the scheme more stable. Also to maintain stability, positivity and boundedness conditions are employed for the turbulence parameters.

The following chapters are organized as follows: Chapter 2 describes the governing equations of the flow, that is, Navier-Stokes equations coupled with two equation turbulence models. This chapter also gives a brief introduction to RANS equations, the closure problem and mixing length hypothesis. Chapter 3 covers the method of discretization, which is based on the type of formulations used by Ni [13]. Handling of viscous and turbulence terms, stability and convergence of the method are explained. Chapter 4 gives the initial and boundary conditions for the partial

differential equations. Chapter 5 presents the results obtained for the test cases to validate the solver and discuss its performance. Chapter 6 summarizes the work by a conclusion and lists some useful ideas for future study.

CHAPTER 2

GOVERNING EQUATIONS

In this study, Navier-Stokes equations are used to model a viscous, heat conducting, and compressible gas which flows under no external or body force, and for which no heat generation occurs within. These equations are written in conservative form in three dimensions, with respect to a stationary reference frame. The conservative form is preferred because this form includes the physics of the flow in the equations and has better shock capturing capabilities.

To calculate the effects of turbulence, Reynolds Averaged Navier-Stokes equations (RANS) are used, and thus "the closure problem of turbulence" is introduced. To close the system of equations, the compressible gas is assumed to be perfect with constant specific heats. Auxiliary relations like Sutherland's law of viscosity - which relates the laminar viscosity of the fluid to its temperature - are used. To calculate turbulent viscosity, turbulence closure approximations are utilized.

2.1 THREE-DIMENSIONAL NAVIER-STOKES EQUATIONS COUPLED WITH TWO-EQUATION TURBULENCE CLOSURES

The compressible Navier-Stokes equations are written in a conservative vectorial form as follows:

$$\frac{\partial U}{\partial t}+\frac{\partial F}{\partial x}+\frac{\partial G}{\partial y}+\frac{\partial H}{\partial z}=\frac{\partial F_{v}}{\partial x}+\frac{\partial G_{v}}{\partial y}+\frac{\partial H_{v}}{\partial z}+S \tag{2.1}$$

where

$$U = \begin{bmatrix} \rho \\ \rho u \\ \rho v \\ \rho w \\ e \\ \rho k \\ \rho \phi \end{bmatrix} \tag{2.2a}$$

$$F = \begin{bmatrix} \rho u \\ \rho u^2 + p \\ \rho uv \\ \rho uw \\ \rho uh \\ \rho uk \\ \rho u\phi \end{bmatrix} \tag{2.2b}$$

$$G = \begin{bmatrix} \rho v \\ \rho uv \\ \rho v^2 + p \\ \rho vw \\ \rho vh \\ \rho vk \\ \rho v\phi \end{bmatrix} \tag{2.2c}$$

$$H = \begin{bmatrix} \rho w \\ \rho uw \\ \rho vw \\ \rho w^2 + p \\ \rho wh \\ \rho wk \\ \rho w\phi \end{bmatrix} \tag{2.2d}$$

$$F_v = \begin{bmatrix} 0 \\ \tau_{xx} \\ \tau_{xy} \\ \tau_{xz} \\ \tau_{xx}u + \tau_{xy}v + \tau_{xz}w - q_x \\ \left(\mu_{lam} + \dfrac{\mu_{turb}}{\sigma_k}\right)\dfrac{\partial k}{\partial x} \\ \left(\mu_{lam} + \dfrac{\mu_{turb}}{\sigma_\phi}\right)\dfrac{\partial \phi}{\partial x} \end{bmatrix} \tag{2.2e}$$

$$G_v = \begin{bmatrix} 0 \\ \tau_{yx} \\ \tau_{yy} \\ \tau_{yz} \\ \tau_{yx}u + \tau_{yy}v + \tau_{yz}w - q_y \\ \left(\mu_{lam} + \dfrac{\mu_{turb}}{\sigma_k}\right)\dfrac{\partial k}{\partial y} \\ \left(\mu_{lam} + \dfrac{\mu_{turb}}{\sigma_\phi}\right)\dfrac{\partial \phi}{\partial y} \end{bmatrix} \tag{2.2f}$$

$$H_v = \begin{bmatrix} 0 \\ \tau_{zx} \\ \tau_{zy} \\ \tau_{zz} \\ \tau_{zx}u + \tau_{zy}v + \tau_{zz}w - q_z \\ \left(\mu_{lam} + \dfrac{\mu_{turb}}{\sigma_k}\right)\dfrac{\partial k}{\partial z} \\ \left(\mu_{lam} + \dfrac{\mu_{turb}}{\sigma_\phi}\right)\dfrac{\partial \phi}{\partial z} \end{bmatrix} \tag{2.2g}$$

where u, v and *w* are the three velocity components in the *x, y* and *z* directions, respectively. ρ is the density, *p* is the static pressure, *k* is the turbulent kinetic energy and ϕ stands for ε in the *k*-ε turbulence closure and for ω in the *k*-ω turbulence closure. For the *k*-ε turbulence model the source term may be expressed as below:

$$S_{k-\varepsilon} = \begin{bmatrix} 0 \\ 0 \\ 0 \\ 0 \\ 0 \\ P_k - \rho\varepsilon - D \\ C_{\varepsilon 1} P_k \dfrac{\varepsilon}{k} - C_{\varepsilon 2} \dfrac{\varepsilon^2 \rho}{k} f_2 - E \end{bmatrix} \tag{2.2h}$$

For k-ω turbulence model, the source term takes the form below:

$$S_{k-\omega} = \begin{bmatrix} 0 \\ 0 \\ 0 \\ 0 \\ 0 \\ P_k - \beta^* \rho k \omega \\ \alpha P_k \dfrac{\omega}{k} - \beta \rho \omega^2 \end{bmatrix} \tag{2.2i}$$

Note that the terms coming from the transport equations for turbulence closure are included at the 6th and 7th row of every vector. Using the equation of state, pressure can be written in terms of the conservative variable as follows:

$$p = (\gamma - 1)\left(e - \frac{1}{2\rho}\left[(\rho u)^2 + (\rho v)^2 + (\rho w)^2 \right] \right) \tag{2.3}$$

where e is the total internal energy per unit volume. The total enthalpy per unit mass, h is defined as:

$$h = \frac{(e + p)}{\rho} \tag{2.4}$$

The stress terms are composed of two parts, laminar and turbulent, as follows:

$$\tau_{xx} = \tau_{xx,lam} + \tau_{xx,tur} \tag{2.5a}$$

$$\tau_{yy} = \tau_{yy,lam} + \tau_{yy,tur} \tag{2.5b}$$

$$\tau_{zz} = \tau_{zz,lam} + \tau_{zz,tur} \tag{2.5c}$$

$$\tau_{xy} = \tau_{xy,lam} + \tau_{xy,tur} \tag{2.5d}$$

$$\tau_{xz} = \tau_{xz,lam} + \tau_{xz,tur} \tag{2.5e}$$

$$\tau_{yz} = \tau_{yz,lam} + \tau_{yz,tur} \tag{2.5f}$$

and,

$$\tau_{yx} = \tau_{xy} \tag{2.5g}$$

$$\tau_{zy} = \tau_{yz} \tag{2.5h}$$

$$\tau_{zx} = \tau_{xz} \tag{2.5i}$$

The subscripts *lam* and *tur* are for laminar and turbulent quantities respectively. The production term for all models is the same and can be expressed as:

$$\begin{aligned} P_k = {} & \tau_{xx,tur}\frac{\partial u}{\partial x} + \tau_{xy,tur}\left(\frac{\partial u}{\partial y} + \frac{\partial v}{\partial x}\right) + \tau_{xz,tur}\left(\frac{\partial u}{\partial z} + \frac{\partial w}{\partial x}\right) + \tau_{yy,tur}\frac{\partial v}{\partial y} \\ & + \tau_{yz,tur}\left(\frac{\partial v}{\partial z} + \frac{\partial w}{\partial y}\right) + \tau_{zz,tur}\frac{\partial w}{\partial z} \end{aligned} \tag{2.6}$$

The laminar stresses given by Stokes law of viscosity can be expressed as:

$$\tau_{xx,lam} = \mu_{lam}\left(\frac{4}{3}\frac{\partial u}{\partial x} - \frac{2}{3}\frac{\partial v}{\partial y} - \frac{2}{3}\frac{\partial w}{\partial z}\right) \tag{2.7a}$$

$$\tau_{yy,lam} = \mu_{lam}\left(\frac{4}{3}\frac{\partial v}{\partial y} - \frac{2}{3}\frac{\partial u}{\partial x} - \frac{2}{3}\frac{\partial w}{\partial z}\right) \tag{2.7b}$$

$$\tau_{zz,lam} = \mu_{lam}\left(\frac{4}{3}\frac{\partial w}{\partial z} - \frac{2}{3}\frac{\partial u}{\partial x} - \frac{2}{3}\frac{\partial v}{\partial y}\right) \tag{2.7c}$$

$$\tau_{xy,lam} = \mu_{lam}\left(\frac{\partial u}{\partial y} + \frac{\partial v}{\partial x}\right) \tag{2.7d}$$

$$\tau_{xz,lam} = \mu_{lam}\left(\frac{\partial u}{\partial z} + \frac{\partial w}{\partial x}\right) \tag{2.7e}$$

$$\tau_{yz,lam} = \mu_{lam}\left(\frac{\partial v}{\partial z} + \frac{\partial w}{\partial y}\right) \tag{2.7f}$$

$$\tau_{yx,lam} = \tau_{xy,lam} \tag{2.7g}$$

$$\tau_{zx,lam} = \tau_{xz,lam} \tag{2.7h}$$

$$\tau_{zy,lam} = \tau_{yz,lam} \tag{2.7i}$$

Relying upon eddy viscosity approximation, the turbulent stresses can be expressed as:

$$\tau_{xx,tur} = \mu_{tur}\left(\frac{4}{3}\frac{\partial u}{\partial x} - \frac{2}{3}\frac{\partial v}{\partial y} - \frac{2}{3}\frac{\partial w}{\partial z}\right) - \frac{2}{3}\rho k \tag{2.8a}$$

$$\tau_{yy,tur} = \mu_{tur}\left(\frac{4}{3}\frac{\partial v}{\partial y} - \frac{2}{3}\frac{\partial u}{\partial x} - \frac{2}{3}\frac{\partial w}{\partial z}\right) - \frac{2}{3}\rho k \tag{2.8b}$$

$$\tau_{zz,tur} = \mu_{tur}\left(\frac{4}{3}\frac{\partial w}{\partial z} - \frac{2}{3}\frac{\partial u}{\partial x} - \frac{2}{3}\frac{\partial v}{\partial y}\right) - \frac{2}{3}\rho k \tag{2.8c}$$

$$\tau_{xy,tur} = \mu_{tur}\left(\frac{\partial u}{\partial y} + \frac{\partial v}{\partial x}\right) \tag{2.8d}$$

$$\tau_{xz,tur} = \mu_{tur}\left(\frac{\partial u}{\partial z} + \frac{\partial w}{\partial x}\right) \tag{2.8e}$$

$$\tau_{yz,tur} = \mu_{tur}\left(\frac{\partial v}{\partial z} + \frac{\partial w}{\partial y}\right) \tag{2.8f}$$

$$\tau_{yx,tur} = \tau_{xy,tur} \tag{2.8g}$$

$$\tau_{zx,tur} = \tau_{xz,tur} \tag{2.8h}$$

$$\tau_{zy,tur} = \tau_{yz,tur} \tag{2.8i}$$

As for shear stresses, the heat fluxes can be assumed to be composing of laminar and turbulent parts:

$$q_x = q_{x,lam} + q_{x,tur} \tag{2.9.a}$$

$$q_y = q_{y,lam} + q_{y,tur} \tag{2.9.b}$$

$$q_z = q_{z,lam} + q_{z,tur} \tag{2.9.c}$$

Laminar stresses can be written as follows:

$$q_x = -\kappa_{lam} \frac{\partial T}{\partial x} \tag{2.10a}$$

$$q_y = -\kappa_{lam} \frac{\partial T}{\partial y} \tag{2.10b}$$

$$q_z = -\kappa_{lam} \frac{\partial T}{\partial z} \tag{2.10c}$$

Turbulent stresses are:

$$q_{x,tur} = -\kappa_{tur} \frac{\partial T}{\partial x} - \frac{2}{3} \rho u k \tag{2.11a}$$

$$q_{y,tur} = -\kappa_{tur} \frac{\partial T}{\partial y} - \frac{2}{3} \rho v k \tag{2.11b}$$

$$q_{z,tur} = -\kappa_{tur} \frac{\partial T}{\partial z} - \frac{2}{3} \rho w k \tag{2.11c}$$

In equations (2.10a-c) and (2.11a-c), T stands for the temperature. Laminar and turbulent thermal conductivities are:

$$\kappa_{lam} = \left(\frac{\mu_{lam}}{Pr_{lam}} \right) \frac{\gamma R}{\gamma - 1} \quad \text{, where } Pr_{lam} = 0.72 \text{ for air} \tag{2.12a}$$

$$\kappa_{tur} = \left(\frac{\mu_{tur}}{Pr_{tur}} \right) \frac{\gamma R}{\gamma - 1} \quad \text{, where } Pr_{tur} = 0.90 \text{ for air} \tag{2.12b}$$

Note that, laminar and turbulent Prandtl numbers are constants.

2.2 CALCULATION OF LAMINAR VISCOSITY

The dynamic viscosity of air is assumed to be a function of temperature only, using Sutherland's law.

$$\mu_{lam} = 1.45x10^{-6} \frac{T^{\frac{3}{2}}}{T + 110.0} \tag{2.13}$$

In the above equation, temperature is in Kelvin and dynamic viscosity is calculated in units of Pa.s.

2.3 CALCULATION OF TURBULENT VISCOSITY

2.3.1 *k-ε* Turbulence Closure

For the **high-Reynolds-number** *k-ε* turbulence closure, $D = E = 0.0$ and f_2=1.0 in equation (2.2h). Chien model is implemented in this work; and hence, the **low-Reynolds-number** turbulence closure source terms take the following form:

$$D = 2\frac{\mu_{lam} k}{y^2} \tag{2.14}$$

$$E = 2\frac{\mu_{lam} \varepsilon}{y^2} \exp\left(-0.5 y^+\right) \tag{2.15}$$

$$f_2 = \left(1 - 0.222\, exp\left(-\frac{Re^{k\varepsilon}{}_T}{6}\right)^2\right) \tag{2.16}$$

$$Re_T^{k\varepsilon} = \frac{\rho k^2}{\mu_{lam}\varepsilon} \tag{2.17}$$

where y^+ is the non-dimensional wall distance calculated as:

$$y^+ = \frac{\rho}{\mu_{lam}} u_\tau \cdot y \tag{2.18}$$

and u_τ is the friction velocity defined as:

$$u_\tau = \sqrt{\frac{\tau_{wall}}{\rho}} \tag{2.19}$$

The eddy viscosity for the k-ε model has the following form:

$$\mu_{tur} = \left\{c_\mu \, \mathrm{Re}_T^{k\varepsilon}\right\} f_\mu \mu_{lam} \tag{2.20}$$

where $f_\mu = 1$ for the high-Reynolds number turbulence closure and for Chien model it is set as follows:

$$f_\mu = 1 - \exp\left(-0.0115 y^+\right) \tag{2.21}$$

The closure coefficients for high-Reynolds number k-ε turbulence closure are:

$$C_{\varepsilon 1} = 1.44, \quad C_{\varepsilon 2} = 1.92 \qquad \sigma_k = 1, \quad \sigma_\varepsilon = 1.3 \qquad \mathrm{Pr}_T = 0.9 \tag{2.22}$$

The closure coefficients for low-Reynolds number k-ε turbulence closure are:

$$C_{\varepsilon 1} = 1.35, \quad C_{\varepsilon 2} = 1.80 \qquad \sigma_k = 1, \quad \sigma_\varepsilon = 1.3 \qquad \mathrm{Pr}_T = 0.9 \tag{2.23}$$

2.3.2 *k-ω* Turbulence Closure

For this model, the eddy viscosity is given as:

$$\mu_{tur} = \alpha^* \frac{\rho k}{\omega} \tag{2.24}$$

The closure coefficients for low-Reynolds-number *k-ω* turbulence closure are:

$$\alpha^* = \frac{\alpha_0^* + \mathrm{Re}_T^{k\omega}/R_k}{1 + \mathrm{Re}_T^{k\omega}/R_k} \qquad \beta^* = \frac{9}{100}\frac{5/18 + \left(\mathrm{Re}_T^{k\omega}/R_\beta\right)^4}{1 + \left(\mathrm{Re}_T^{k\omega}/R_\beta\right)^4}$$
$$\alpha = \frac{5}{9}\frac{\alpha_0 + \mathrm{Re}_T^{k\omega}/R_\omega}{1 + \mathrm{Re}_T^{k\omega}/R_\omega}\left(\alpha^*\right)^{-1} \qquad \sigma_k = \sigma_\omega = 2 \tag{2.25}$$

$$\beta = 3/40, \quad \alpha_0^* = \beta/3, \quad \alpha_0 = 1/10 \quad R_\beta = 8, \quad R_k = 6, \quad R_\omega = 27/10 \tag{2.25}$$

and the turbulent Reynolds number for *k-ω* model is defined by

$$\mathrm{Re}_T^{k\omega} = \frac{\rho k}{\omega \mu_{lam}} \tag{2.27}$$

The closure coefficients for high-Reynolds number *k-ω* turbulence closure are:

$$\alpha^* = 1.0, \quad \alpha = \frac{5}{9}, \quad \beta^* = \frac{9}{100}, \quad \sigma_k = \sigma_\omega = 2 \tag{2.28}$$

2.3.3 Positivity and Boundedness for *k-ε* and *k-ω* Closures

During computations, *k*, *ε* and *ω* must be bounded by limiters, otherwise their values may attain negative values, which are non-physical and meaningless.

Furthermore this may create stability problems. So if k, ε and ω are found to be negative during the computations, the boundedness suggested by Gerolymos [19] are used in this study, which are

$$k = \varepsilon = 10^{-23} \tag{2.29}$$

For k and ω the lower limits are set as follows:

$$k = 10^{-6} \quad \omega = 5 \tag{2.30}$$

According to Liu [15], the production of turbulent kinetic energy must be limited to the twice of the dissipation expressed as:

$$P_k = \min\left(P_k, 2\rho\varepsilon\right) \tag{2.31}$$

2.4 ZERO-EQUATION (ALGEBRAIC) TURBULENCE MODELS

Zero-equation models retain the Boussinesq eddy-viscosity (turbulent viscosity) approximation to compute the turbulent stresses, as in two-equation turbulence models. Their difference is that the turbulent viscosity is formulated using the mixing-length hypothesis. Closure coefficients and auxiliary functions are used to support their formulations to take into account the effects of wake, intermittency and separation.

The coupling of zero-equation models with the Navier-Stokes equations is very similar to two-equation models. The differences are:

i. As their name (zero-equation) implies, no additional partial differential equation is solved, so the last two equations are dropped from the system of equations (2.2.a-h).

ii. The terms involving turbulence kinetic energy, $\frac{2}{3}\rho k$, $\frac{2}{3}\rho uk$, $\frac{2}{3}\rho vk$ and $\frac{2}{3}\rho wk$ are cancelled in the equations (2.8.a-c) and (2.11.a-c).

2.4.1 Cebeci-Smith Turbulence Closure

The Cebeci-Smith model is a two-layer algebraic model with the turbulent viscosity given by separate expressions in each layer as

$$\mu_{tur} = \begin{pmatrix} (\mu_{tur})_{inner}, & y \le y_m \\ (\mu_{tur})_{outer}, & y > y_m \end{pmatrix} \tag{2.32}$$

where y_m is the smallest value of y for which $(\mu_{tur})_{inner} = (\mu_{tur})_{outer}$ whereas y denotes the normal distance from the wall. The values of μ_{tur} in the inner layer, $(\mu_{tur})_{inner}$, and the outer layer, $(\mu_{tur})_{outer}$, are computed as follows

Inner Layer Formulation:

$$(\mu_{tur})_{inner} = \rho \cdot l_{mix}{}^2 \cdot \sqrt{\left(\frac{\partial u}{\partial y}\right)^2 + \left(\frac{\partial v}{\partial x}\right)^2} \tag{2.33}$$

where l_{mix} is the mixing length calculated by

$$l_{mix} = \kappa y \left(1 - e^{\frac{-y^+}{A^+}}\right) \tag{2.34}$$

and y^+ is the distance from the wall and is calculated as in equation (2.18).

Outer Layer Formulation:

$$(\mu_{tur})_{outer} = \alpha \rho U_e \delta_v^* F_{Kleb}(y;\delta) \tag{2.35}$$

where U_e is the boundary layer edge velocity taken as:

$$U_e = 0.995 U_\infty \tag{2.36}$$

δ_v^* is the velocity thickness defined by the integral

$$\delta_v^* = \int_0^\delta (1 - \frac{u}{U_e}) dy \tag{2.37}$$

where δ is the boundary layer thickness. $F_{Kleb}(y;\delta)$ is the Klebanoff intermittency function given as:

$$F_{Kleb}(y;\delta) = \frac{1}{1 + 5.5\left(\frac{C_{Kleb} y}{y_{max}}\right)^6} \tag{2.38}$$

Finally the closure coefficients for Cebeci-Smith model are expressed as

$$\kappa = 0.41 \quad C_{Kleb} = 0.3 \quad \alpha = 0.0168 \quad A^+ = 26\left[1 + y\frac{dP/dx}{\rho u_\tau}\right]^{-1/2} \tag{2.39}$$

where u_τ is the friction velocity defined by equation (2.19).

Alternative Outer Layer Formulation:

The eddy viscosity in the outer layer can simply be formulated in a different way as follows:

$$(\mu_{tur})_{outer} = \rho \cdot l_{mix}{}^{2} \cdot \sqrt{\left(\frac{\partial u}{\partial y}\right)^{2} + \left(\frac{\partial v}{\partial x}\right)^{2}} \tag{2.40}$$

Note that the form of the eddy-viscosity is the same as it is in the inner layer, but this time the mixing length is given by:

$$l_{mix} = 0.085\delta \tag{2.41}$$

2.2.2 Michel et. al. Turbulence Closure

The model by Michel et. al. postulates a single layer approach, where turbulent viscosity is calculated by a single formulation throughout the whole boundary layer. The turbulent viscosity is

$$\mu_{tur} = \rho \cdot l_{mix}{}^{2} \cdot \sqrt{\left(\frac{\partial u}{\partial y}\right)^{2} + \left(\frac{\partial v}{\partial x}\right)^{2}} \tag{2.42}$$

where the mixing length is given as:

$$l_{mix} = 0.085\delta \cdot \left(1 - e^{\frac{-y^{+}}{A^{+}}}\right) \cdot tanh\left(\frac{\kappa}{0.085\delta} y\right) \tag{2.43}$$

The closure coefficients A^{+} and κ have the same values as in Cebeci-Smith model.

2.2.3 Baldwin-Lomax Turbulence Closure

Like the Cebeci-Smith closure, the Baldwin-Lomax model is also a two-layer algebraic model. The turbulent viscosity is the same as in equation (3.32) However,

the values of μ_{tur} in the inner layer, $(\mu_{tur})_{inner}$, and the outer layer, $(\mu_{tur})_{outer}$, are computed as follows:

Inner Layer Formulation:

$$(\mu_{tur})_{inner} = \rho \cdot {l_{mix}}^2 \cdot |\vec{\omega}| \tag{2.44}$$

where the mixing length is given by

$$l_{mix} = \kappa y \cdot \left(1 - e^{\frac{-y^+}{A^+}}\right) \tag{2.45}$$

and $|\vec{\omega}|$ is the magnitude of vorticity vector given by

$$|\vec{\omega}| = \sqrt{\left(\frac{\partial w}{\partial y} - \frac{\partial v}{\partial z}\right)^2 + \left(\frac{\partial u}{\partial z} - \frac{\partial w}{\partial x}\right)^2 + \left(\frac{\partial v}{\partial x} - \frac{\partial u}{\partial y}\right)^2} \tag{2.46}$$

For wake regions and separated boundary layers, mixing length is calculated from:

$$l_{mix} = \kappa y \tag{2.47}$$

Outer Layer Formulation:

$$(\mu_{tur})_{outer} = \rho \alpha C_{cp} F_{wake} F_{Kleb}(y; \frac{y_{max}}{C_{kleb}}) \tag{2.48}$$

$$F_{wake} = min\left(y_{max} F_{max}, C_{wk} y_{max} \frac{V_{dif}^2}{F_{max}}\right) \tag{2.49}$$

$$F_{max} = \frac{1}{\kappa} max\left(l_{mix} \left| \vec{\omega} \right| \right) \tag{2.50}$$

$$F_{Kleb}(y; \frac{y_{max}}{C_{kleb}}) = \frac{1}{1 + 5.5\left(\frac{C_{Kleb} y}{y_{max}} \right)^6} \tag{2.51}$$

y_{max} is the value of y at which $l_{mix} \cdot \left| \vec{\omega} \right|$ achieves its maximum value. V_{dif} is calculated as:

$$V_{dif} = V_{\max} - V_{\min} \tag{2.52}$$

where V denotes the magnitude of the velocity vector. V_{max} is the maximum value of the velocity along the profile. For wall bounded flows, V_{min} is zero, and for free shear layers, V_{min} corresponds to the velocity at y_{max}.

Finally, the closure coefficients for Baldwin-Lomax model are as follows:

$$\begin{aligned} &\kappa = 0.41 \qquad \alpha = 0.0168 \qquad A^+ = 26 \\ &C_{cp} = 1.6 \qquad C_{Kleb} = 0.3 \qquad C_{wk} = 0.25 \end{aligned} \tag{2.53}$$

CHAPTER 3

NUMERICAL METHOD

This chapter presents and discusses the numerical technique used for the discretization of the three-dimensional Navier-Stokes equations, coupled with turbulence transport equations for k-ε and k-ω models. Calculation of the time step and artificial smoothing terms, which are necessary for the stability and convergence of the numerical scheme, will be explained in detail as well.

3.1. DISCRETIZATION

The discretization technique used in this study is a hybrid finite volume technique: Hybrid in the sense that *cell-vertex* approach is used for the inviscid and first order source terms; and *cell-centered* approach is used for the second order inviscid terms and first order viscous terms. This will be discussed in detail in this chapter. The technique is based on a one-step Lax-Wendroff scheme, which is of explicit time marching type. It was first introduced by Ni [7] for the solution of Euler equations and further improved to solve for Navier-Stokes equations [9]. The derivation of the scheme starts with the second order Taylor series expansion of the conservative vector variable U:

$$U^{n+1} = U^n + \Delta t\left(\frac{\partial U}{\partial t}\right)^n + \frac{\Delta t^2}{2}\left(\frac{\partial^2 U}{\partial t^2}\right)^n \tag{3.1}$$

In the above equation, the superscript n denotes the time step. Using equation (2.1), the term $\frac{\partial U}{\partial t}$ can be written as

$$\frac{\partial U}{\partial t} = -\frac{\partial F}{\partial x} - \frac{\partial G}{\partial y} - \frac{\partial H}{\partial z} + \frac{\partial F_v}{\partial x} + \frac{\partial G_v}{\partial y} + \frac{\partial H_v}{\partial z} + S \tag{3.2}$$

Define the residual as $\delta U = U^{n+1} - U^n$ and insert (3.2) into Equation (3.1) to get:

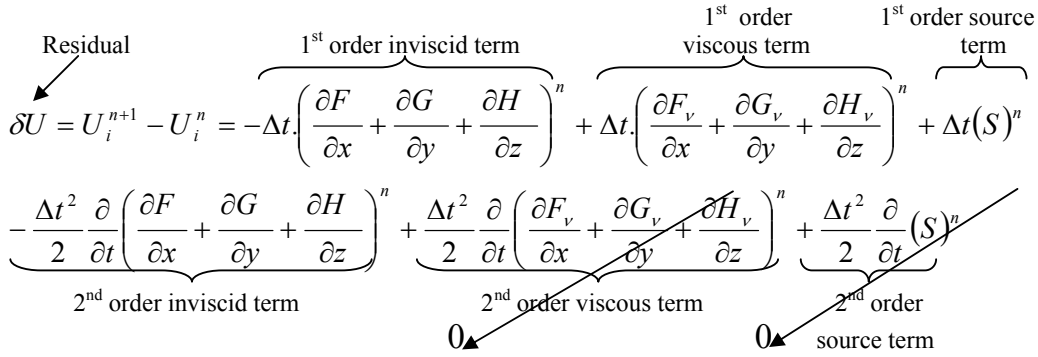

(3.3)

Note that in the above equation; the terms are grouped according their degrees and physical meanings. The effect of the second order viscous and the source terms on the convergence history and final solution has been found to be entirely negligible so that they will be neglected. So, the second order contributions will only be due to the inviscid fluxes. Also the superscript *n* can safely be dropped so that the right hand side of the following equations will stand for the same time level. The remaining equation is:

$$\begin{aligned}\delta U = &-\Delta t.\left(\frac{\partial F}{\partial x} + \frac{\partial G}{\partial y} + \frac{\partial H}{\partial z}\right) + \Delta t.\left(\frac{\partial F_v}{\partial x} + \frac{\partial G_v}{\partial y} + \frac{\partial H_v}{\partial z}\right) + \Delta t(S) \\ &-\frac{\Delta t^2}{2}\frac{\partial}{\partial t}\left(\frac{\partial F}{\partial x} + \frac{\partial G}{\partial y} + \frac{\partial H}{\partial z}\right)\end{aligned} \tag{3.4}$$

The second order inviscid flux terms can be modified as follows:

$$\begin{aligned}
\frac{\Delta t^2}{2}\cdot\frac{\partial}{\partial t}\left(\frac{\partial F}{\partial x}+\frac{\partial G}{\partial y}+\frac{\partial H}{\partial z}\right) &= \frac{\Delta t^2}{2}\left[\frac{\partial}{\partial x}\left(\frac{\partial F}{\partial t}\right)+\frac{\partial}{\partial y}\left(\frac{\partial G}{\partial t}\right)+\frac{\partial}{\partial z}\left(\frac{\partial H}{\partial t}\right)\right] \\
&= \frac{\Delta t^2}{2}\left[\frac{\partial}{\partial x}\left(\frac{\partial F}{\partial U}\frac{\partial U}{\partial t}\right)+\frac{\partial}{\partial y}\left(\frac{\partial G}{\partial U}\frac{\partial U}{\partial t}\right)+\frac{\partial}{\partial z}\left(\frac{\partial H}{\partial U}\frac{\partial U}{\partial t}\right)\right] \\
&= \frac{\Delta t}{2}\left[\frac{\partial}{\partial x}\left(\frac{\partial F}{\partial U}\frac{\partial U}{\partial t}\Delta t\right)+\frac{\partial}{\partial y}\left(\frac{\partial G}{\partial U}\frac{\partial U}{\partial t}\Delta t\right)+\frac{\partial}{\partial z}\left(\frac{\partial H}{\partial U}\frac{\partial U}{\partial t}\Delta t\right)\right] \\
&= \frac{\Delta t}{2}\left[\frac{\partial}{\partial x}\left(\frac{\partial F}{\partial U}\Delta U\right)+\frac{\partial}{\partial y}\left(\frac{\partial G}{\partial U}\Delta U\right)+\frac{\partial}{\partial z}\left(\frac{\partial H}{\partial U}\Delta U\right)\right]
\end{aligned} \tag{3.3}$$

where,

$$\Delta U = \frac{\partial U}{\partial t}\Delta t \tag{3.6}$$

The Jacobians of the inviscid flux vectors can be expressed as [7]

$$\begin{aligned}
\Delta F &= \frac{\partial F}{\partial U}\Delta U \\
\Delta G &= \frac{\partial G}{\partial U}\Delta U \\
\Delta H &= \frac{\partial H}{\partial U}\Delta U
\end{aligned} \tag{3.7}$$

Substitute these definitions into Equation (3.2) to obtain

$$\begin{aligned}
\delta U = &-\Delta t\left(\frac{\partial F}{\partial x}+\frac{\partial G}{\partial y}+\frac{\partial H}{\partial z}\right)+\Delta t\left(\frac{\partial F_v}{\partial x}+\frac{\partial G_v}{\partial y}+\frac{\partial H_v}{\partial z}\right)+\Delta t S \\
&-\frac{\Delta t}{2}\left(\frac{\partial(\Delta F)}{\partial x}+\frac{\partial(\Delta G)}{\partial y}+\frac{\partial(\Delta H)}{\partial z}\right)
\end{aligned} \tag{3.8}$$

The finite volume approximation yields the following expressions for change ΔU , and for Jacobians of inviscid fluxes F, G, H as:

$$\Delta U = \begin{bmatrix} \Delta\rho \\ \Delta(\rho u) \\ \Delta(\rho v) \\ \Delta(\rho w) \\ \Delta e \\ \Delta(\rho k) \\ \Delta(\rho \phi) \end{bmatrix} \tag{3.9a}$$

$$\Delta F = \left(\frac{\partial F}{\partial U}\right)\Delta U = \begin{bmatrix} \Delta(\rho u) \\ u\Delta(\rho u) + \rho u \Delta u + \Delta p \\ v\Delta(\rho u) + \rho u \Delta v \\ w\Delta(\rho u) + \rho u \Delta w \\ h\Delta(\rho u) + \rho u \Delta h \\ k\Delta(\rho u) + u\Delta(\rho k) - uk\Delta\rho \\ \phi\Delta(\rho u) + u\Delta(\rho \phi) - u\phi\Delta\rho \end{bmatrix} \tag{3.9b}$$

$$\Delta G = \left(\frac{\partial G}{\partial U}\right)\Delta U = \begin{bmatrix} \Delta(\rho v) \\ u\Delta(\rho v) + (\rho v)\Delta u \\ v\Delta(\rho v) + (\rho v)\Delta v + \Delta p \\ w\Delta(\rho v) + (\rho v)\Delta w \\ h\Delta(\rho v) + (\rho v)\Delta h \\ k\Delta(\rho v) + v\Delta(\rho k) - (vk)\Delta\rho \\ \phi\Delta(\rho v) + v\Delta(\rho \phi) - v\phi\Delta\rho \end{bmatrix} \tag{3.9c}$$

$$\Delta H = \left(\frac{\partial H}{\partial U}\right)\Delta U = \begin{bmatrix} \Delta(\rho w) \\ u\Delta(\rho w) + (\rho w)\Delta u \\ v\Delta(\rho w) + (\rho w)\Delta v \\ w\Delta(\rho w) + (\rho w)\Delta w + \Delta p \\ h\Delta(\rho w) + (\rho w)\Delta h \\ k\Delta(\rho w) + w\Delta(\rho k) - (wk)\Delta\rho \\ \phi\Delta(\rho w) + w\Delta(\rho \phi) - (w\phi)\Delta\rho \end{bmatrix} \tag{3.9d}$$

Note that ϕ represents ε and ω for k-ε and k-ω turbulence closure, respectively. Also note that,

$$\Delta u = \frac{1}{\rho}\left[\Delta(\rho u) - u\Delta\rho\right]$$

$$\Delta v = \frac{1}{\rho}\left[\Delta(\rho v) - v\Delta\rho\right]$$

$$\Delta w = \frac{1}{\rho}\left[\Delta(\rho w) - w\Delta\rho\right] \tag{3.10}$$

$$\Delta p = (\gamma - 1)\left[\Delta e - \frac{1}{2}\left(u\Delta(\rho u) + v\Delta(\rho v) + w\Delta(\rho w) + \rho u\Delta u + \rho v\Delta v + \rho w\Delta w\right)\right]$$

$$\Delta h = \frac{1}{\rho}\left[\Delta e + \Delta p - h\Delta\rho\right]$$

Before starting the explanation of the integration procedure, it will be useful to examine a typical cell as given in Figure 3.1. The nodes of the cell are locally numbered in counter clockwise order as shown. First order inviscid changes are calculated using the nodes shown with the solid circles, •, and the second order inviscid and first order viscous changes are calculated using the "imaginary" node shown by the white circle, o, representing cell averaged values at the center of the cell.

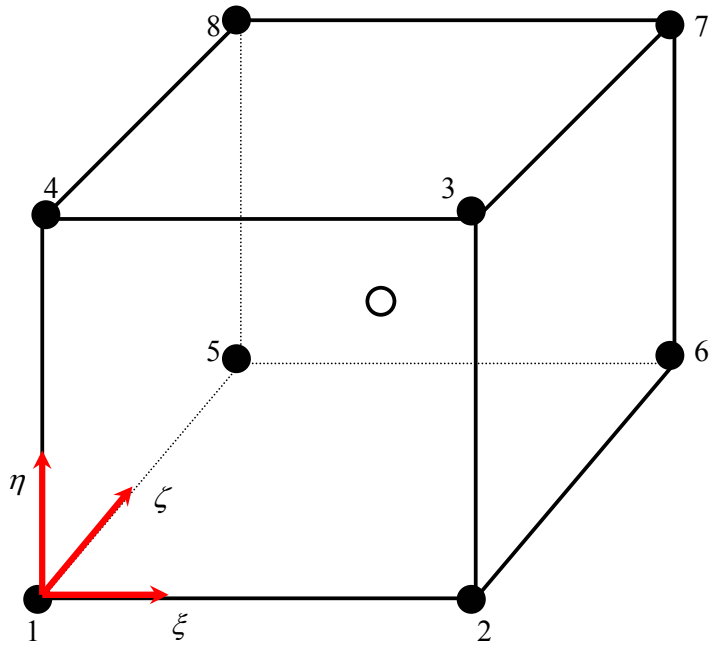

Figure 3.1 Local cell numbering notation

All nodes are surrounded by eight cells, as shown for node 1 in Figure 3.2. Two kinds of control volume are used: The one formed by joining the nodes of the computational domain and the other one formed by joining the cell centers of these, which is a transformed control volume. Figure 3.2 also illustrates these.

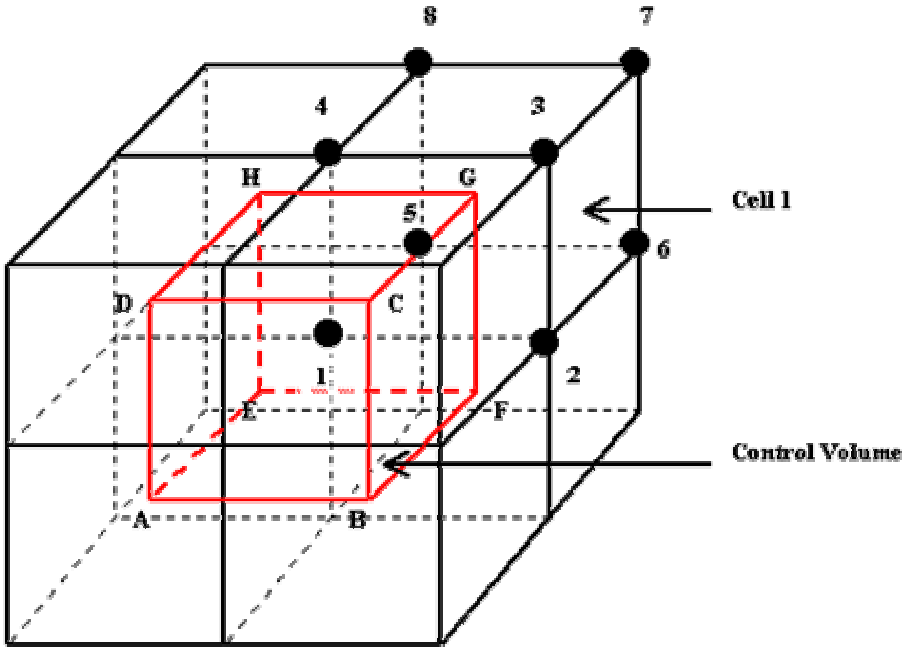

Figure 3.2 Representation of the cells surrounding node 1 of Figure 3.1.

The transformed control volume shown by A-B-C-D-E-F-G-H in Figure 3.2 is the combination of one eighth of every primary cell, which is shown by 1-2-3-4-5-6-7-8. Such a transformed control volume is used to calculate the second order inviscid and the first order viscous changes. On the other hand the primary cell shown in Figure 3.1 is used for the calculation of the first order inviscid changes and the first order source term.

Now the integration procedure can be explained. First integrate Equation (3.8) over a random control volume to get the average change in U:

$$\int_{\delta\forall}\delta U d\forall = -\int_{\delta\forall}\Delta t\left(\frac{\partial F}{\partial x}+\frac{\partial G}{\partial y}+\frac{\partial H}{\partial z}\right)d\forall + \int_{\delta\forall}\Delta t\left(\frac{\partial F_v}{\partial x}+\frac{\partial G_v}{\partial y}+\frac{\partial H_v}{\partial z}\right)d\forall$$
$$+\int_{\delta\forall}(\Delta t S)d\forall - \int_{\delta\forall}\frac{\Delta t}{2}\left(\frac{\partial(\Delta F)}{\partial x}+\frac{\partial(\Delta G)}{\partial y}+\frac{\partial(\Delta H)}{\partial z}\right)d\forall \tag{3.11}$$

The above integration is for any control volume, which will later be applied to the control volumes formed by the primary cell and the transformed control volume. But before, it will be illustrative to check the below figure:

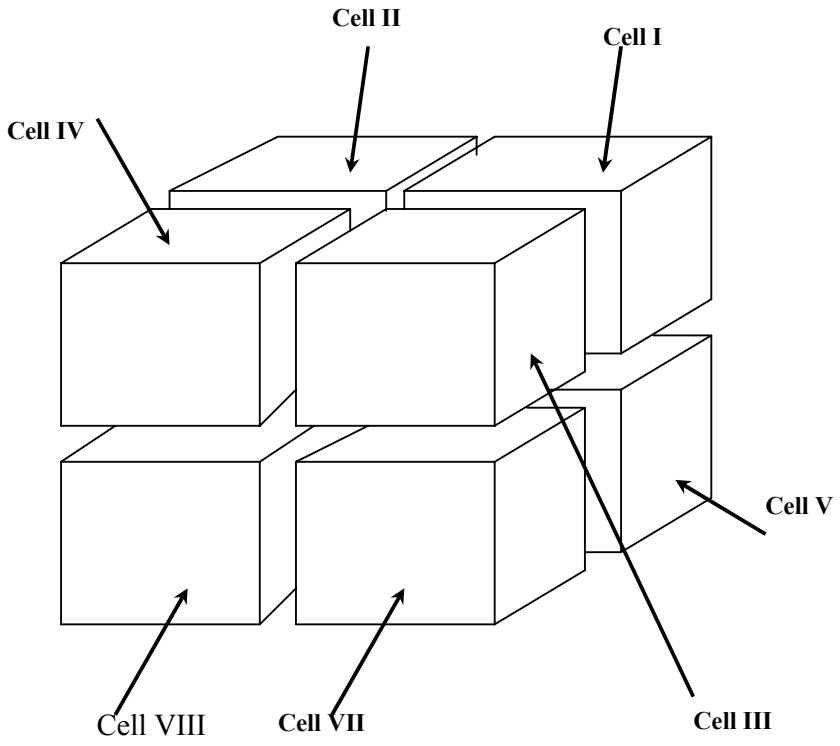

Figure 3.3 Disassembled cells that surround node 1

Figure 3.3 depicts the numbering notation of the eight cells that are shown in Figure 3.2. Here it is worth noting that the cells of the computational domain are not always regular shapes like cubes or prisms, rather, they are generally irregular and can be thought as three dimensional trapezoids. In this work they are shown as cubes just for the sake of illustration.

So, the total contribution of the changes on node 1 is the summation of the contributions from the surrounding eight cells, which can be written as follows:

$$\delta U_1 = \delta U_{1I} + \delta U_{1II} + \delta U_{1III} + \delta U_{1IV} + \delta U_{1V} + \delta U_{1VI} + \delta U_{1VII} + \delta U_{1VIII} \qquad (3.12)$$

In the above equation, the subscripts show the node (which is node 1 here) and cell numbers (*I to VIII*), respectively, at a given time step. Figure 3.4 shows the part of the transformed control volume; 1abcdefgh drawn by the dark lines, within the primary cell, 12345678. This part is used to calculate δU_{1I}, which stands for the contribution of cell I to node 1.

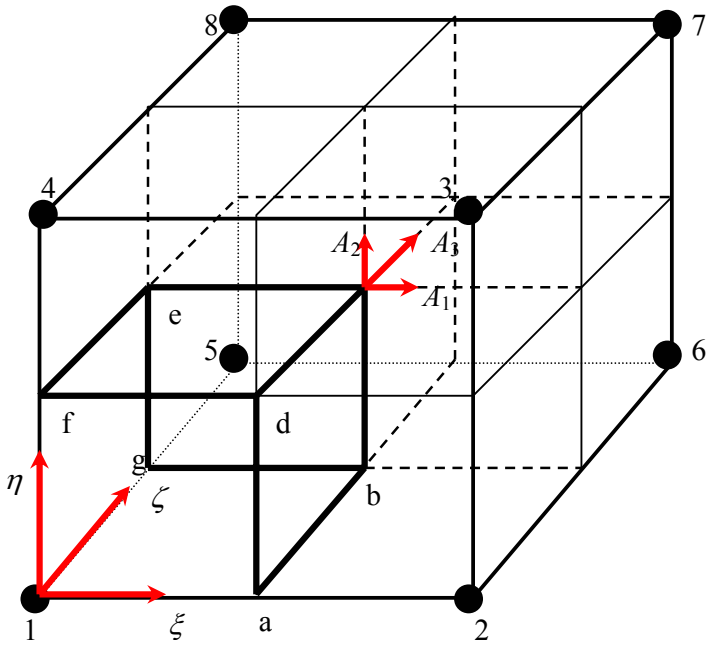

Figure 3.4 Part of the transformed control volume remaining in cell I and cell center face area notation

So, the contribution of cell I to node 1 can be written as follows

$$\delta U_{1I} = -\frac{1}{8}\frac{\Delta t}{\Delta \forall_I}\int_{cell-I}\left(\frac{\partial F}{\partial x}+\frac{\partial G}{\partial y}+\frac{\partial H}{\partial z}\right)d\forall + \frac{\Delta t}{\Delta \forall_I}\int_{1abcdefg}\left(\frac{\partial F_v}{\partial x}+\frac{\partial G_v}{\partial y}+\frac{\partial H_v}{\partial z}\right)d\forall$$
$$+\frac{1}{8}\frac{\Delta t}{\Delta \forall_I}\int_{cell-I} Sd\forall \quad -\frac{\Delta t}{2\Delta \forall_I}\int_{1abcdefg}\left(\frac{\partial(\Delta F)}{\partial x}+\frac{\partial(\Delta G)}{\partial y}+\frac{\partial(\Delta H)}{\partial z}\right)d\forall$$

(3.13)

The above integration calculates the contributions of the change in cell I together with contributions coming from the part of the "transformed" control volume inside cell I. The contributions are calculated for node 1. The first and third integrals on the right hand side of Equation (3.13) stand for the contributions coming from first order inviscid flux and first order source term, respectively, calculated in cell I. The second and the fourth integrals evaluate the contributions coming from first order viscous and second order inviscid fluxes, using the transformed control volume.

The coefficient 1/8 is due to the fact that the contribution on node 1 is from the surrounding eight cells or can be thought as an average contribution of a cell to one of its eight nodes. However, the second and fourth terms in the above integral does not contain the coefficient 1/8, which is logical since the integral is performed on one-eighth of the transformed control volume.

Now, using divergence theorem to convert the volume integrals (except the one for the source terms) in Equation (3.13) to surface integrals one gets:

$$\delta U_{1I} = -\frac{1}{8}\frac{\Delta t}{\Delta \forall_I}\int_{cell-I}\left(FdS_x + GdS_y + HdS_z\right) + \frac{\Delta t}{\Delta \forall_I}\int_{1abcdefg}\left(F_v dS_x + G_v dS_y + H_v dS_z\right)$$
$$+\frac{1}{8}\frac{\Delta t}{\Delta \forall_I}\int_{cell-I} Sd\forall \quad -\frac{\Delta t}{2\Delta \forall_I}\int_{1abcdefg}\left(\Delta F dS_x + \Delta G dS_y + \Delta H dS_z\right)$$

(3.14)

For the ease of representation, group the terms in Equation (3.14) as shown below:

$$\Delta U_i = -\frac{\Delta t}{\Delta \forall_I} \int_{cell-1} \left(F dS_x + G dS_y + H dS_z \right) \tag{3.15a}$$

$$\Delta U_v = \frac{\Delta t}{\Delta \forall_I} \int_{1abcdefg} \left(F_v dS_x + G_v dS_y + H_v dS_z \right) \tag{3.15b}$$

$$\Delta^2 U_i = -\frac{\Delta t}{2\Delta \forall_I} \int_{1abcdefg} \left(\Delta F dS_x + \Delta G dS_y + \Delta H dS_z \right) \tag{3.15c}$$

$$\Delta U_s = \frac{\Delta t}{\Delta \forall_I} \int_{cell-I} \left(S d\forall \right) \tag{3.15d}$$

Substitute the above-defined groups back into Equation (3.14), to get

$$\delta U_{1I} = \frac{1}{8}\left(\Delta U_i + \Delta U_s \right) + \Delta U_v + \Delta^2 U_i \tag{3.16}$$

Now, using trapezoidal integration around cell I, the term ΔU_i in the above equation can be evaluated as follows

$$\begin{aligned} \Delta U_i = \frac{\Delta t}{\Delta \forall_I} [& \left(F_{1,x}.S_{1,x} + G_{1,y}.S_{1,y} + H_{1,z}.S_{1,z} \right) \\ & - \left(F_{2,x}.S_{2,x} + G_{2,y}.S_{2,y} + H_{2,z}.S_{2,z} \right) \\ & + \left(F_{3,x}.S_{3,x} + G_{3,y}.S_{3,y} + H_{3,z}.S_{3,z} \right) \\ & - \left(F_{4,x}.S_{4,x} + G_{4,y}.S_{4,y} + H_{4,z}.S_{4,z} \right) \\ & + \left(F_{5,x}.S_{5,x} + G_{5,y}.S_{5,y} + H_{5,z}.S_{5,z} \right) \\ & - \left(F_{6,x}.S_{6,x} + G_{6,y}.S_{6,y} + H_{6,z}.S_{6,z} \right)] \end{aligned} \tag{3.17}$$

where the fluxes through each cell face are taken to be the average of the corner nodes as shown below for the fluxes in *x* direction:

$$
\begin{aligned}
F_{1,x} &= \frac{F_5 + F_1 + F_4 + F_8}{4} \qquad & F_{2,x} &= \frac{F_6 + F_2 + F_3 + F_7}{4} \\
F_{3,x} &= \frac{F_1 + F_2 + F_6 + F_5}{4} & F_{4,x} &= \frac{F_4 + F_3 + F_7 + F_8}{4} \\
F_{5,x} &= \frac{F_1 + F_2 + F_3 + F_4}{4} & F_{6,x} &= \frac{F_5 + F_6 + F_7 + F_8}{4}
\end{aligned}
\tag{3.18}
$$

Figure (3.5) depicts the surface vectors used in Equation (3.17) in order to explain the calculation of the average fluxes over each face of cell I. The inviscid first-order changes are thus calculated (or estimated). Calculation procedure for the surface vectors can be seen in Appendix A.

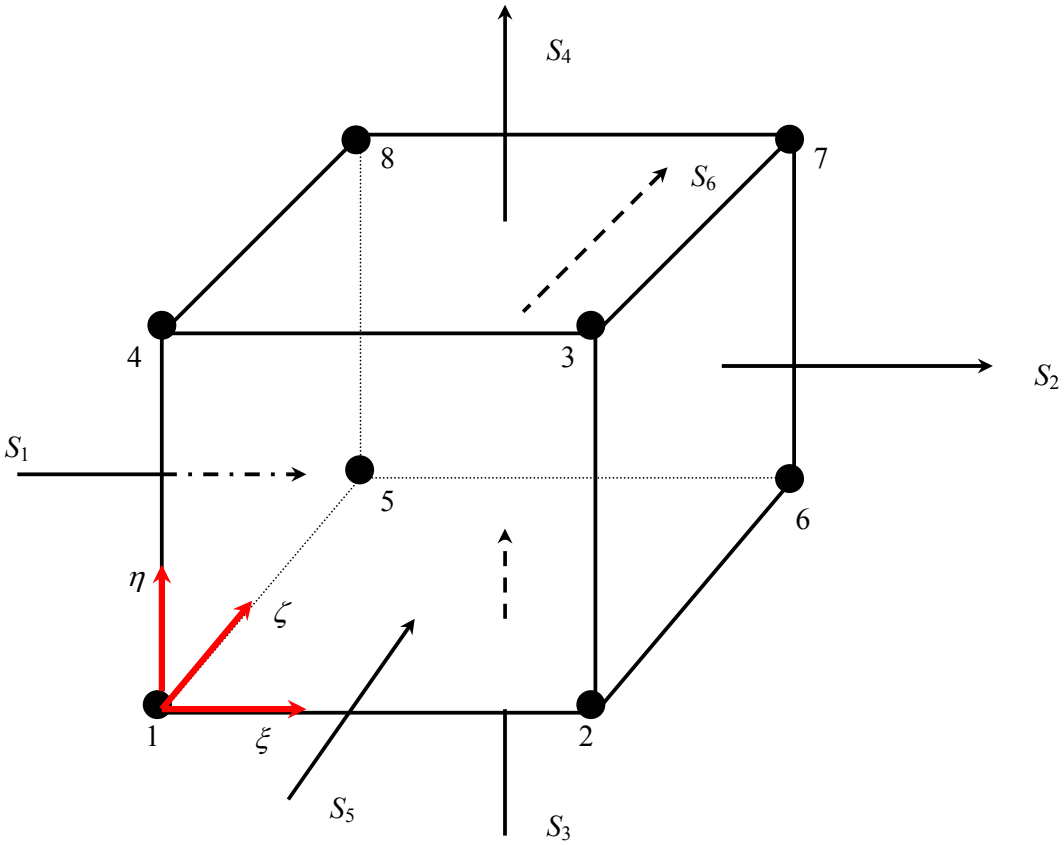

Figure 3.5 Surface vectors on cell I

After a similar interpretation for the fluxes in the other directions, namely, G and H, insert these equations for F, G, H into (3.17), to get:

$$\Delta U_i = \frac{\Delta t}{\Delta \forall_I}\left\{\frac{F_5+F_1+F_4+F_8}{4}S_{1,x}+\frac{G_5+G_1+G_4+G_8}{4}S_{1,y}+\frac{H_5+H_1+H_4+H_8}{4}S_{1,z}\right.$$
$$-\left(\frac{F_6+F_2+F_3+F_7}{4}S_{2,x}+\frac{G_6+G_2+G_3+G_7}{4}S_{2,y}+\frac{H_6+H_2+H_3+H_7}{4}S_{2,z}\right)$$
$$+\frac{F_1+F_2+F_6+F_5}{4}S_{3,x}+\frac{G_1+G_2+G_6+G_5}{4}S_{3,y}+\frac{H_1+H_2+H_6+H_5}{4}S_{3,z}$$
$$-\left(\frac{F_4+F_3+F_7+F_8}{4}S_{4,x}+\frac{G_4+G_3+G_7+G_8}{4}S_{4,y}+\frac{H_4+H_3+H_7+H_8}{4}S_{4,z}\right)$$
$$+\frac{F_1+F_2+F_3+F_4}{4}S_{5,x}+\frac{G_1+G_2+G_3+G_4}{4}S_{5,y}+\frac{H_1+H_2+H_3+H_4}{4}S_{5,z}$$
$$\left.-\left(\frac{F_5+F_6+F_7+F_8}{4}S_{6,x}+\frac{G_5+G_6+G_7+G_8}{4}S_{6,y}+\frac{H_5+H_6+H_7+H_8}{4}S_{6,z}\right)\right\}$$

(3.19)

Calculation of the first order inviscid changes is thus completed. Before plunging into the calculation procedure for the viscous change term, it should once again be noted that the necessary integration will be carried out on the portion of the transformed control volume remaining in cell I, which is the volume 1abcdefg. Thereby, the viscous terms are averaged over a cell and defined at the cell center. The surface area that is to be used for the surface integration will be taken as the part of the face of the transformed control volume abcdefgh, which lies in the cell I. This approximately amount to one fourth of the area of cell I at the cell center for random cells. (It exactly amounts to one-fourth, for perfectly rectangular cells) For this integration, three surface vectors A_1, A_2, A_3 are used as shown in Figure 3.4. The calculation of these vectors is discussed in Appendix A. So now, ΔU_v can be written as

$$\Delta U_v = \frac{\Delta t}{4\Delta \forall_I}\left\{F_v\left(A_{1x}+A_{2x}+A_{3x}\right)+G_v\left(A_{1y}+A_{2y}+A_{3y}\right)+H_v\left(A_{1z}+A_{2z}+A_{3z}\right)\right\}$$

(3.20)

Introduce the following notation into Equation (3.20)

$$\Delta f_v = F_v \cdot A_{1x} + G_v \cdot A_{1y} + H_v \cdot A_{1z} \tag{3.21a}$$

$$\Delta g_v = F_v \cdot A_{2x} + G_v \cdot A_{2y} + H_v \cdot A_{2z} \tag{3.21b}$$

$$\Delta h_v = F_v \cdot A_{3x} + G_v \cdot A_{3y} + H_v \cdot A_{3z} \tag{3.21c}$$

to obtain

$$\Delta U_v = \frac{\Delta t}{4\Delta \forall_I}\left(\Delta f_v + \Delta g_v + \Delta h_v\right) \tag{3.22}$$

Here, it should be noted that F_v, G_v and H_v are calculated separately for each node of the cell. This calculation procedure will be explained later in this chapter. Now the calculation of viscous terms is thus completed.

The second-order inviscid flux terms can be evaluated in a similar way as the viscous flux terms as

$$\begin{aligned}\Delta^2 U_i = -\frac{\Delta t}{2\Delta \forall_I}\frac{1}{4}\{&\Delta F\left(A_{1x} + A_{2x} + A_{3x}\right)\\ &+\Delta G\left(A_{1y} + A_{2y} + A_{3y}\right)\\ &+\Delta H\left(A_{1z} + A_{2z} + A_{3z}\right)\ \}\end{aligned} \tag{3.23}$$

with the following notation

$$\Delta f_i = \Delta F \cdot A_{1x} + \Delta G \cdot A_{1y} + \Delta H \cdot A_{1z} \tag{3.24a}$$

$$\Delta g_i = \Delta F \cdot A_{2x} + \Delta G \cdot A_{2y} + \Delta H \cdot A_{2z} \tag{3.24b}$$

$$\Delta h_i = \Delta F \cdot A_{3x} + \Delta G \cdot A_{3y} + \Delta H \cdot A_{3z} \tag{3.24c}$$

Substitute Equation (3.24) into Equation (3.23) to get

$$\Delta^2 U_i = \frac{1}{8}\frac{\Delta t}{\Delta \forall_{\mathrm{I}}}\left(-\Delta f_i - \Delta g_i - \Delta h_i\right) \tag{3.25}$$

This completes the calculation of the second order inviscid terms. Now, considering the first and second order source terms in Equation (3.15) as

$$\Delta U_s = \frac{\Delta t}{\Delta \forall_I}\int_{cell-1}\left(S d\forall\right) \tag{3.26}$$

ΔU_s is formulated by carrying out the integral in the primary control volume. Thus,

$$\Delta U_s = \frac{\Delta t}{\Delta \forall_I} S_{center}\,\Delta \forall_I = \Delta t S_{center} \tag{3.27}$$

Here note that S_{center} is not the average of eight nodes over the cell. That is $S_{\mathrm{center}} \neq \frac{1}{8}\sum_{i=1}^{8} S_i$. The conservative variables are first averaged over a cell and it is followed by a cell-based evaluation of all source terms.

Thus, summing up all the terms formulated up to now, the formulation for total changes of each node that forms cell-I becomes

$$\delta U_{1I} = \frac{1}{8}\left\{\Delta U_i + \frac{\Delta t}{\Delta \forall_I}\left(\left(-\Delta f_i - \Delta g_i - \Delta h_i\right) - 2\left(-\Delta f_v - \Delta g_v - \Delta h_v\right) + \Delta \forall_I S_{center}\right)\right\} \tag{3.28a}$$

$$\delta U_{2I} = \frac{1}{8}\left\{\Delta U_i + \frac{\Delta t}{\Delta \forall_I}\left(\left(+\Delta f_i - \Delta g_i - \Delta h_i\right) - 2\left(+\Delta f_v - \Delta g_v - \Delta h_v\right) + \Delta \forall_I S_{center}\right)\right\} \tag{3.28b}$$

$$\delta U_{3I} = \frac{1}{8}\left\{\Delta U_i + \frac{\Delta t}{\Delta \forall_I}\left(\left(+\Delta f_i + \Delta g_i - \Delta h_i\right) - 2\left(+\Delta f_v + \Delta g_v - \Delta h_v\right) + \Delta \forall_I S_{center}\right)\right\} \tag{3.28c}$$

$$\delta U_{4I} = \frac{1}{8}\left\{\Delta U_i + \frac{\Delta t}{\Delta \forall_I}\left(\left(-\Delta f_i + \Delta g_i - \Delta h_i\right) - 2\left(-\Delta f_v + \Delta g_v - \Delta h_v\right) + \Delta \forall_I S_{center}\right)\right\} \quad (3.28d)$$

$$\delta U_{5I} = \frac{1}{8}\left\{\Delta U_i + \frac{\Delta t}{\Delta \forall_I}\left(\left(-\Delta f_i - \Delta g_i + \Delta h_i\right) - 2\left(-\Delta f_v - \Delta g_v + \Delta h_v\right) + \Delta \forall_I S_{center}\right)\right\} \quad (3.28e)$$

$$\delta U_{6I} = \frac{1}{8}\left\{\Delta U_i + \frac{\Delta t}{\Delta \forall_I}\left(\left(+\Delta f_i - \Delta g_i + \Delta h_i\right) - 2\left(+\Delta f_v - \Delta g_v + \Delta h_v\right) + \Delta \forall_I S_{center}\right)\right\} \quad (3.28f)$$

$$\delta U_{7I} = \frac{1}{8}\left\{\Delta U_i + \frac{\Delta t}{\Delta \forall_I}\left(\left(+\Delta f_i + \Delta g_i + \Delta h_i\right) - 2\left(+\Delta f_v + \Delta g_v + \Delta h_v\right) + \Delta \forall_I S_{center}\right)\right\} \quad (3.28g)$$

$$\delta U_{8I} = \frac{1}{8}\left\{\Delta U_i + \frac{\Delta t}{\Delta \forall_I}\left(\left(-\Delta f_i + \Delta g_i + \Delta h_i\right) - 2\left(-\Delta f_v + \Delta g_v + \Delta h_v\right) + \Delta \forall_I S_{center}\right)\right\} \quad (3.28h)$$

The above formulas are called the "distribution" formulas, as stated by Ni [13].

After the calculation of the change for each cell (here for cell I) and its distribution to its corresponding nodes, the conservative variables can be updated at every node of the cell as follows:

$$U_i^{n+1} = U_i^n + \delta U_{iI} \quad (3.29)$$

where the subscript i=1,2,...,8 .

3.2. CALCULATION OF VISCOUS AND HEAT CONDUCTION TERMS

The terms containing a derivative of a conservative variable written in Cartesian coordinate system (x, y, z) can be transformed into curvilinear coordinates (ξ, η, ζ) for any conservative variable U.

$$(x, y, z) \rightarrow (\xi, \eta, \zeta)$$

Where

$$\begin{aligned} \xi &= \xi(x, y, z) \\ \eta &= \eta(x, y, z) \\ \zeta &= \zeta(x, y, z), \end{aligned} \tag{3.30}$$

Using the chain rule, the transformation of derivatives in Cartesian coordinates to the ones in curvilinear (local) coordinates can be written as:

$$\begin{bmatrix} \frac{\partial}{\partial x} \\ \frac{\partial}{\partial y} \\ \frac{\partial}{\partial z} \end{bmatrix} = \begin{bmatrix} \frac{\partial \xi}{\partial x} & \frac{\partial \eta}{\partial x} & \frac{\partial \zeta}{\partial x} \\ \frac{\partial \xi}{\partial y} & \frac{\partial \eta}{\partial y} & \frac{\partial \zeta}{\partial y} \\ \frac{\partial \xi}{\partial z} & \frac{\partial \eta}{\partial z} & \frac{\partial \zeta}{\partial z} \end{bmatrix} \begin{bmatrix} \frac{\partial}{\partial \xi} \\ \frac{\partial}{\partial \eta} \\ \frac{\partial}{\partial \zeta} \end{bmatrix} \tag{3.31}$$

The Jacobian of transformation can be written as

$$J = \frac{\partial(\xi, \eta, \zeta)}{\partial(x, y, z)} = \frac{1}{\frac{\partial x}{\partial \xi}\left(\frac{\partial y}{\partial \eta}\frac{\partial z}{\partial \zeta} - \frac{\partial y}{\partial \zeta}\frac{\partial z}{\partial \eta}\right) - \frac{\partial x}{\partial \eta}\left(\frac{\partial y}{\partial \xi}\frac{\partial z}{\partial \zeta} - \frac{\partial y}{\partial \zeta}\frac{\partial z}{\partial \xi}\right) + \frac{\partial x}{\partial \zeta}\left(\frac{\partial y}{\partial \xi}\frac{\partial z}{\partial \eta} - \frac{\partial y}{\partial \eta}\frac{\partial z}{\partial \xi}\right)} \tag{3.32}$$

and the equations for the metric terms in the Jacobian matrix are

$$\frac{\partial \xi}{\partial x} = J\left(\frac{\partial y}{\partial \eta}\frac{\partial z}{\partial \zeta} - \frac{\partial y}{\partial \zeta}\frac{\partial z}{\partial \eta}\right) \tag{3.33a}$$

$$\frac{\partial \xi}{\partial y} = J\left(\frac{\partial x}{\partial \zeta}\frac{\partial z}{\partial \eta} - \frac{\partial x}{\partial \eta}\frac{\partial z}{\partial \zeta}\right) \tag{3.33b}$$

$$\frac{\partial \xi}{\partial z} = J\left(\frac{\partial x}{\partial \eta}\frac{\partial y}{\partial \zeta} - \frac{\partial x}{\partial \zeta}\frac{\partial y}{\partial \eta}\right) \tag{3.33c}$$

$$\frac{\partial \eta}{\partial x} = J\left(\frac{\partial y}{\partial \zeta}\frac{\partial z}{\partial \xi} - \frac{\partial y}{\partial \xi}\frac{\partial z}{\partial \zeta}\right) \tag{3.33d}$$

$$\frac{\partial \eta}{\partial y} = J\left(\frac{\partial x}{\partial \xi}\frac{\partial z}{\partial \zeta} - \frac{\partial x}{\partial \zeta}\frac{\partial z}{\partial \xi}\right) \tag{3.33e}$$

$$\frac{\partial \eta}{\partial z} = J\left(\frac{\partial x}{\partial \zeta}\frac{\partial y}{\partial \xi} - \frac{\partial x}{\partial \xi}\frac{\partial y}{\partial \zeta}\right) \tag{3.33f}$$

$$\frac{\partial \zeta}{\partial x} = J\left(\frac{\partial y}{\partial \xi}\frac{\partial z}{\partial \eta} - \frac{\partial y}{\partial \eta}\frac{\partial z}{\partial \zeta}\right) \tag{3.33g}$$

$$\frac{\partial \zeta}{\partial y} = J\left(\frac{\partial x}{\partial \eta}\frac{\partial z}{\partial \xi} - \frac{\partial x}{\partial \xi}\frac{\partial z}{\partial \eta}\right) \tag{3.33h}$$

$$\frac{\partial \zeta}{\partial z} = J\left(\frac{\partial x}{\partial \xi}\frac{\partial y}{\partial \eta} - \frac{\partial x}{\partial \eta}\frac{\partial y}{\partial \zeta}\right) \tag{3.33i}$$

Now, the shear stresses can be expressed in terms of gradients in curvilinear coordinates as follows

$$\tau_{xx} = \mu\left(\frac{4}{3}\left(\frac{\partial\xi}{\partial x}\frac{\partial u}{\partial\xi}+\frac{\partial\eta}{\partial x}\frac{\partial u}{\partial\eta}+\frac{\partial\zeta}{\partial x}\frac{\partial u}{\partial\zeta}\right)\right.$$
$$\left.-\frac{2}{3}\left(\left(\frac{\partial\xi}{\partial y}\frac{\partial v}{\partial\xi}+\frac{\partial\eta}{\partial y}\frac{\partial v}{\partial\eta}+\frac{\partial\zeta}{\partial y}\frac{\partial v}{\partial\zeta}\right)+\left(\frac{\partial\xi}{\partial z}\frac{\partial w}{\partial\xi}+\frac{\partial\eta}{\partial z}\frac{\partial w}{\partial\eta}+\frac{\partial\zeta}{\partial z}\frac{\partial w}{\partial\zeta}\right)\right)\right) \tag{3.34a}$$

$$\tau_{yy} = \mu\left(\frac{4}{3}\left(\frac{\partial\xi}{\partial y}\frac{\partial v}{\partial\xi}+\frac{\partial\eta}{\partial y}\frac{\partial v}{\partial\eta}+\frac{\partial\zeta}{\partial y}\frac{\partial v}{\partial\zeta}\right)\right.$$
$$\left.-\frac{2}{3}\left(\left(\frac{\partial\xi}{\partial x}\frac{\partial u}{\partial\xi}+\frac{\partial\eta}{\partial x}\frac{\partial u}{\partial\eta}+\frac{\partial\zeta}{\partial x}\frac{\partial u}{\partial\zeta}\right)+\left(\frac{\partial\xi}{\partial z}\frac{\partial w}{\partial\xi}+\frac{\partial\eta}{\partial z}\frac{\partial w}{\partial\eta}+\frac{\partial\zeta}{\partial z}\frac{\partial w}{\partial\zeta}\right)\right)\right) \tag{3.34b}$$

$$\tau_{zz} = \mu\left(\frac{4}{3}\left(\frac{\partial\xi}{\partial z}\frac{\partial w}{\partial\xi}+\frac{\partial\eta}{\partial z}\frac{\partial w}{\partial\eta}+\frac{\partial\zeta}{\partial z}\frac{\partial w}{\partial\zeta}\right)\right.$$
$$\left.-\frac{2}{3}\left(\left(\frac{\partial\xi}{\partial x}\frac{\partial u}{\partial\xi}+\frac{\partial\eta}{\partial x}\frac{\partial u}{\partial\eta}+\frac{\partial\zeta}{\partial x}\frac{\partial u}{\partial\zeta}\right)+\left(\frac{\partial\xi}{\partial y}\frac{\partial v}{\partial\xi}+\frac{\partial\eta}{\partial y}\frac{\partial v}{\partial\eta}+\frac{\partial\zeta}{\partial y}\frac{\partial v}{\partial\zeta}\right)\right)\right) \tag{3.34c}$$

$$\tau_{yz} = \mu\left(\left(\frac{\partial\xi}{\partial z}\frac{\partial w}{\partial\xi}+\frac{\partial\eta}{\partial z}\frac{\partial w}{\partial\eta}+\frac{\partial\zeta}{\partial z}\frac{\partial w}{\partial\zeta}\right)+\left(\frac{\partial\xi}{\partial y}\frac{\partial v}{\partial\xi}+\frac{\partial\eta}{\partial y}\frac{\partial v}{\partial\eta}+\frac{\partial\zeta}{\partial y}\frac{\partial v}{\partial\zeta}\right)\right) \tag{3.34d}$$

$$\tau_{xz} = \mu\left(\left(\frac{\partial\xi}{\partial z}\frac{\partial w}{\partial\xi}+\frac{\partial\eta}{\partial z}\frac{\partial w}{\partial\eta}+\frac{\partial\zeta}{\partial z}\frac{\partial w}{\partial\zeta}\right)+\left(\frac{\partial\xi}{\partial x}\frac{\partial u}{\partial\xi}+\frac{\partial\eta}{\partial x}\frac{\partial u}{\partial\eta}+\frac{\partial\zeta}{\partial x}\frac{\partial u}{\partial\zeta}\right)\right) \tag{3.34e}$$

$$\tau_{xy} = \mu\left(\left(\frac{\partial\xi}{\partial y}\frac{\partial v}{\partial\xi}+\frac{\partial\eta}{\partial y}\frac{\partial v}{\partial\eta}+\frac{\partial\zeta}{\partial y}\frac{\partial v}{\partial\zeta}\right)+\left(\frac{\partial\xi}{\partial x}\frac{\partial u}{\partial\xi}+\frac{\partial\eta}{\partial x}\frac{\partial u}{\partial\eta}+\frac{\partial\zeta}{\partial x}\frac{\partial u}{\partial\zeta}\right)\right) \tag{3.34f}$$

and the heat flux equations can be expressed as

$$q_x = -\left(\frac{\mu}{\mathrm{Pr}}\right)\frac{1}{(\gamma-1)}\left(\frac{\partial\xi}{\partial x}\frac{\partial T}{\partial\xi}+\frac{\partial\eta}{\partial x}\frac{\partial T}{\partial\eta}+\frac{\partial\zeta}{\partial x}\frac{\partial T}{\partial\zeta}\right) \tag{3.35a}$$

$$q_y = -\left(\frac{\mu}{\mathrm{Pr}}\right)\frac{1}{(\gamma-1)}\left(\frac{\partial\xi}{\partial y}\frac{\partial T}{\partial\xi}+\frac{\partial\eta}{\partial y}\frac{\partial T}{\partial\eta}+\frac{\partial\zeta}{\partial y}\frac{\partial T}{\partial\zeta}\right) \tag{3.35b}$$

$$q_z = -\left(\frac{\mu}{\mathrm{Pr}}\right)\frac{1}{(\gamma-1)}\left(\frac{\partial\xi}{\partial z}\frac{\partial T}{\partial\xi}+\frac{\partial\eta}{\partial z}\frac{\partial T}{\partial\eta}+\frac{\partial\zeta}{\partial z}\frac{\partial T}{\partial\zeta}\right) \tag{3.35c}$$

Ni [13] suggested that, first order finite difference approximation to the above derivatives can be formulated in each cell separately for each node as follows:

Let Q denote any conservative variable or, a Cartesian coordinate *x*, *y*, or *z*. Then for node 1 in cell I, shown in Figure 3.1, one can write the expressions for $\left(\frac{\partial Q}{\partial\xi}\right)_1$, $\left(\frac{\partial Q}{\partial\eta}\right)_1$ *and* $\left(\frac{\partial Q}{\partial\zeta}\right)_1$ as follows:

$$\left(\frac{\partial Q}{\partial\xi}\right)_1 \cong \frac{\Delta Q}{\Delta\xi} = \frac{Q_2 - Q_1}{\xi_2 - \xi_1} = \frac{Q_2 - Q_1}{\Delta\xi} = Q_2 - Q_1 \tag{3.36a}$$

$$\left(\frac{\partial Q}{\partial\eta}\right)_1 \cong \frac{\Delta Q}{\Delta\eta} = \frac{Q_4 - Q_1}{\eta_4 - \eta_1} = \frac{Q_4 - Q_1}{\Delta\eta} = Q_4 - Q_1 \tag{3.36b}$$

$$\left(\frac{\partial Q}{\partial\zeta}\right)_1 \cong \frac{\Delta Q}{\Delta\zeta} = \frac{Q_5 - Q_1}{\zeta_5 - \zeta_1} = \frac{Q_5 - Q_1}{\Delta\zeta} = Q_5 - Q_1 \tag{3.36c}$$

The derivatives for the other nodes can be handled in a similar way: The idea is to remain in the cell, and use either a forward or a backward difference, whichever appropriate.

3.3. ARTIFICIAL SMOOTHING

The one-step, second-order Lax-Wendroff scheme operates satisfactorily in the regions where the variation of the properties is smooth. In such regions, stability can be preserved if a fine mesh is used together with the help physical diffusion inherent in the scheme. However, the scheme has a major drawback that it causes

oscillations around discontinuities, i.e. around a shock wave or in the boundary layer. So, artificial smoothing terms must be introduced, to damp those oscillations.

These terms don't have much effect on the final converged solution, since they almost converge to zero, as the solution converges. Admittedly, they introduce some error in the calculations. However they are necessary for the convergence of the solution and assure stability around discontinuities (i.e. a shock wave), suppressing the oscillations in those regions. It should here be noted that, in spite of its second order accuracy and simplicity, Lax-Wendroff scheme's behavior around discontinuities is not fully satisfactory, as stated by Hirsch [5].

Therefore, in this study, artificial smoothing terms are added to the distribution formulas, given by Equations 3.28a - 3.28h. The artificial smoothing is calculated for each node within a cell in two steps in the following way: First the second order smoothing term is calculated and then, the fourth order smoothing is applied to the second order smoothed term. The resulting formulation is added to the distribution formulas. In this study, the second order smoothing strategy is taken from Ni [11] whereas the fourth order smoothing is supplied by Tınaztepe [15]. They can be given as:

$$\delta^2 U_i = \sigma^2 \frac{\Delta t}{8\Delta V} \Delta A\left(\overline{U} - U_i\right) \tag{3.37a}$$

$$\delta^4 U_i = \sigma^4 \frac{\Delta t}{8\Delta V} \Delta A\left(\overline{\delta^2 U} - \delta^2 U_i\right) \tag{3.37b}$$

where the subscript i=1,2,...,8 denotes the node number of a cell and the over bar indicates the conservative variables averaged over the cell. A is the area at the cell center, given in Figure 3.4:

$$\Delta A = \sqrt{\left|\vec{A}_1\right|^2 + \left|\vec{A}_2\right|^2 + \left|\vec{A}_3\right|^2} \tag{3.38}$$

Also, σ^2 and σ^4 stand for the second and fourth order artificial smoothing coefficients, respectively. σ^4 is taken as 1/32 of σ^2 and σ^2 should be chosen to be smaller than 0.1 as given in Tınaztepe [15].

Near solid boundaries, the viscous fluxes in the momentum equations are quite large and adequate to provide smoothing [9]. Hence, in these regions, the second and fourth order smoothing terms can introduce unwanted errors to the solution, giving rise to very large nonphysical values of total dissipation in the near-wall regions.

So, to account for this fact, a local Mach number scaling can be utilized, to decrease the level of artificial smoothing near walls where the flow slows down, as given by Tınaztepe[15]

$$\left(\sigma^2\right)_{scaled} = \left(\frac{M}{M_\infty}\right)^2 \sigma^2 \tag{3.39}$$

Now, the total change of a node can be written as

$$\delta U_i = \delta U_i + \delta^2 U_i + \delta^4 U_i \tag{3.40}$$

where i=1,2,...,8

3.4. TIME STEPPING CONTROL

The Lax-Wendroff scheme is an explicit scheme, which marches in time; In all explicit methods, a limit must be prescribed for the time step at every iteration, otherwise the stability of the method will be endangered. This limit is superimposed on the time step Δt by the CFL condition [16].

In this study, Ni's [9] formulation is used to restrict the time step for the solution of the Navier-Stokes equations. This formulation is also used by El Khoury [9], which can be given as

$$\Delta t = CFL \cdot min\left[\frac{\left|\vec{L}_x\right|}{\left|V \cdot \vec{l}\right| + c + \frac{2\mu}{\left|\vec{L}_x\right|}}, \quad \frac{\left|\vec{L}_y\right|}{\left|V \cdot \vec{l}\right| + c + \frac{2\mu}{\left|\vec{L}_y\right|}}, \quad \frac{\left|\vec{L}_z\right|}{\left|V \cdot \vec{l}\right| + c + \frac{2\mu}{\left|\vec{L}_z\right|}} \right] \tag{3.41}$$

where $\vec{L}$ is the displacement vector crossing the cell in the streamwise direction and $\vec{l}$ is a unit vector in the direction $\vec{L}$. c is the local speed of sound in the cell and μ is taken as the laminar viscosity for this study.

$\vec{L}$ can be expressed in the *x, y* and *z* directions, as follows [9]:

in *x*-direction

$$\begin{aligned} \vec{L}_x = \Bigg\{ & \left[\frac{1}{4}\left(x_2 + x_3 + x_6 + x_7\right) - \frac{1}{4}\left(x_1 + x_4 + x_5 + x_8\right) \right] \vec{i} \\ & + \left[\frac{1}{4}\left(y_2 + y_3 + y_6 + y_7\right) - \frac{1}{4}\left(y_1 + y_4 + y_5 + y_8\right) \right] \vec{j} \\ & + \left[\frac{1}{4}\left(z_2 + z_3 + z_6 + z_7\right) - \frac{1}{4}\left(z_1 + z_4 + z_5 + z_8\right) \right] \vec{k} \Bigg\} \end{aligned} \tag{3.42a}$$

in *y*-direction

$$\begin{aligned} \vec{L}_y = \Bigg\{ & \left[\frac{1}{4}\left(x_3 + x_4 + x_7 + x_8\right) - \frac{1}{4}\left(x_1 + x_2 + x_5 + x_6\right) \right] \vec{i} \\ & + \left[\frac{1}{4}\left(y_3 + y_4 + y_7 + y_8\right) - \frac{1}{4}\left(y_1 + y_2 + y_5 + y_6\right) \right] \vec{j} \\ & + \left[\frac{1}{4}\left(z_3 + z_4 + z_7 + z_8\right) - \frac{1}{4}\left(z_1 + z_2 + z_5 + z_6\right) \right] \vec{k} \Bigg\} \end{aligned} \tag{3.42b}$$

in z-direction

$$\vec{L}_z = \left\{ \left[\frac{1}{4}\left(x_5 + x_6 + x_7 + x_8\right) - \frac{1}{4}\left(x_1 + x_2 + x_3 + x_4\right) \right] \vec{i} \right.$$
$$+ \left[\frac{1}{4}\left(y_5 + y_6 + y_7 + y_8\right) - \frac{1}{4}\left(y_1 + y_2 + y_3 + y_4\right) \right] \vec{j} \qquad (3.42c)$$
$$\left. + \left[\frac{1}{4}\left(z_5 + z_6 + z_7 + z_8\right) - \frac{1}{4}\left(z_1 + z_2 + z_3 + z_4\right) \right] \vec{k} \right\}$$

For stability of the scheme, CFL number stays below 1.0 for every cell in the computational domain. Local time stepping control is employed, that is a different Δt value is imposed on each cell. All of the variables used in this method are taken as average values over a cell.

CHAPTER 4

INITIAL AND BOUNDARY CONDITIONS

In Chapters 2 and 3, the governing equations and their discretization technique are discussed. In this chapter, the initial and boundary conditions, which are necessary to obtain a solution out of these equations, will be explained.

Initial conditions are used to set up the initial flow field, which is a must for all time marching schemes like the one used in this study. On the other hand, boundary conditions are necessary to get a solution unique to the special flow domain of concern. Different types of boundary conditions are used in this study, including characteristic type boundary conditions.

4.1 INITIAL CONDITIONS

To start the iterative solution procedure, the flow domain should be initialized at all points of the computational domain. To achieve this, one should keep in mind the following criteria: the final converged solution should be independent of the initialization of the flow. In this study, initialization is done using the input Mach number and the direction cosines of the flow as follows:

$$U=\begin{bmatrix}\rho\\ \rho u\\ \rho v\\ \rho w\\ e\\ \rho k\\ \rho\varepsilon\end{bmatrix}=\begin{bmatrix}\rho_{total}\left(1+\frac{\gamma-1}{2}M_{far}^{2}\right)^{\frac{-1}{\gamma-1}}\\ \rho_{total}a_{total}\cos\alpha_1\left(1+\frac{\gamma-1}{2}M_{far}^{2}\right)^{\frac{-(\gamma-1)}{2(\gamma-1)}}\\ \rho_{total}a_{total}\cos\alpha_2\left(1+\frac{\gamma-1}{2}M_{far}^{2}\right)^{\frac{-(\gamma-1)}{2(\gamma-1)}}\\ \rho_{total}a_{total}\cos\alpha_3\left(1+\frac{\gamma-1}{2}M_{far}^{2}\right)^{\frac{-(\gamma-1)}{2(\gamma-1)}}\\ \left(\frac{p_{total}}{\gamma-1}+\frac{1}{2}\rho_{total}a_{total}^{2}M_{far}^{2}\right)\left(1+\frac{\gamma-1}{2}M_{far}^{2}\right)^{\frac{-\gamma}{2(\gamma-1)}}\\ \frac{(\rho u)^2}{\rho}K\\ \frac{(\rho u)^2}{\rho}K\end{bmatrix} \tag{4.1}$$

Here note that isentropic relations are also utilized. Also note that K stands for the free stream turbulence intensity, which has an empirically determined value ranging between 0.005 % and 1 %.

In this study, the free stream values of turbulence parameters, which are used to initialize the flow field, are taken as follows:

For *k*-ε turbulence closure,

$$k_\infty = 10^{-6}u_\infty$$

$$\varepsilon_\infty = 10^{-6}u_\infty \tag{4.2}$$

and for *k*- ω turbulence closure:

$$k_\infty = 10^{-6}$$

$$\omega_\infty = 5.0 \tag{4.3}$$

It is worth reminding here that the k value is taken to have a small value so as to guarantee that the freestream eddy viscosity is much smaller than the molecular viscosity. This is because, from mixing length hypothesis, turbulent kinetic energy is related to the turbulent eddy viscosity as follows:

$$\mu_{T\infty} \sim \rho k_{\infty}^{1/2} \ell \tag{4.4}$$

4.2 APPLICATION OF BOUNDARY CONDITIONS

The characteristic boundary conditions used in this study are formulated in a predictor-corrector form. The predictor step consists of the solution procedure for conservative variables at the boundary nodes carried out by the Lax-Wendroff scheme and the corrector step consists of the application of the characteristic boundary conditions to the boundary nodes.

Accordingly, the solution is updated as follows:

$$\delta U_{boundary} = U_{corrected} - U_{predicted} \tag{4.5}$$

where $U_{corrected}$ and $U_{predicted}$ stands for the corrected and predicted conservative variables respectively.

4.3 CHARACTERISTIC TYPE BOUNDARY CONDITIONS

To derive the characteristic type boundary conditions, the Euler equations are written in terms of primitive variables in the normal, tangential and binormal directions at a boundary as follows:

$$\frac{\partial \widetilde{U}}{\partial t} + \frac{\partial \widetilde{F}}{\partial n} + \frac{\partial \widetilde{G}}{\partial s} + \frac{\partial \widetilde{H}}{\partial b} = 0 \tag{4.6}$$

where *n*, *s* and *b* denotes the local coordinates in the normal, tangential and binormal directions, respectively. Since the variations assumed to be much larger in the normal direction than the other two, their derivatives can be dropped from the equation to get the following form

$$\frac{\partial \widetilde{U}}{\partial t} + \frac{\partial \widetilde{F}}{\partial n} = 0 \tag{4.7}$$

and in a quassi-linear form, it can be written as

$$\frac{\partial \widetilde{U}}{\partial t} + \widetilde{A}\frac{\partial \widetilde{U}}{\partial n} = 0 \tag{4.8}$$

where $\widetilde{U}$ and $\widetilde{A}$ represents the primitive vector variable and the Jacobian matrix respectively, which can be given as follows

$$\widetilde{U} = \begin{bmatrix} \rho \\ u_n \\ u_s \\ u_b \\ p \end{bmatrix} \tag{4.9}$$

and

$$\widetilde{A} = \begin{bmatrix} \overline{u}_n & \overline{\rho} & 0 & 0 & 0 \\ 0 & \overline{u}_n & 0 & 0 & \dfrac{1}{\overline{\rho}} \\ 0 & 0 & \overline{u}_n & 0 & 0 \\ 0 & 0 & 0 & \overline{u}_n & 0 \\ 0 & \overline{\rho c}^2 & 0 & 0 & \overline{u}_n \end{bmatrix} \tag{4.10}$$

where u_n, u_s and u_b correspond to normal, tangential and binormal velocity vector components and c represents the speed of sound. The barred quantities represent the averaged values and are taken as constants.

The Jacobian matrix can be diagonalized by performing a similarity transformation as follows:

$$L^{-1}\widetilde{A}\,L = \Lambda \tag{4.11}$$

where

$$L = \begin{bmatrix} 1 & 0 & 0 & \frac{\overline{\rho}}{2\overline{c}} & \frac{\overline{\rho}}{2\overline{c}} \\ 0 & 0 & 0 & \frac{1}{2} & -\frac{1}{2} \\ 0 & 0 & -1 & 0 & 0 \\ 0 & 1 & 0 & 0 & 0 \\ 0 & 0 & 0 & \frac{\overline{\rho}}{2\overline{c}} & \frac{\overline{\rho}}{2\overline{c}} \end{bmatrix} \tag{4.12a}$$

$$L^{-1} = \begin{bmatrix} 1 & 0 & 0 & 0 & \frac{-1}{\overline{c}^2} \\ 0 & 0 & 0 & 1 & 0 \\ 0 & 0 & -1 & 0 & 0 \\ 0 & 1 & 0 & 0 & \frac{1}{\overline{\rho c}} \\ 0 & -1 & 0 & 0 & \frac{1}{\overline{\rho c}} \end{bmatrix} \tag{4.12b}$$

and

$$\Lambda = \begin{bmatrix} \overline{u}_n & 0 & 0 & 0 & 0 \\ 0 & \overline{u}_n & 0 & 0 & 0 \\ 0 & 0 & \overline{u}_n & 0 & 0 \\ 0 & 0 & 0 & \overline{u}_n + \overline{c} & 0 \\ 0 & 0 & 0 & 0 & \overline{u}_n - \overline{c} \end{bmatrix} \tag{4.13a}$$

or

$$\Lambda = \begin{bmatrix} \lambda_1 & 0 & 0 & 0 & 0 \\ 0 & \lambda_2 & 0 & 0 & 0 \\ 0 & 0 & \lambda_3 & 0 & 0 \\ 0 & 0 & 0 & \lambda_4 & 0 \\ 0 & 0 & 0 & 0 & \lambda_5 \end{bmatrix} \tag{4.13b}$$

where $\lambda_1, \lambda_2, \lambda_3, \lambda_4, \lambda_5$ are called the eigenvalues of the Jacobian matrix $\widetilde{A}$. Equation (4.11) can be solved for the Jacobian matrix $\widetilde{A}$ to get:

$$\widetilde{A} = L\Lambda L^{-1} \tag{4.14}$$

Substitute Equation (4.14) into Equation (4.8), to get

$$\frac{\partial \widetilde{U}}{\partial t} + L\Lambda L^{-1} \frac{\partial \widetilde{U}}{\partial n} = 0 \tag{4.15}$$

Left multiplying Equation (4.8) by L^{-1} yields

$$L^{-1} \frac{\partial \widetilde{U}}{\partial t} + \Lambda L^{-1} \frac{\partial \widetilde{U}}{\partial n} = 0 \tag{4.16}$$

The characteristic vector variable, which stands for the perturbations in characteristic variables, is defined as follows:

$$\delta W = L^{-1} \delta \widetilde{U} \tag{4.17}$$

Now substituting Equation (4.17) into Equation (4.16), it is possible to obtain

$$\frac{\partial W}{\partial t} + \Lambda \frac{\partial W}{\partial n} = 0 \tag{4.18}$$

where W is the vector of linearized characteristic variables and written as follows:

$$W = \begin{bmatrix} \rho - \dfrac{p}{\bar{c}^2} \\ u_b \\ u_s \\ u_n + \dfrac{p}{\bar{c}^2} \\ -u_n + \dfrac{p}{\bar{c}^2} \end{bmatrix} \tag{4.19}$$

At this point it should be reminded that two kinds of boundary condition will be used: physical and numerical. Applying physical boundary condition means to impose the physical values of the characteristics at the boundary, which are generally the far field values. Applying numerical boundary condition means to impose the value of the characteristics coming from the interior of the domain calculated by the numerical method. The type of boundary condition to be applied is decided by the signs of the eigenvalues of the characteristics that depend on the Mach number of the flow at the boundary. Positive eigenvalues mean that characteristics enter the flow domain, whereas zero or negative values mean that the characteristics leave the domain.

Physical boundary conditions are imposed utilizing the fact that ideally the boundary conditions should not reflect the characteristics back into the flow domain. Therefore the so called “non-reflective” boundary conditions express the physical boundary conditions as the requirement that the local perturbations propagated along incoming characteristics must be made to vanish [15]. Thus,

$$\frac{\partial W}{\partial t} = 0 \tag{4.20}$$

or equivalently

$$\Lambda \frac{\partial W}{\partial n} = 0 \tag{4.21}$$

in a discretized form

$$\Delta W = 0 \tag{4.22}$$

4.3.1 Subsonic Inlet

For the case of subsonic inlet, $c > u_n > 0$ so the eigenvalues $\lambda_1, \lambda_2, \lambda_3, \lambda_4$ are positive and λ_5 is negative. This means that the fifth characteristic variable has to be determined from the interior domain and the other four physical boundary conditions are to be specified at the boundary. Therefore,

$$\Delta W_1 = 0 \Rightarrow \qquad \rho_{corrected} - \frac{p_{corrected}}{\overline{c}^2} = \rho_{far} - \frac{p_{far}}{\overline{c}^2} \tag{4.23a}$$

$$\Delta W_2 = 0 \Rightarrow \qquad u_{b,corrected} = u_{b,far} \tag{4.23b}$$

$$\Delta W_3 = 0 \Rightarrow \qquad u_{s,corrected} = u_{s,far} \tag{4.23c}$$

$$\Delta W_4 = 0 \Rightarrow \qquad u_{n,corrected} + \frac{p_{corrected}}{\overline{\rho c}} = u_{n,far} + \frac{p_{far}}{\overline{\rho c}} \tag{4.23d}$$

$$\Delta W_5 = 0 \Rightarrow \qquad -u_{n,corrected} + \frac{p_{corrected}}{\overline{\rho c}} = -u_{n,predicted} + \frac{p_{predicted}}{\overline{\rho c}} \tag{4.23e}$$

where the subscript *corrected* denotes the corrected value whereas the subscript *predicted* stands for the value predicted by Lax-Wendroff scheme. Solving the above set of equations for the corrected primitive variables to get

$$p_{corrected} = \frac{1}{2}\left[p_{far} + p_{predicted} + \overline{\rho c}\left(u_{n,far} - u_{n,predicted}\right)\right] \tag{4.24a}$$

$$\rho_{corrected} = \rho_{far} + \frac{p_{corrected} - p_{far}}{\overline{c}^2} \tag{4.24b}$$

$$u_{n,corrected} = u_{n,far} + \frac{p_{far} - p_{corrected}}{\overline{\rho c}} \tag{4.24c}$$

$$u_{s,corrected} = u_{s,far} \tag{4.24d}$$

$$u_{b,corrected} = u_{b,far} \tag{4.24e}$$

Finally, for the k-ε closure.

$$k = u^2 K \tag{4.25a}$$

and

$$\varepsilon = u^2 K \tag{4.25b}$$

and for the k-ω turbulent closure [21],

$$k = 10^{-6} \tag{4.26a}$$

and

$$\omega_\infty = \mathrm{O}\left(10\frac{U_\infty}{L}\right) \tag{4.26b}$$

Note that in the above equations, free stream values are used.

4.3.2 Supersonic Inlet

Since $u_n > c$, all the eigenvalues $\lambda_1, \lambda_2, \lambda_3$ in Equation (4.13) are positive. Resultantly, at the inlet, all the characteristic values are corrected using the free stream values. Thus,

$$\Delta W_1 = 0 \Rightarrow \qquad \rho_{corrected} - \frac{p_{corrected}}{\overline{c}^2} = \rho_{far} - \frac{p_{far}}{\overline{c}^2} \tag{4.27a}$$

$$\Delta W_2 = 0 \Rightarrow \qquad u_{b,corrected} = u_{b,far} \tag{4.27b}$$

$$\Delta W_3 = 0 \Rightarrow \qquad u_{s,corrected} = u_{s,far} \tag{4.27c}$$

$$\Delta W_4 = 0 \Rightarrow \qquad u_{n,corrected} + \frac{p_{corrected}}{\overline{\rho c}} = u_{n,far} + \frac{p_{far}}{\overline{\rho c}} \tag{4.27d}$$

$$\Delta W_5 = 0 \Rightarrow \qquad -u_{n,corrected} + \frac{p_{corrected}}{\overline{\rho c}} = -u_{n,far} + \frac{p_{far}}{\overline{\rho c}} \tag{4.27e}$$

Primitive variables can be solved for as follows:

$$p_{corrected} = p_{far} \tag{4.28a}$$

$$\rho_{corrected} = \rho_{far} \tag{4.28b}$$

$$u_{n,corrected} = u_{n,far} \tag{4.28c}$$

$$u_{s,corrected} = u_{s,far} \tag{4.28d}$$

$$u_{b,corrected} = u_{b,far} \tag{4.28e}$$

Finally, it should be noted that, the supersonic inlet boundary conditions used for the k-ε and k-ω closure are just the same as the ones in the subsonic case.

4.3.3 Subsonic Exit

For the case of subsonic outflow, $u_n < 0$ and $|u_n| < \bar{c}$. That's why, λ_4 becomes positive, and $\lambda_{1,}, \lambda_2, \lambda_3$ and λ_5 become negative. Hence at the exit, only one physical boundary condition will be imposed which corresponds to W_4. Therefore,

$$\Delta W_1 = 0 \Rightarrow \qquad \rho_{corrected} - \frac{p_{corrected}}{\bar{c}^2} = \rho_{predicted} - \frac{p_{predicted}}{\bar{c}^2} \tag{4.29a}$$

$$\Delta W_2 = 0 \Rightarrow \qquad u_{b,corrected} = u_{b,predicted} \tag{4.29b}$$

$$\Delta W_3 = 0 \Rightarrow \qquad u_{s,corrected} = u_{s,predicted} \tag{4.29c}$$

$$\Delta W_4 = 0 \Rightarrow \qquad u_{n,corrected} - \frac{p_{corrected}}{\overline{\rho c}} = u_{n,far} - \frac{p_{far}}{\overline{\rho c}} \tag{4.29d}$$

$$\Delta W_5 = 0 \Rightarrow \qquad -u_{n,corrected} + \frac{p_{corrected}}{\overline{\rho c}} = -u_{n,predicted} + \frac{p_{predicted}}{\overline{\rho c}} \tag{4.29e}$$

The above set of equations can be reduced to the following form:

$$p_{corrected} = p_{far} \tag{4.30a}$$

$$\rho_{corrected} = \rho_{predicted} + \frac{p_{corrected} - p_{predicted}}{\bar{c}^2} \tag{4.30b}$$

$$u_{n,corrected} = u_{n,predicted} + \frac{p_{corrected} - p_{predicted}}{\overline{\rho c}} \tag{4.30c}$$

$$u_{s,corrected} = u_{s,predicted} \tag{4.30d}$$

$$u_{b,corrected} = u_{b,predicted} \tag{4.30e}$$

Finally, at the exit, a first order extrapolation is used for the *k*-ε and *k*-ω turbulence closures, as follows:

$$U_{i,j} = 2\,U_{i+1,j} - U_{i+2,j} \tag{4.31}$$

where *U* stands for the conservative variables representing $\rho k, \rho\varepsilon,$ and $\rho\omega$.

4.3.4 Supersonic Exit

For the case of supersonic outflow, $u_n < 0$, therefore all the eigenvalues become negative. No physical boundary conditions are used; the values of the primitive variables are extrapolated from the inner flow domain. Therefore,

$$\Delta W_1 = 0 \Rightarrow \qquad \rho_{corrected} - \frac{p_{corrected}}{\bar{c}^2} = \rho_{predicted} - \frac{p_{predicted}}{\bar{c}^2} \tag{4.32a}$$

$$\Delta W_2 = 0 \Rightarrow \qquad u_{b,corrected} = u_{b,predicted} \tag{4.32b}$$

$$\Delta W_3 = 0 \Rightarrow \qquad u_{s,corrected} = u_{s,predicted} \tag{4.32c}$$

$$\Delta W_4 = 0 \Rightarrow \qquad u_{n,corrected} + \frac{p_{corrected}}{\overline{\rho c}} = u_{n,predicted} + \frac{p_{predicted}}{\overline{\rho c}} \tag{4.32d}$$

$$\Delta W_5 = 0 \Rightarrow \qquad -u_{n,corrected} + \frac{p_{corrected}}{\overline{\rho c}} = -u_{n,predicted} + \frac{p_{predicted}}{\overline{\rho c}} \tag{4.32e}$$

And for the corrected primitive variables one obtains

$$p_{corrected} = p_{far} \tag{4.33a}$$

$$\rho_{corrected} = \rho_{predicted} \tag{4.33b}$$

$$u_{n,corrected} = u_{n,predicted} \tag{4.33c}$$

$$u_{s,corrected} = u_{s,predicted} \tag{4.33d}$$

$$u_{b,corrected} = u_{b,predicted} \tag{4.33e}$$

For the two-equation turbulence closure, the same first order extrapolation procedure, carried out for the subsonic exit, is used.

4.4 SYMMETRY BOUNDARY CONDITION

The symmetry boundary condition asserts that, the flow velocity is tangent to the surface; thus, normal component of the velocity is set to zero on the boundary. $\lambda_1, \lambda_2, \lambda_3$ and λ_5 becomes negative, and λ_4 positive. Therefore,

$$\Delta W_1 = 0 \Rightarrow \qquad \rho_{corrected} - \frac{p_{corrected}}{\bar{c}^2} = \rho_{predicted} - \frac{p_{predicted}}{\bar{c}^2} \tag{4.34a}$$

$$\Delta W_2 = 0 \Rightarrow \qquad u_{b,corrected} = u_{b,predicteed} \tag{4.34b}$$

$$\Delta W_3 = 0 \Rightarrow \qquad u_{s,corrected} = u_{s,predicted} \tag{4.34c}$$

$$\Delta W_4 = 0 \Rightarrow \qquad u_{n,corrected} - \frac{p_{corrected}}{\overline{\rho c}} = u_{n,wall} - \frac{p_{wall}}{\overline{\rho c}} \tag{4.34d}$$

$$\Delta W_5 = 0 \Rightarrow \qquad -u_{n,corrected} + \frac{p_{corrected}}{\overline{\rho c}} = -u_{n,predicted} + \frac{p_{predicted}}{\overline{\rho c}} \tag{4.34e}$$

Keeping in mind that $u_{n,wall}$ is set to zero, one can obtain

$$u_{n,corrected} = u_{n,wall} = 0 \tag{4.35a}$$

$$u_{s,corrected} = u_{s,predicted} \tag{4.35b}$$

$$u_{b,corrected} = u_{b,predicted} \tag{4.35c}$$

$$p_{corrected} = p_{predicted} - \rho \bar{c} u_{n,predicted} \tag{4.35d}$$

$$\rho_{corrected} = \rho_{predicted} + \frac{p_{corrected} - p_{predicted}}{\bar{c}^2} \tag{4.35e}$$

and for the k-ε and k-ω turbulent closure, a first order extrapolation yields:

$$U_{i,j} = U_{i,j\pm1} \tag{4.36}$$

4.5 SOLID WALL BOUNDARY CONDITION

The action of attractive molecular forces between the flowing fluid and the solid wall boundary causes the fluid particles stick to the wall. Therefore, just on the solid wall boundary, it is assumed that the relative velocity between the fluid and the solid body becomes zero, preventing slip. Thus, this type of boundary condition is also called the no-slip boundary condition. Mathematically, it can be expressed as follows:

$$u = v = w = 0 \tag{4.37}$$

For the energy equation, the appropriate solid wall boundary condition would be either to specify the temperature or heat flux on the wall, that is,

$$T = T_{wall} \tag{4.38}$$

or

$$-k^{thermal}\frac{\partial T}{\partial n} = q_{wall} \tag{4.39}$$

In this study, adiabatic boundary condition is used, that is, heat flux on the wall is set to zero.

$$q_{wall} = 0 \tag{4.40}$$

or accordingly,

$$\frac{\partial T}{\partial n} = 0 \tag{4.41}$$

In the normal direction to the solid boundary, using boundary layer assumptions, *y*-momentum equation reduces to

$$\frac{\partial p}{\partial n} = 0 \tag{4.42}$$

For the k-ε equations solid wall boundary conditions are

$$k_{wall} = \varepsilon_{wall} = 0.0 \tag{4.43}$$

and for the k-ω turbulent closure,

$$k_{wall} = 0.0 \tag{4.44}$$

and for ω Wilcox [21] suggested that

$$\omega = \frac{2500\upsilon_{\omega}}{k_R^2} \tag{4.45}$$

where k_R is the average height of a sand-grain roughness element. k_R must be small enough to insure a correct skin friction distribution when applied to a smooth wall, otherwise the skin friction values will be larger than the correct values [9].

4.6 FAR FIELD BOUNDARY CONDITION

Ideally, at a farfield boundary, the propagating waves should neither be reflected nor emitted. Rather, by the action of viscosity, they should be dissipated. To implement such an ideal farfield condition means that the boundary should be placed sufficiently far, say 50-60 or sometimes 100 characteristic lengths away [15]. Then the implementation would become a simple matter, the free stream values could directly be specified at the boundary.

However, this kind of a method is practically inconvenient because it will necessitate the use of large number of grid points and result in a considerable increase of computational time.

A practical approach would be to put the farfield boundary closer, say 5 – 6 characteristic lengths away, but this time special corrections will be added to the free stream values [15].

In this study, the free stream values of primitive variables are directly imposed on the far field boundaries.

CHAPTER 5

RESULTS

To evaluate the performance of the turbulence models adapted into the Navier-Stokes solver, a case of two dimensional, subsonic, laminar - transition fixed - turbulent flow over a flat plate is chosen. This test case was also handled by several other researchers, like Jameson [20], El Khoury [11], Haliloğlu [16], Tınaztepe [15]. These researchers used a free stream Mach number of 0.3.

But before applying any turbulence models into the Navier-Stokes solver, it is first tested for a two dimensional laminar flow over a flat plate, with the same Mach number as the turbulent case, but with a different Reynolds number. The Reynolds number is chosen to keep the flow in the laminar regime. This case aims to validate the performance of the Navier-Stokes solver that the turbulence models will be included in.

A total number of five turbulence models are applied, and the computed results are compared with analytical and empirical results. These results include velocity, local skin friction distribution and boundary layer thickness plots, which are seen necessary to evaluate the performance of the computations. Residual histories are also included for further evaluation.

In addition to the results, grid properties, some basic issues of the numerical work and important pinpoints in model implementation are discussed.

5.1 GRID AND FLOW PROPERTIES

To verify the accuracy of the Navier-Stokes solver that the turbulence models will be based on, a two dimensional laminar flow with zero pressure gradient is considered. Mach number is set to be 0.3 as in the turbulent case, but the length of the flat plate is properly adjusted to keep the Reynolds number less than $5x10^5$, the widely accepted value for transition to turbulence. To adjust the length of the flat plate which is initially 1 meter (lying between $0 < x < 1$), the grid data is scaled with a factor of 0.005. This scaling reduces the flat plate length to 5 mm. Thus a maximum Reynolds number of $3.5x10^4$ could be obtained, and the flow could be kept in the pure laminar regime.

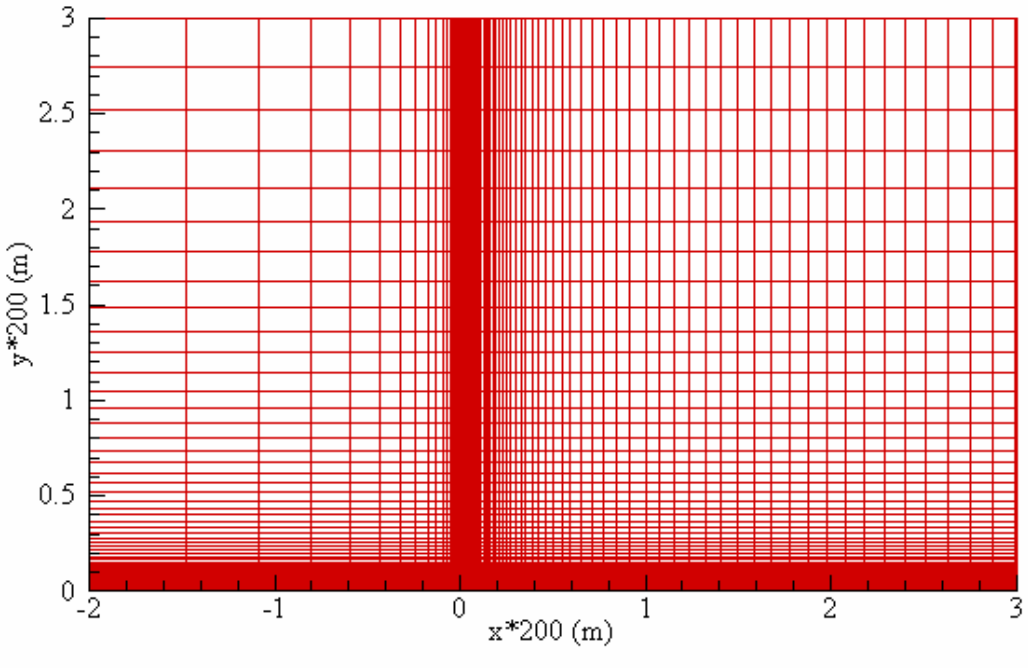

Figure 5.1 The grid used for the laminar flat plate problem (scaled).

The grid used for this case is shown with its scale indicated on the axis in Figure 5.1. It is basically a structured H-type grid formed of 121x81 grid points (9801 nodes, 9600 cells). This discretized domain has a length of 5 chords and a width of 3 chords. In this domain, in the horizontal direction, there are 30 nodes before the flat plate, 70 nodes on the flat plate and 21 nodes in the wake region. The

grid is clustered exponentially at the leading edge and over the flat plate, making minimum Δx and Δy equal to 0.00022 and 0.00025 of the chord length, respectively.

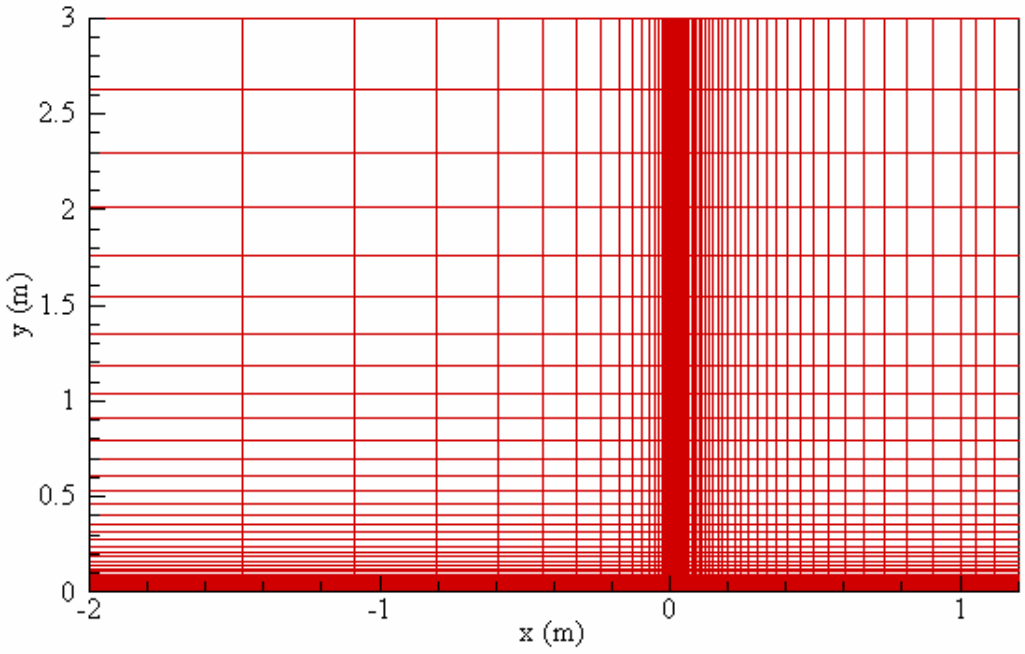

Figure 5.2 The first grid (grid-1) used for the turbulent flat plate problem.

Apart from the laminar flow case, two different grids are considered for the turbulent flow case. For both grids, flat plate lies at $0 < x < 1$, dimensions given in meters. The first grid used is shown in Figure 5.2. It has 121x81 grid points that are clustered at the leading edge and near the wall. There are 37 nodes upstream, 81 nodes on the flat plate and 3 nodes in the wake region. The grid is clustered such that minimum Δx and Δy are equal to 0.00004 and 0.000015, respectively. Clustering at the leading edge is done to ensure that there are enough grid points to capture the gradients of pressure and velocity along the x-direction which occur due to flow stagnation. In addition to this, transition occurs near the leading edge, therefore this clustering helps to capture the sudden changes in flow properties during transition. Along the normal direction to the plate, the turbulent velocity profiles are expected to be much steeper than they are for laminar flow. For this reason, the grid should be compressed more in the y-direction to capture property variations along the boundary layer correctly. Therefore during the grid generation, minimum value of Δy is

adjusted such that there is at least one grid line in the laminar sublayer. In other words, there is at least one grid point below $y^+ < 5$, keeping in mind the fact that the same y value above the flat plate can attain different y^+ values along the plate, depending on the value of the wall shear stress. Consequently, such a grid clustering along normal direction to the wall helps to increase the accuracy of calculations in the boundary layer.

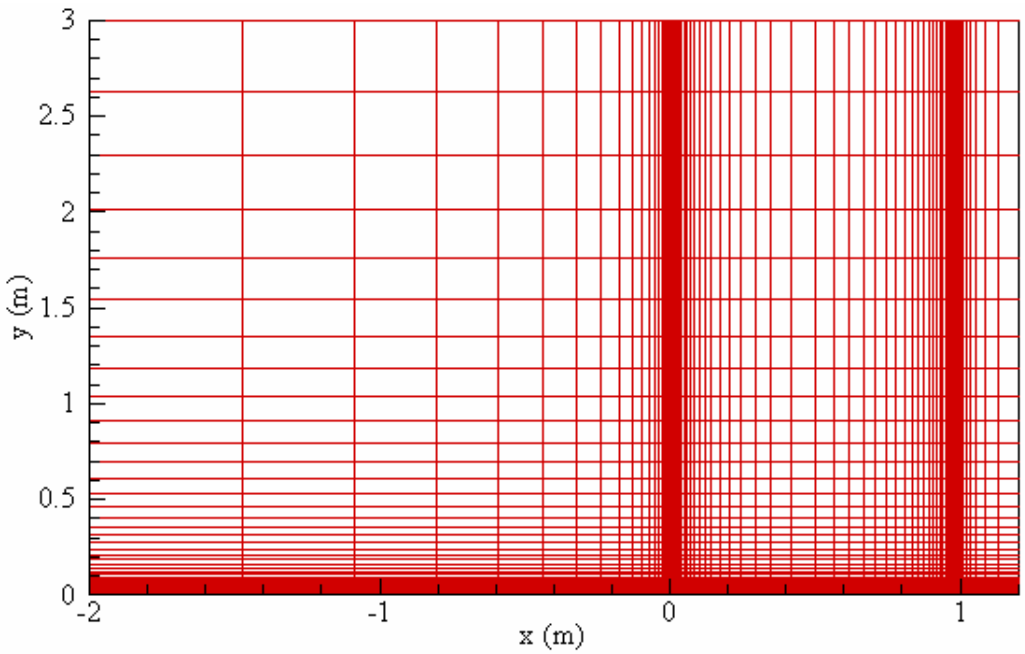

Figure 5.3 The second grid (grid-2) used for the turbulent flat plate problem.

The second grid used for the flat plate problem is shown in Figure 5.3. This grid have the same number of nodes, 121x81, but it is clustered at the trailing edge as well. Minimum Δy is set to be the same as it is in grid-1, but minimum Δx is now set to be 0.000032. In this grid, there are 37 nodes in the upstream region, 70 nodes on the flat plate, and 8 nodes in the wake region. It can be said that grid-2 is a more clustered version of grid-1 at the trailing edge. The other difference is that a few grid lines are transferred from the flat plate to the wake region. Again note that, for this grid, the flat plate lies at $0 < x < 1$, same as in grid-1.

For the turbulent case, the free stream Mach number of the air flow over the flat plate is 0.3, and the free stream Reynolds number based on the length of the flat plate corresponds to 6,000,000. In accordance with references [11],[15],[16] and [20], transition to turbulence is fixed at $X_{cr} = 0.054$, which corresponds to a Reynolds number of 324,000. Actually, fixing transition is setting an empirical x-value in the solver after which the turbulence models are coupled with the Navier-Stokes equations in the domain. Finally, it should once again be noted that the flows considered in this study have no streamwise pressure gradient and can be considered incompressible.

In this study, the initial flow properties are taken as:

i. $M_\infty = 0.3$, flow being in parallel direction to the flat plate (purely in x-direction),
ii. $(P_o)_\infty = 100{,}000$ Pa, for stagnation pressure,
iii. $(T_o)_\infty = 298$ K, for stagnation temperature.

Notice that, for two-equation models, initial values for turbulence parameters are given in Section 4.1. Boundary conditions for the turbulent case are set as follows:

i. For inlet and exit (inlet at $x = -2$, $0 < y < 3$ and exit at $x = 1.2$, $0 < y < 3$) characteristic boundary conditions are applied, as explained in Section 4.3.
ii. On the lower boundary along the regions excluding the flat plate (at $y = 0$, $-2 < x < 0$ and $1 < x < 1.2$), symmetry boundary condition is applied, as explained in Section 4.4.
iii. On the flat plate (at $y = 0$, $0 < x < 1$), no-slip boundary condition is applied, as explained in Section 4.5.
iv. Finally on the upper boundary (at $y = 3$, $-2 < x < 1.2$), free stream boundary condition is applied.

5.2 PERFORMANCE OF THE NAVIER-STOKES SOLVER

To test the performance of the Navier-Stokes solver, the velocity outputs - obtained along different vertical positions on the flat plate - are compared with Blasius similarity solution. The similarity variable η and non-dimensional velocity u^+ are defined as such:

$$\eta = \frac{y}{x}\sqrt{Re_x} \tag{5.1a}$$

$$u^+ = \frac{u}{U_\infty} \tag{5.1b}$$

Re_x is the Reynolds number at position x on the plate defined as

$$Re_x = \frac{\rho_\infty U_\infty x}{\mu_\infty} \tag{5.2}$$

Finally, the result for local skin friction coefficient is compared with the Blasius exact solution which is calculated to be

$$C_f = 0.664\left(Re_x\right)^{-0.5} \tag{5.3}$$

The results for skin friction distribution and tangential and normal velocities are presented in Figures 5.4, 5.5 and 5.6. Note that the velocity data is obtained at four different positions on the plate, and plotted on top of each other. After several runs for different grids, it has been observed that the slight deviation for skin friction result at the leading edge is due to grid clustering in the y direction, not due to the solver. This deviation could further be decreased by compressing the grid more along the horizontal direction.

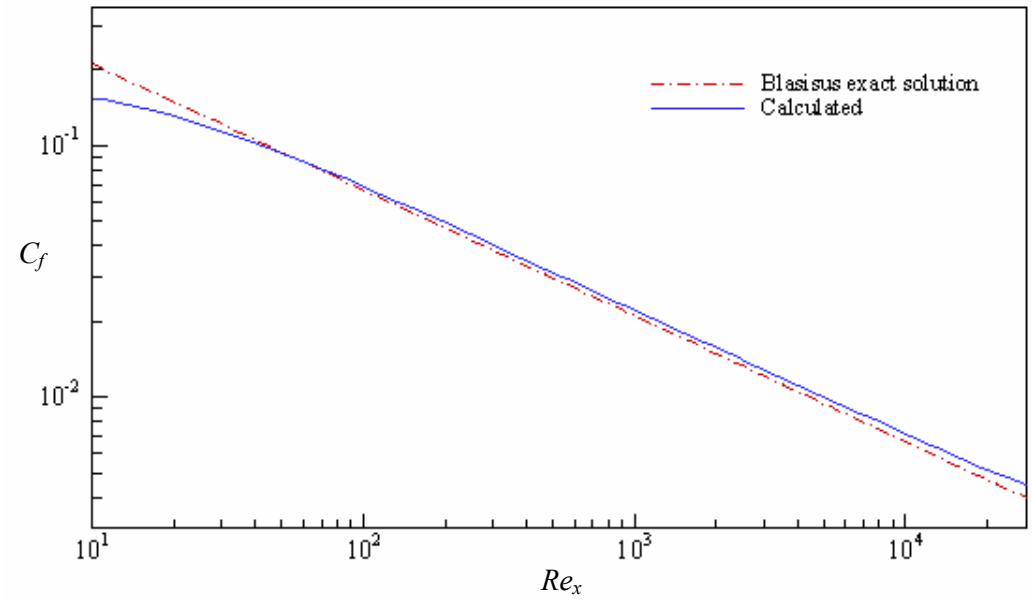

Figure 5.4 Local skin friction coefficient along the flat plate (Laminar Case).

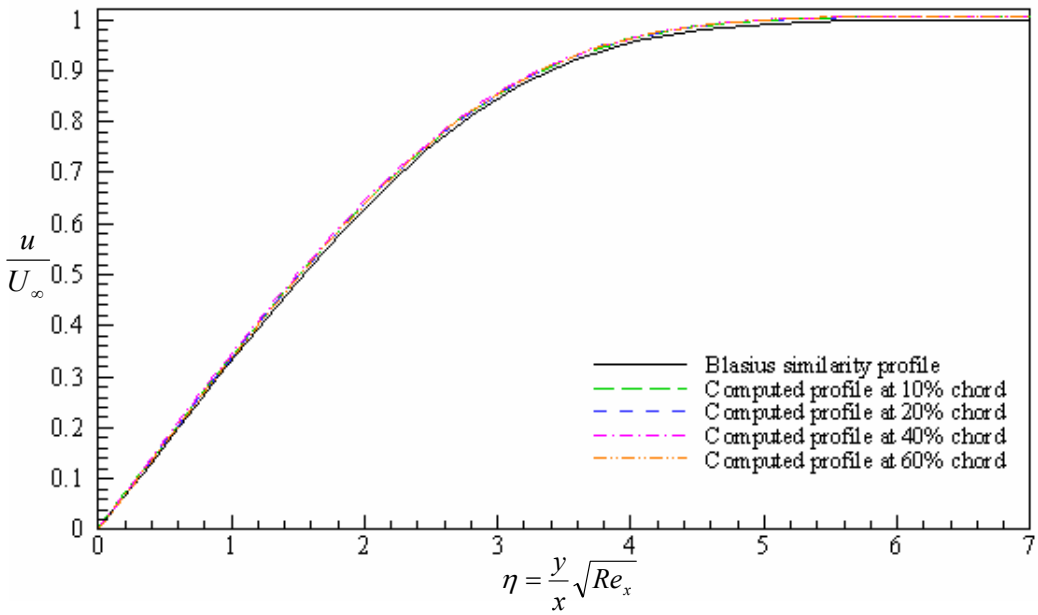

Figure 5.5 Non-dimensional tangential velocity profiles (Laminar Case).

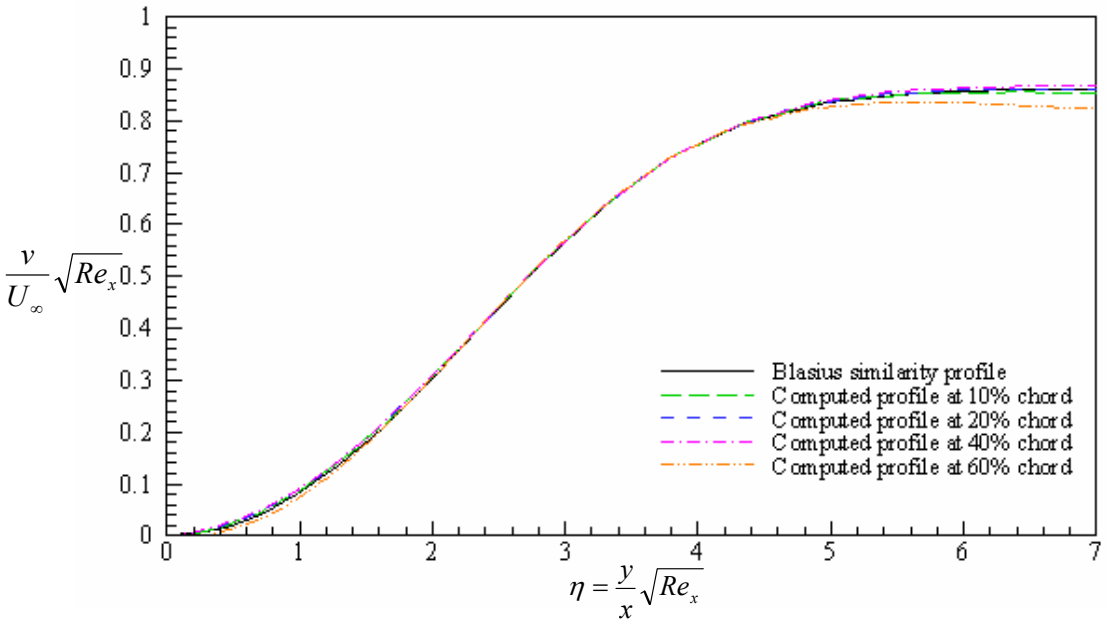

Figure 5.6 Non-dimensional normal velocity profiles (Laminar Case).

These plots validate the Navier-Stokes solver well enough to remove any doubt in mind about its performance for laminar flows. It is thus concluded that the considered turbulence models can be applied with enough comfort, and the accuracy of the Navier-Stokes formulation is acceptable for this purpose.

5.3 PERFORMANCE OF THE TURBULENCE MODELS

To evaluate the performance of the models, both empirical and analytical results have been employed. The calculated local skin friction coefficient and boundary layer thickness have been compared with Blasius exact and approximate solutions. Calculated turbulent velocity profiles have been compared with empirically obtained universal velocity distributions. As a summary, the analytical and empirical relations for the flat plate problem utilized in this study can be given as follows:

For local skin friction, Blasius exact solution for laminar regime is used, as given in Equation (5.3). For turbulent region Prandtl's 1/5 law is used, as given below:

$$C_f = 0.0592\left(Re_x\right)^{-0.2} \tag{5.4}$$

where Re_x is the Reynolds number based on distance from the leading edge, x, defined as in Equation (5.2) and C_f is the local skin friction coefficient given as,

$$C_f = \frac{\tau_w}{\frac{1}{2}\rho_\infty U_\infty{}^2} \tag{5.5}$$

noting that ρ_∞ and U_∞ are free stream values for density and velocity, and τ_w is the value of wall friction calculated locally on the flat plate.

For turbulent non-dimensional velocity profiles, the following generally accepted correlation [18], which is also plotted in linear-log scale in Figure 5.7, is used:

$$u^+ = \begin{cases} y^+ & , \quad 0 < y^+ < 5 \qquad (5.6a) \\ 5.0\,log(y^+) - 3.05, & 5 < y^+ < 30 \qquad (5.6b) \\ 2.5\,log(y^+) + 5.5 & , \quad 30 < y^+ \qquad (5.6c) \end{cases}$$

In the above correlation, y^+ is defined by Equation (2.18) and non-dimensional velocity u^+ can be given as,

$$u^+ = \frac{u}{u_\tau} \tag{5.6b}$$

where u_τ is the friction velocity defined by Equation (2.19). Here note that this definition of non-dimensional velocity is different than in Equation (5.1b).

For boundary layer thickness, the following analytical results are used:

$$\delta = 5.0\,x\left(Re_x\right)^{-0.5} \quad \text{- for laminar regime,} \tag{5.7a}$$

$$\delta = 0.2882\,x\left(Re_x\right)^{-0.2} \quad \text{- for turbulent regime.} \tag{5.7b}$$

Before evaluating the results, it must be noted that skin friction and velocity distributions are plotted on a log-log and linear-log scale respectively. (Velocity plots are in linear scale for u^+ and in logarithmic scale for the Reynolds number.)

Finally, it is worth mentioning that, for all algebraic models, the artificial dissipation coefficient is set to 0.001, similar to the original Navier-Stokes solver. Higher values are used for two-equation models. For all models, the CFL value is set to 0.5, and local time stepping technique is applied.

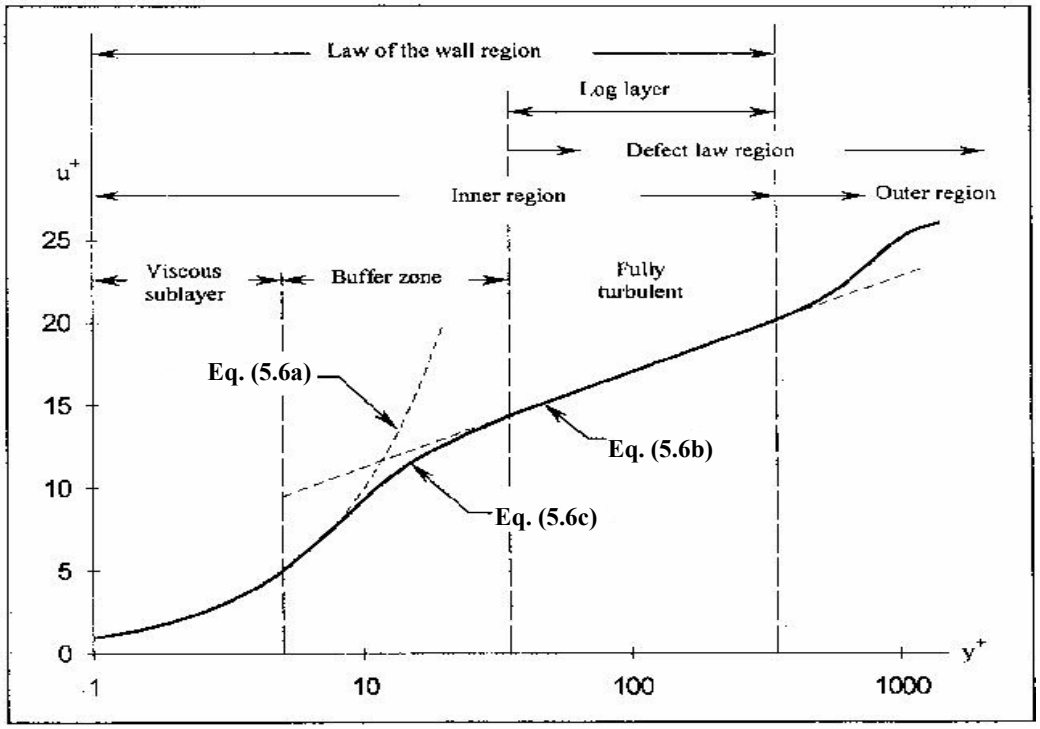

Figure 5.7 Non-dimensional velocity profile for an incompressible turbulent flow over a flat plate and identification of different regions within the turbulent boundary layer (Adapted from reference [18]).

5.2.1 Cebeci-Smith Model

This model is tested on grid-2. Clustering the grid at the trailing edge is preferred to prevent the under prediction of the skin friction result which was observed for grid-1. In other words, the skin friction result obtained by grid-2 was notably better than that obtained by grid-1.

The results of computations for Cebeci-Smith model are shown in Figure 5.8, Figure 5.9 and Figure 5.10. The local skin friction coefficient result is compared with Prandtl's 1/5 law, that is, with Equation (5.4). Note that the skin friction result for the turbulent part is slightly under predicted. Here it should once again be noted that, the skin friction distributions are plotted on a log-log scale and therefore, the curves in the turbulent zone are pushed to the trailing edge of the flat plate. In the linear graph, turbulent zone constitutes almost all the flat plate.

The deviation near the end of the boundary layer in the velocity plot, as seen in Figure 5.9 is expected. This is because, such a defect or deviation from the log-law in the outer region of the boundary layer is also observed in various experimental results in the literature and thus this region is given the name "defect layer" (see Figure 5.7). As its name implies, in this region, the actual velocity profile deviates from the logarithmic profile, so that there is a defect.

Boundary layer thickness calculation is necessary for the Cebeci-Smith model, in order to calculate velocity thickness. Velocity thickness data is then used to calculate the outer layer turbulent viscosity, as explained in Section 2.4.1. In this regard, boundary layer thickness calculation has an indirect effect on turbulence properties, entering directly into the formula for turbulent viscosity. Therefore, to ensure the accuracy of the computations, such a plot was seen to be necessary, and a small routine is developed and added to the code to get an output of the boundary layer thickness, as shown in Figure 5.10.

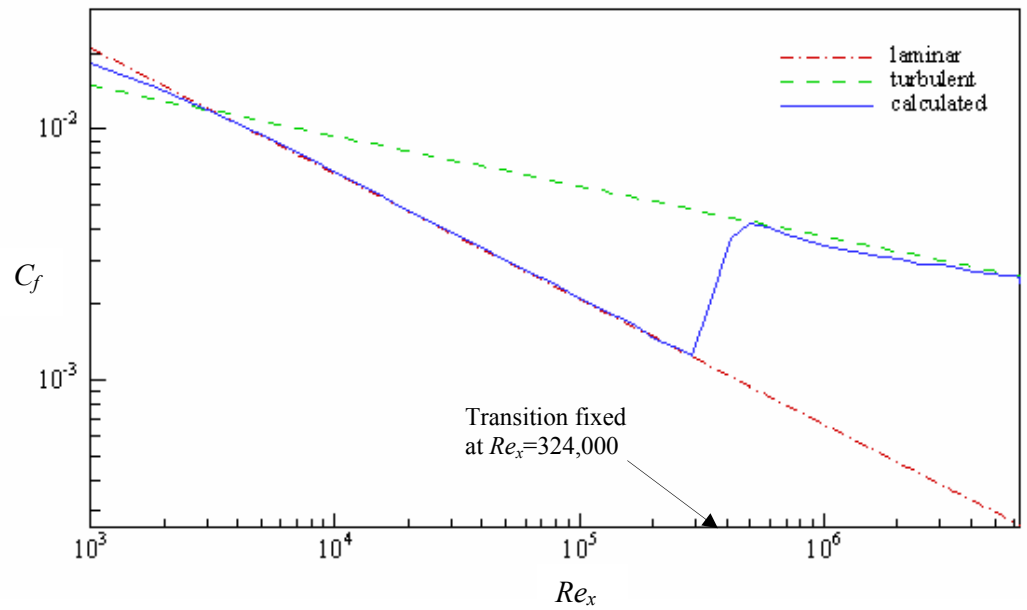

Figure 5.8 Local skin friction coefficient along the flat plate (Cebeci-Smith model).

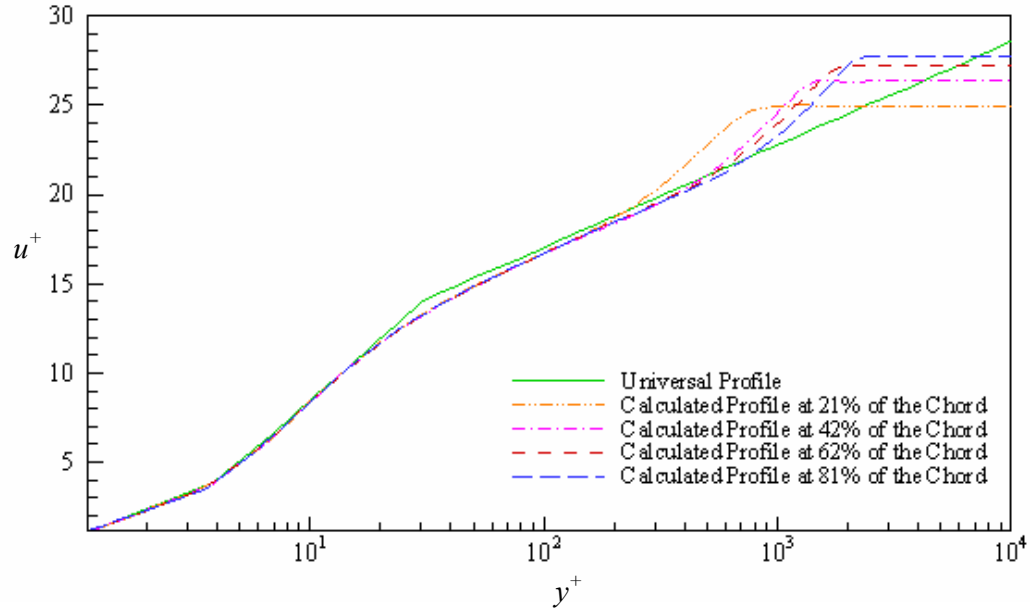

Figure 5.9 Non-dimensional turbulent velocity profiles (Cebeci-Smith model).

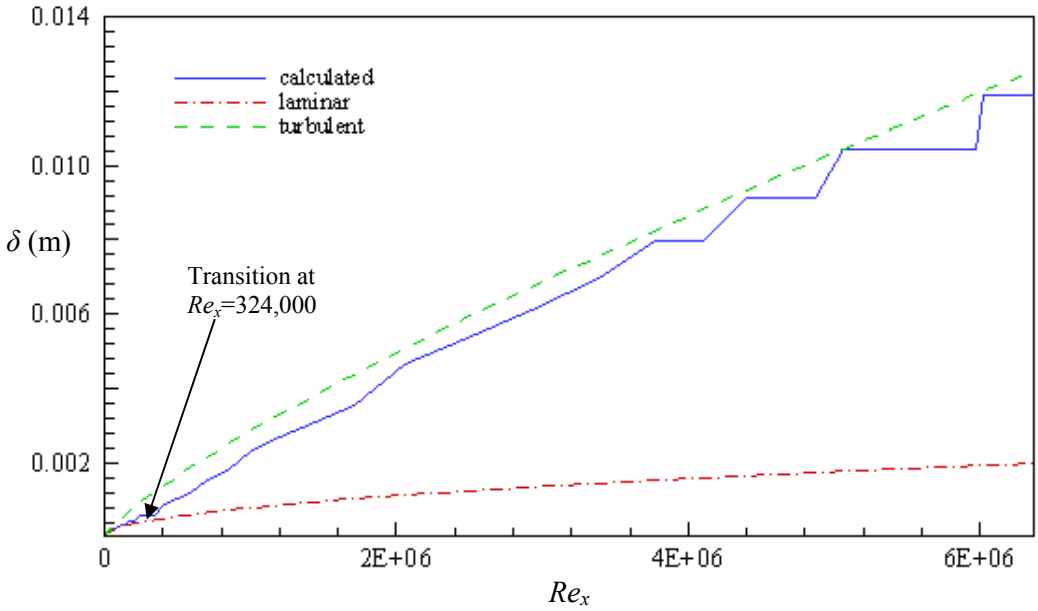

Figure 5.10 Boundary layer thickness along the flat plate (Cebeci-Smith model).

For this model, results show fairly good agreement, except for the boundary layer thickness: the stepwise oscillations near the leading edge are thought to be because of the grid coarsening near the boundary layer edge, far above the flat plate. And as seen from the other plots, this small inconsistency has a minor effect on the model performance, and it is acceptable. (The result deviates from the analytical solution at most by only 0.001 of the length of the flat plate, one-thousandth of a meter.)

5.2.2 Michel et. al. Turbulence Model

This model is the easiest one to implement, among others considered in this study. It has a single layer approach, where the turbulent viscosity is calculated by a single formula. In spite of this fact, the results show almost the same performance with the Cebeci-Smith model. (Figures 5.11, 5.12, 5.13) It is observed that when grid-1 is used, skin friction result is slightly over predicted at the trailing edge. So similar to the Cebeci-Smith model, grid-2 is selected for this model, too.

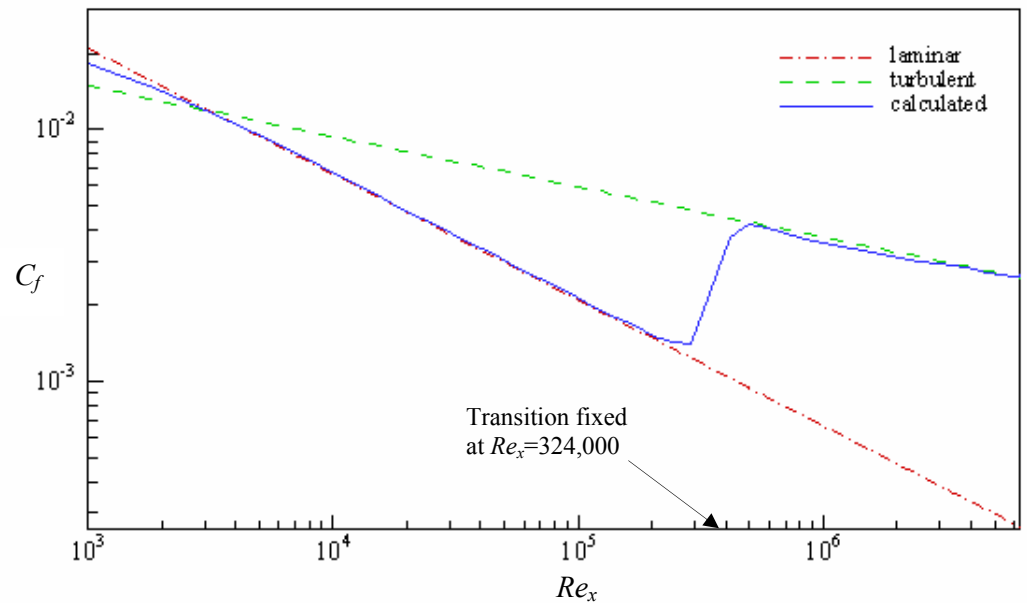

Figure 5.11 Local skin friction coefficient along the flat plate (Michel et. al. model).

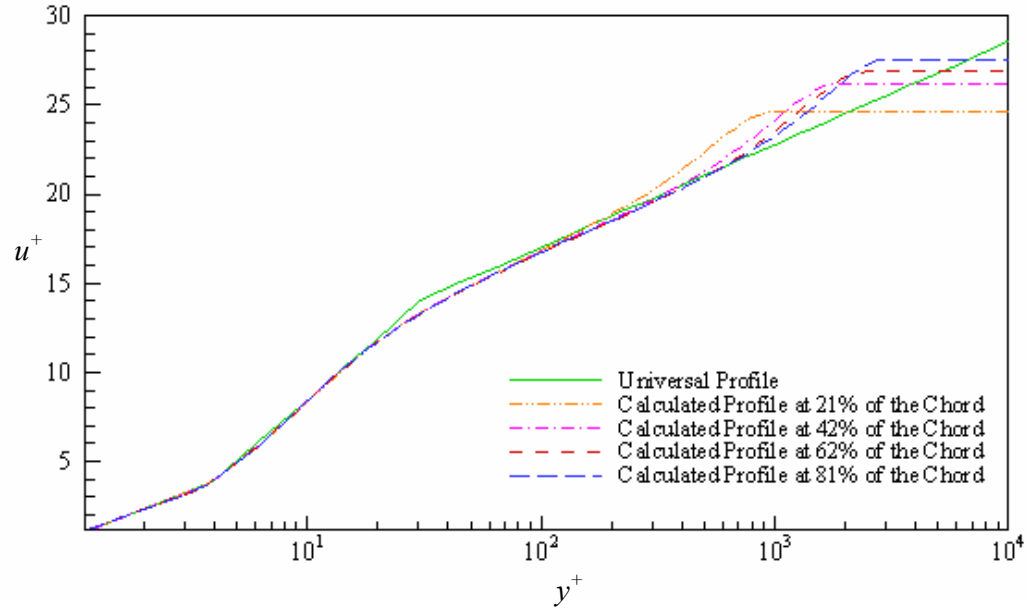

Figure 5.12 Non-dimensional turbulent velocity profiles (Michel et. al. model).

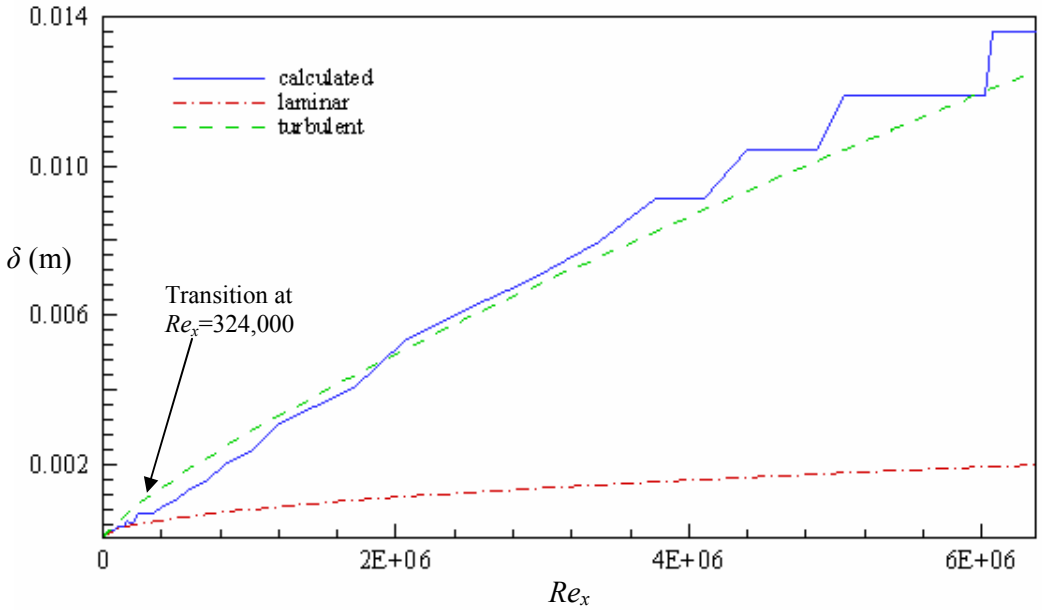

Figure 5.13 Boundary layer thickness along the flat plate (Michel et. al. model).

Conclusively, successful results are obtained with Michel et. al. model, with its simplicity as a plus. Also, the deviation in the boundary layer thickness plot is acceptable, again due to the grid coarsening effect which is explained for the Cebeci-Smith model.

5.2.3 Baldwin-Lomax Model

This model is the last algebraic model considered in this study. The results obtained with this model are shown in Figures 5.14 and 5.15. As in the case of other algebraic models used in this study, to maintain a better accuracy at the trailing edge, the second grid (grid-2) is selected. The results are in close agreement with the analytical solutions, both for skin friction and velocity distribution. Boundary layer thickness plot is not included in the results, because boundary layer thickness calculation is unnecessary for this model. In fact, this is the main advantage of the model over other algebraic formulations. Eliminating the boundary layer thickness data is really an advantage for separated flows, for which its calculation might create

stability problems. However, this fact is unimportant for attached boundary layers like in our case.

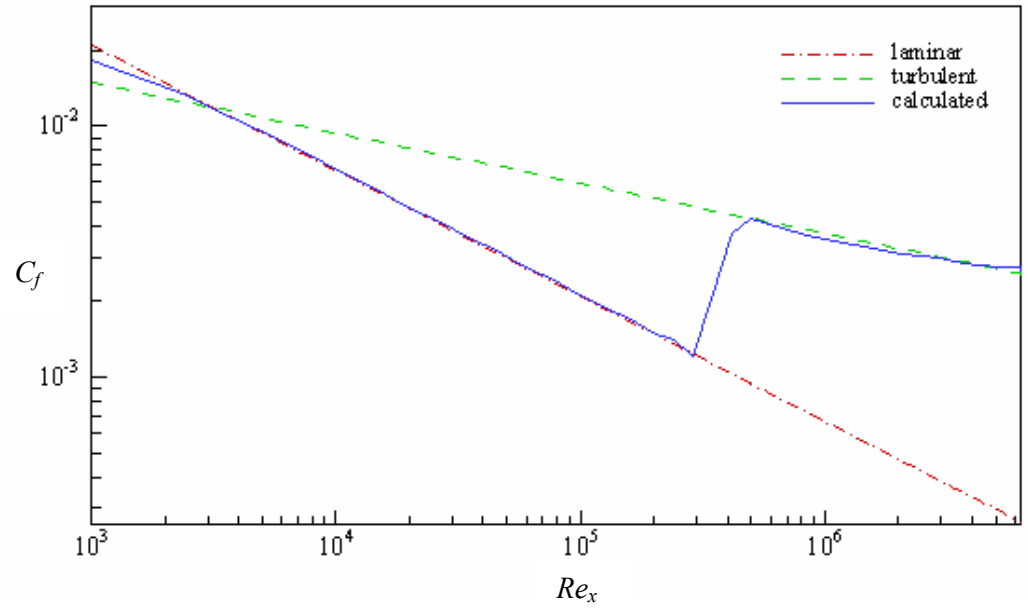

Figure 5.14 Local skin friction coefficient along the flat plate (Baldwin-Lomax model).

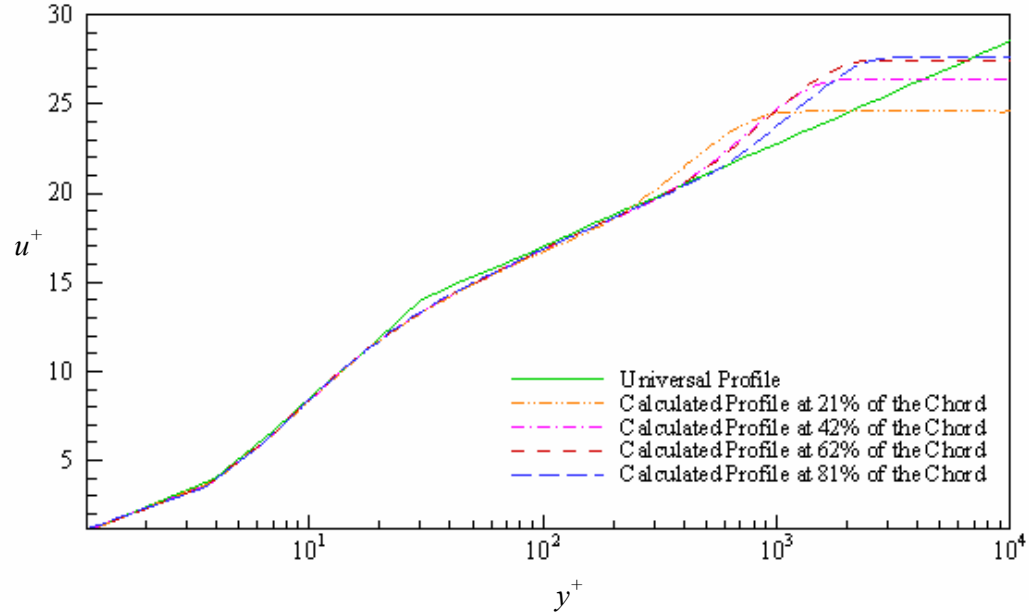

Figure 5.15 Non-dimensional turbulent velocity profiles (Baldwin-Lomax model).

With the above results, the implementation of Baldwin-Lomax model is shown to be successful. Generally, algebraic models are simple, easy to implement and do not create stability problems. They are the best alternatives for simple flow cases like the one considered in this study.

For all algebraic models used in this study, a second order smoothing coefficient (or artificial dissipation coefficient) of 0.001 is used. This value is adapted from references [9] and [16]. While implementing the algebraic models into the Navier-Stokes solver, no other extra numerical treatment was imposed.

5.2.4 Chien's *k*-*ε* model

Since two additional equations are solved with Navier-Stokes equations, this model needs a more intricate numerical work. Numerical experimentation showed that to maintain stability, artificial dissipation coefficient must be increased by approximately 3 orders of magnitude, in agreement with reference [9]. This stability concern, that is increasing the amount of artificial dissipation, brings an extra burden for the numerical scheme. Due to the Lax-Wendroff scheme explained in Chapter 3, the non-physical artificial dissipation acts more on coarser grids than on finer ones. Increased artificial dissipation means decreased distribution of changes at each cell to its nodes at each time step. Thus, the convergence speed of the solver decreases, and extra care should be given to the grid structure, because the solver becomes more sensitive to the grid used. Accordingly, many runs have been performed with several grids and the only successful result is obtained by grid-2.

During iterations, k and ε may attain negative values. This situation violates the physics of the problem because turbulence kinetic energy and its dissipation can not be negative. What's more, this unwanted situation can cause stability problems. Therefore, when this occurs, values of k and ε are set to very small positive numbers, immediately after the iteration.

The skin friction result for this model is shown in Figure 5.16. Note that, a close match with the analytical solutions is observed. The small downward trend of the curve just before transition is also observed by reference [9], and it is thought to be due to the model's interaction with the laminar part of the flow. In any case, the model's performance for the turbulent part is much more important, and in this regard, the accuracy of the computation is acceptable.

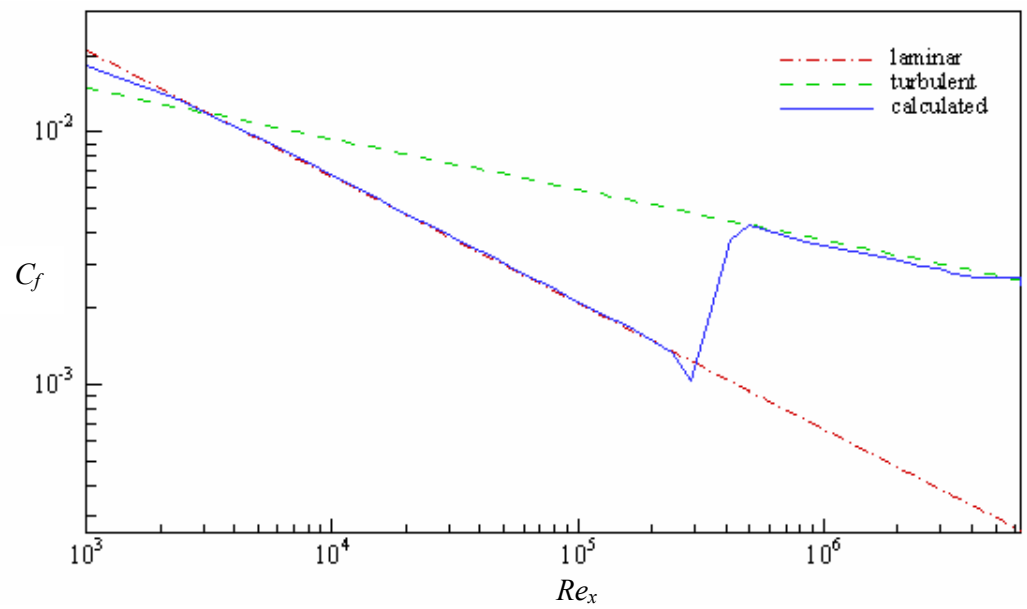

Figure 5.16 Local skin friction coefficient along the flat plate (Chien's *k-ε* model).

5.2.5 Wilcox's *k-ω* model

The implementation of *k-ω* model is similar to the *k-ε* model. While discretizing the two additional transport equations, the value of the artificial dissipation coefficient (which is originally 0.001) was increased by a factor of 5000 [9]. Note that the value of artificial dissipation coefficient remains unchanged for the Navier-Stokes equations. The value of ω at the wall and at the first and second grid points above the wall is set according to Equation (4.45). The value of k_R in Equation (4.45) is set to be $2\text{x}10^{-7}$ and reduced to its half after 20,000 iterations. During the iterations, if negative values of k and ω are encountered, they are set to their free

stream values, similar to the *k-ε* model. With these numerical considerations, the stability of the calculations could be maintained.

Different than other models, grid-1 is used for this case. Actually this is the only model where grid-1 is used. Trailing edge clustering was found to be unnecessary and it can be said that this model is less sensitive to the grid structure than the *k-ε* model. However, the final converged solution is again highly dependent on artificial damping, similar to the *k-ε* model. From the experience gained by this case, it can clearly be said that, for wall boundary layer flows, Wilcox's *k-ω* formulation is far less stiff than Chien's *k-ε* model and good performance is obtained with less effort. On the contrary, it is observed that *k-ω* model is more sensitive to the free stream flow region after the flat plate. And it should be reminded to the reader that all the results obtained in this study exclude free stream regions.

The skin friction result obtained for this model is presented in Figure 5.17 below.

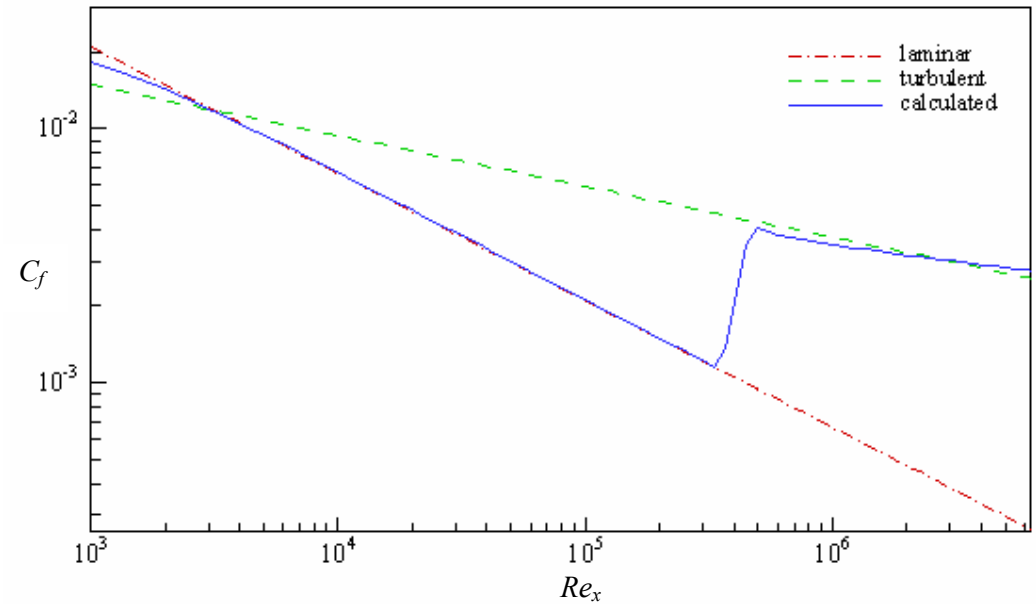

Figure 5.17 Local skin friction coefficient along the flat plate (Wilcox's *k-ω* model).

Finally the residual histories of models are plotted on the same graph in Figure 5.18. This plot shows the *x*-momentum residual behavior and it is given to show the convergence behavior of each model. Note that, for models which use high artificial damping coefficient, oscillations tend to get suppressed. This is the very case for especially the Chien's *k-ε* model, where the increased damping coefficient is applied to the whole system of equations. A very smooth curve is obtained for this case. For the *k-ω* model on the other hand, still some oscillations are observed. This is thought to be because high artificial damping is applied only to the additional two equations solved.

For zero-equation models, approximately 70,000 iterations were enough for convergence. But for two-equation models, the solver is run for approximately 90,000 iterations. Finally it should be noted that the residual graph is incapable of showing the convergence speed, that is, the time necessary for any model to reach a solution. This is because; a single iteration takes different time for different models. In this study, P4 processors are used with 2.4 GHz clock speeds. For zero equation models it took approx. 3.5 hours for the results to converge, whereas for two equation models it took almost 5.5 hours to reach the converged solutions.

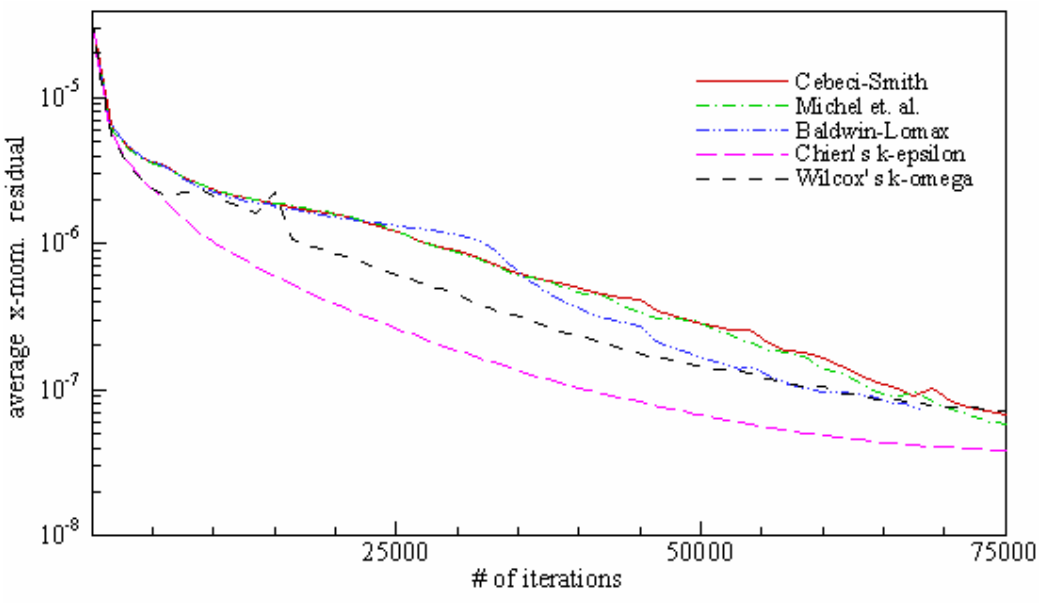

Figure 5.18 Average *x*-momentum residual history for the turbulence models.

CHAPTER 6

DISCUSSION AND CONCLUSION

6.1 SUMMARY

A previously developed Navier-Stokes solver capable of solving laminar flows is improved to handle turbulent flows, using several eddy-viscosity turbulence models (EVM's) which are of zero-equation and two-equation type. The improved solver is tested for a case of subsonic, laminar - transition fixed - turbulent flow over a flat plate. Transition to turbulence calculations is fixed by a certain value of x, that is, the distance from the leading edge of the flat plate. Before the transition point, only Navier-Stokes equations are solved. Over the flat plate, wall bounded turbulence formulations are used. After the flat plate in the wake region, free stream formulations of the turbulence models are implemented.

While evaluating the performance of the solver, it must be kept in mind that the model and the numerical scheme can not be thought independently, they must be considered as a whole. In this regard, the results show the characteristics of the model, as well as the efficiency of the numerical discretization. This is especially the case for two-equation models, where the discretization of the turbulence transport equations has a major effect on the results. Apart from this interaction, it is also observed that the results are sensitive to space discretization or in other words the grid used. It was observed that the clustering of the grid at the trailing edge yielded better results, especially for the k- ε closure.

Zero equation models implemented in this study are Cebeci-Smith, Michel et. al., and Baldwin-Lomax models. These models utilize the mixing length hypothesis, which was set forth by Prandtl in 1925. This hypothesis asserts that in turbulent flow, fluid particles coalesce into lumps and move as a single unit. The mixing length is an empirically determined length scale which gives us the distance that these lumps of fluid particles can move freely with respect to each other. The mixing length theory is highly inspired by the kinetic theory gases (with analogy to molecular mean free path of gases), and models using this theory give successful results for flows with no or low adverse pressure gradients. For simple flows like the one considered in this work, mixing length models are the best alternatives, due to their simplicity and the ease of implementation. Especially the mixing length model developed by Michel et. al. is the easiest one to implement and performs as good as others. However, it is reported that this model is only applicable for flat plate boundary layers [25]. Here it must be noted that, Michel et. al. and Cebeci-Smith models have the drawback of calculating boundary layer thickness, which would be hard especially for separated flows. On the other hand, Baldwin-Lomax model has the capacity to predict separated wall bounded flows but it is reported that their performance is still questionable [6].

The two-equation models considered in this study are Wilcox's k-ω and Chien's k-ε models. These models are selected due to their popularity and accepted success in predicting turbulent flows. They use the turbulence kinetic energy equation which is an additional partial differential equation modeling the transport of turbulence within the flow and it is derived by taking the moments of Navier-Stokes equations. With this equation, turbulence history effects can be introduced into the solutions. This consideration is supposed to increase the accuracy of the calculations. It must however be kept in mind that the two-equation models are based on the assumption of isotropy. However, real life turbulence is almost always anisotropic because it has a preferred direction. In parallel to the assumption of isotropy, all eddy-viscosity models assume the turbulent flow to be in equilibrium state, which asserts that in turbulent flow, the energy cascade of the turbulent eddies are in equilibrium. This is almost never the case as well. In the shadow of these

assumptions, it can be said that, wall bounded turbulence (or wall shear turbulent flows) is a harder case for turbulence modeling studies than free shear turbulence. Therefore, application of these models to the flat plate problem is only a first step towards the testing of the solver on more complex geometries. On more complex test cases, the effects of pressure gradient, flow curvature, separation and shock-boundary layer interaction on turbulence can be investigated.

Numerical study for the two-equation models showed that the result obtained with k-ε model is rather sensitive to grid clustering at the trailing edge. However, it is also observed that k-ε model performs better than k-ω in the wake region. k-ω model on the other hand performs well enough without such a grid clustering. However, k-ω model is rather sensitive to free stream values of ω, which was also reported by Menter [22]. The disadvantage of k-ε model is that it is rather stiff and needs the use of high values for artificial dissipation coefficient to render the solution stable.

Conclusively, zero equation models perform well enough for turbulent flat plate problem, and they are the best choice for this kind of a flow where small amount of adverse pressure is present. In our case, their performance is adequate with the two-equation models for which greater effort is spent. However, two-equation models have the potential to perform better for complex flow field calculations. They are considered in this study to show their application and this will form the basis of future studies.

6.2 RECOMMENDATIONS FOR FUTURE STUDY

This study has witnessed the successful implementation of algebraic models on the Navier-Stokes solver for flat plate problem. It will be a good practice to go one step further to Johnson-King turbulence model, which is a successful model, tested by various researchers on airfoil geometries for transonic separated flows. In addition to this, it is much easier to implement than two-equation models. In this model, only an ordinary differential equation is solved. An algebraic version of this

model is also presented by Cebeci and Chang [27], rendering the model even simpler.

Many improvements can be made on the two-equation turbulence kinetic energy models used in this study. First of all there are various different versions of these models which are suitable for different flow fields. To see their contributions, these versions may be applied on the Navier-Stokes solver. A rather interesting approach is reported by Menter [17], where he proposed to combine the k-ε and k-ω closures to compensate for the deficiencies of each other. He offered to combine the success of k-ω model in the near wall region with the success of k-ε model in the free stream region. To do this, he proposed a blending function to determine how much of these models will be utilized in different regions of the flow, without user intervention [26]. Menter could thus offer a powerful combination of the two models and his approach has been the subject of industrial applications in the past years due to its success.

In the mid-way between two-equation and algebraic models, one equation models may also be considered. Due to their less computational demands and acceptable success, they have found quite wide applications in research studies and in industry.

Finally, all models developed into the present solver can be easily applied to any finite volume Navier-Stokes solver, with similar discretization. However, the use of a higher order numerical scheme would yield better results for more complex flow geometries.

REFERENCES

[1] Gerritsma, M. I., "Computational Fluid Dynamics, Incompressible Flows", Delft University Press, 2002.

[2] Ferziger, J. M., Perić, M., "Computational Methods for Fluid Dynamics", 3rd Edition, Springer, Germany, 2002.

[3] Wendt, J. F., "Computational Fluid Dynamics", Springer, Germany, 1996.

[4] Versteeg, H. K., Malalasekera, W., "An Introduction to Computational Fluid Dynamics, The Finite Volume Method", Longman, 1995.

[5] Hirsch C., "Numerical Computation of Internal and External Flows", Vol 1-2, John Wiley & Sons, Great Britain, 1988-1990.

[6] Wilcox, D. C., "Turbulence Modeling for CFD", DCW Industries Inc., USA, 1994.

[7] Chen C. J., Jaw S. Y., "Fundamentals of Turbulence Modeling", Taylor & Francis, USA, 1998.

[8] Tennekes, H., Lumley J. L., "A First Course in Turbulence", MIT Press, USA, 1994.

[9] El Khoury, M., "Development of a Three Dimensional Object Oriented Navier Stokes Solver Using Two Equation Turbulence Models", M. Sc. Thesis, METU, Turkey, June 2001.

[10] Batchelor, G. K., "The Theory of Homogeneous Turbulence", Cambridge University Press, USA, 1993.

[11] El Khoury, M., "An Improved Wall Distance Free Version of the Baldwin-Barth Turbulence Model", Proceedings of IMECE, November 16-21, 2003.

[12] Mathieu, J., Scott, J., "An Introduction to Turbulent Flow", Cambridge University Press, USA, 2000.

[13] Ni, R.H., "A Multiple-Grid Scheme for Solving the Euler Equations", AIAA Journal, Vol. 20, pp. 1565-71, 1982.

[14] Caughey, D. A., "Hafez, M. M., Frontiers of Computational Fluid Dynamics 1994", John Wiley & Sons, USA, 1994.

[15] Tınaztepe, H. T., "A Finite Volume Method for Compressible Viscous Flows", Ph. D. Thesis, METU, Turkey, March 1997.

[16] Haliloğlu, M. U., "Development of a Three Dimensional Object Oriented Navier Stokes Solver Using C++ Programming Language", M. Sc. Thesis, METU, Turkey, June 2000.

[17] Menter, F. R., "Zonal Two-Equation Turbulence Model for Aerodynamic Flows", AIAA paper, 1993-2906, 1993.

[18] Hoffman, K. A., Chiang, S.T., "Computational Fluid Dynamics", Vol. 1-2-3, Engineering Education System Publication, USA, August 2000.

[19] Gerolymos, G.A., and Vallet, I., "Implicit Computation of Three-Dimensional Compressible Navier-Stokes Equations Using k-ε Closure", AIAA Journal, Vol. 34, pp. 1321-1330, 1996.

[20] Liu, F., and Jameson, A., "Multigrid Navier-Stokes Calculations for Three-Dimensional Cascades", AIAA Journal, Vol. 31, pp. 1785-1791, 1993.

[21] Wilcox, D.C., "Reassessment of the Scale-Determining Equation for Advanced Turbulence Models", AIAA Journal, Vol. 26, pp. 1299-1310, 1988.

[22] Menter, F. R., "Influence of Freestream Values on k-ω Turbulence Model Predictions", AIAA Journal,Vol. 30, pp. 1657-1659, 1992.

[23] Menter, F. R., "Performance of a Popular Turbulence Models for Attached and Separated Adverse Pressure Gradient Flows", AIAA Paper 91-1784, June 1991.

[24] Kordulla, W., Vinokur, M., "Efficient Computation of Volume in Flow Prediction", AIAA Journal, Vol.21, pp.917-8, 1983.

[25] Cebeci, T., Cousteix, J., "Modelling and Computation of Boundary-Layer Flows", Horizons Publishing Inc., Long Beach, CA, 1999.

[26] Menter, F. R., Kuntz, M., Langtry, R., "Ten Years of Industrial Experience with the SST Turbulence Model", in Proc. Turbulence Heat and Mass Transfer, Eds. Hanjalic, Nagano, Tummers, Antalya, 2003.

[27] Cebeci, T., and Chang, K. C., "An improved Cebeci-Smith Turbulence Model for Boundary-Layer and Navier-Stokes Methods", 20th Congress of the International Council of the Aeronautical Sciences, paper no. ICAS-96-1.7.3, Sorrento, Italy, September 8-13, 1996.

APPENDIX A

CALCULATION OF SURFACE VECTORS

This short summary is intended to demonstrate the calculation procedure of the surface areas used in Chapter 3 in the calculation of the first- and second-order changes. The surface vectors are decomposed into three components in each of the three Cartesian directions. The following calculations are carried out in correspondence with Figure 3.5. The surface vector S_1 can be expressed as follows:

$$\vec{S}_1 = \frac{1}{2}\left(\vec{r}_{54} \times \vec{r}_{18}\right) \tag{A.1}$$

Here, r stands for the displacement vector between two nodes and the subscripts denote the node numbers of the corresponding vector. The open form of the displacement vectors can be expressed as follows:

$$\vec{r}_{54} = \left(x_4 - x_5\right)\vec{i} + \left(y_4 - y_5\right)\vec{j} + \left(z_4 - z_5\right)\vec{k} \tag{A.2a}$$

$$\vec{r}_{18} = \left(x_8 - x_1\right)\vec{i} + \left(y_8 - y_1\right)\vec{j} + \left(z_8 - z_1\right)\vec{k} \tag{A.2b}$$

Substituting the above vectors into (A.1) and rearranging to get

$$\vec{S}_1 = \frac{1}{2}\left(\vec{r}_{54} \times \vec{r}_{18}\right) = \begin{vmatrix} \vec{i} & \vec{j} & \vec{k} \\ x_4 - x_5 & y_4 - y_5 & z_4 - z_5 \\ x_8 - x_1 & y_8 - y_1 & z_8 - z_1 \end{vmatrix} \tag{A.3}$$

The open form of Equation (A.3) can be expressed as:

$$\begin{aligned}\vec{S}_1 = \frac{1}{2}\{&\vec{i}\left[(y_4 - y_5)(z_8 - z_1) - (y_8 - y_1)(z_4 - z_5)\right] \\ &- \vec{j}\left[(x_4 - x_5)(z_8 - z_1) - (x_8 - x_1)(z_4 - z_5)\right] \\ &+ \vec{k}\left[(x_4 - x_5)(y_8 - y_1) - (x_8 - x_1)(y_4 - y_5)\right]\}\end{aligned} \tag{A.4a}$$

where the first, second and third terms stand for the three Cartesian components $S_{1,x}$, $S_{2,x}$, $S_{3,x}$ respectively, which are used in Chapter 3. The rest of the five surface vectors can be given as follows:

$$\begin{aligned}\vec{S}_2 &= \frac{1}{2}(\vec{r}_{63} \times \vec{r}_{27}) \\ &= \frac{1}{2}\{\vec{i}\left[(y_3 - y_6)(z_7 - z_2) - (y_7 - y_2)(z_3 - z_7)\right] \\ &\quad - \vec{j}\left[(x_3 - x_6)(z_7 - z_2) - (x_7 - x_2)(z_3 - z_6)\right] \\ &\quad + \vec{k}\left[(x_3 - x_6)(y_7 - y_2) - (x_7 - x_2)(y_3 - y_6)\right]\}\end{aligned} \tag{A.4b}$$

$$\begin{aligned}\vec{S}_3 &= \frac{1}{2}(\vec{r}_{52} \times \vec{r}_{61}) \\ &= \frac{1}{2}\{\vec{i}\left[(y_2 - y_5)(z_1 - z_6) - (y_1 - y_6)(z_2 - z_5)\right] \\ &\quad - \vec{j}\left[(x_2 - x_5)(z_1 - z_6) - (x_1 - x_6)(z_2 - z_5)\right] \\ &\quad + \vec{k}\left[(x_2 - x_5)(y_1 - y_6) - (x_1 - x_6)(y_2 - y_5)\right]\}\end{aligned} \tag{A.4c}$$

$$\begin{aligned}\vec{S}_4 &= \frac{1}{2}(\vec{r}_{83} \times \vec{r}_{74}) \\ &= \frac{1}{2}\{\vec{i}\left[(y_3 - y_8)(z_4 - z_7) - (y_4 - y_7)(z_3 - z_8)\right] \\ &\quad - \vec{j}\left[(x_3 - x_8)(z_4 - z_7) - (x_4 - x_7)(z_3 - z_8)\right] \\ &\quad + \vec{k}\left[(x_3 - x_8)(y_4 - y_7) - (x_4 - x_7)(y_3 - y_8)\right]\}\end{aligned} \tag{A.4d}$$

$$\begin{aligned}\vec{S}_5 &= \frac{1}{2}\left(\vec{r}_{13}\times\vec{r}_{24}\right)\\ &= \frac{1}{2}\{\vec{i}\left[\left(y_3-y_1\right)\left(z_4-z_2\right)-\left(y_4-y_2\right)\left(z_3-z_1\right)\right]\\ &\quad -\vec{j}\left[\left(x_3-x_1\right)\left(z_4-z_2\right)-\left(x_4-x_2\right)\left(z_3-z_1\right)\right]\\ &\quad +\vec{k}\left[\left(x_3-x_1\right)\left(y_4-y_2\right)-\left(x_4-x_2\right)\left(y_3-y_1\right)\right]\}\end{aligned} \tag{A.4e}$$

$$\begin{aligned}\vec{S}_6 &= \frac{1}{2}\left(\vec{r}_{57}\times\vec{r}_{68}\right)\\ &= \frac{1}{2}\{\vec{i}\left[\left(y_7-y_5\right)\left(z_8-z_6\right)-\left(y_8-y_6\right)\left(z_7-z_5\right)\right]\\ &\quad -\vec{j}\left[\left(x_7-x_5\right)\left(z_8-z_6\right)-\left(x_8-x_6\right)\left(z_7-z_5\right)\right]\\ &\quad +\vec{k}\left[\left(x_7-x_5\right)\left(y_8-y_6\right)-\left(x_8-x_6\right)\left(y_7-y_5\right)\right]\}\end{aligned} \tag{A.4f}$$

Referring to Figure A.1, the cross products of surface vectors that are used in the calculation of the second-order inviscid and first-order viscous terms as denoted by Figure 3.5 in Chapter 3 are derived as follows:

$$\vec{A}_1 = \frac{1}{4}\vec{S}_{mnop} = \frac{1}{4}\left(\vec{r}_{np}\times\vec{r}_{om}\right) \tag{A.5a}$$

Each of the above displacement vectors ($\vec{r}_{np}$ and $\vec{r}_{om}$) can be expressed using the corners of the main cell, as follows:

$$\vec{A}_1 = \frac{1}{4}\left(\frac{\left(\vec{r}_7+\vec{r}_8\right)-\left(\vec{r}_1+\vec{r}_2\right)}{2}\times\frac{\left(\vec{r}_5+\vec{r}_6\right)-\left(\vec{r}_3+\vec{r}_4\right)}{2}\right) \tag{A.5b}$$

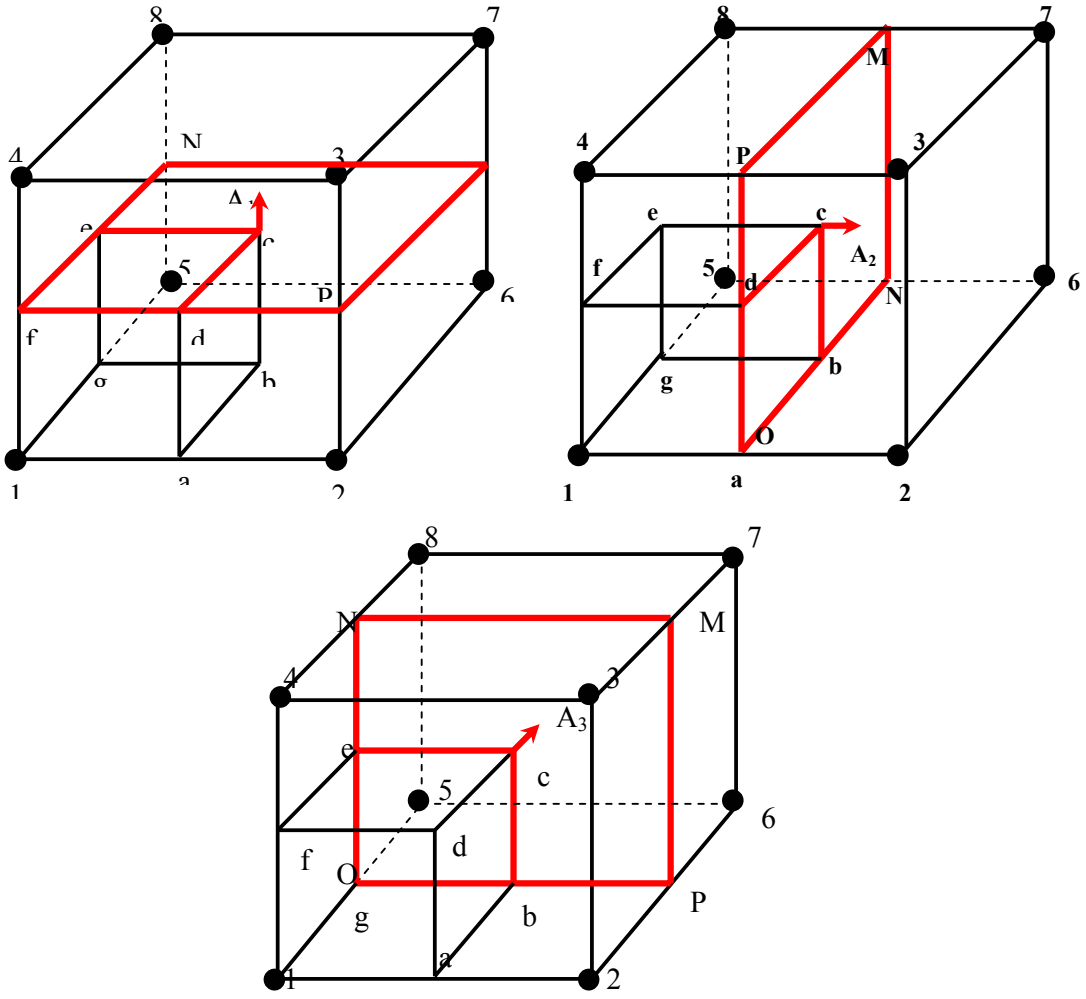

Figure A.1 Surface vectors

Evaluating the cross product along with further manipulation, the above equation can be expressed in x, y and z directions as follows:

$$A_{1,x} = \frac{1}{8}\left[\left(y_8 + y_7 - y_1 - y_2\right)\left(z_5 + z_6 - z_4 - z_3\right) - \left(z_8 + z_7 - z_1 - z_2\right)\left(y_5 + y_6 - y_4 - y_3\right)\right] \quad \text{(A.6a)}$$

$$A_{1,y} = \frac{1}{8}\left[\left(x_8 + x_7 - x_1 - x_2\right)\left(z_5 + z_6 - z_4 - z_3\right) - \left(z_8 + z_7 - z_1 - z_2\right)\left(x_5 + x_6 - x_4 - x_3\right)\right] \tag{A.6b}$$

$$A_{1,z} = \frac{1}{8}\left[\left(x_8 + x_7 - x_1 - x_2\right)\left(y_5 + y_6 - y_4 - y_3\right) - \left(y_8 + y_7 - y_1 - y_2\right)\left(y_5 + y_6 - y_4 - y_3\right)\right] \tag{A.6c}$$

Similarly the surface vectors A_2 and A_3 can also be expressed as shown below

$$A_{2,x} = \frac{1}{8}\left[\left(y_8 + y_5 - y_3 - y_2\right)\left(z_1 + z_4 - z_6 - z_7\right) - \left(z_8 + z_5 - z_3 - z_2\right)\left(y_1 + y_4 - y_6 - y_7\right)\right] \tag{A.7a}$$

$$A_{2,y} = \frac{1}{8}\left[\left(x_8 + x_5 - x_3 - x_2\right)\left(z_1 + z_4 - z_6 - z_7\right) - \left(z_8 + z_5 - z_3 - z_2\right)\left(x_1 + x_4 - x_6 - x_7\right)\right] \tag{A.7b}$$

$$A_{2,z} = \frac{1}{8}\left[\left(x_8 + x_5 - x_3 - x_2\right)\left(y_1 + y_4 - y_6 - y_7\right) - \left(y_8 + y_5 - y_3 - y_2\right)\left(x_1 + x_4 - x_6 - x_7\right)\right] \tag{A.7c}$$

$$A_{3,x} = \frac{1}{8}\left[\left(y_1 + y_5 - y_3 - y_7\right)\left(z_8 + z_4 - z_6 - z_2\right) - \left(z_1 + z_5 - z_3 - z_7\right)\left(y_8 + y_4 - y_6 - y_2\right)\right] \tag{A.8a}$$

$$A_{3,y} = \frac{1}{8}\left[\left(x_1 + x_5 - x_3 - x_7\right)\left(z_8 + z_4 - z_6 - z_2\right) - \left(z_1 + z_5 - z_3 - z_7\right)\left(x_8 + x_4 - x_6 - x_2\right)\right] \tag{A.8b}$$

$$A_{3,z} = \frac{1}{8}\left[\left(x_1 + x_5 - x_3 - x_7\right)\left(y_8 + y_4 - y_6 - y_2\right) - \left(y_1 + y_5 - y_3 - y_7\right)\left(x_8 + x_4 - x_6 - x_2\right)\right] \tag{A.8c}$$

Calculation of cell volume is carried out using the method introduced by Kordulla and Vinokur [24]. This method was also used by Haliloğlu [16] and El Khoury [9].

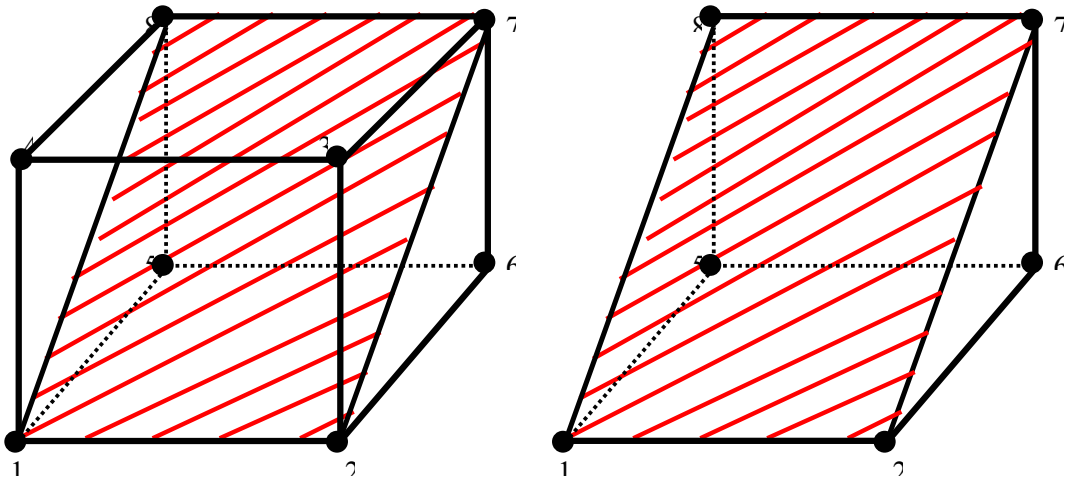

Figure A.2 Cell division

Figure A.2 shows the cell division while the half of the cell is composed of three tetrahedral. These tetrahedral are shown below

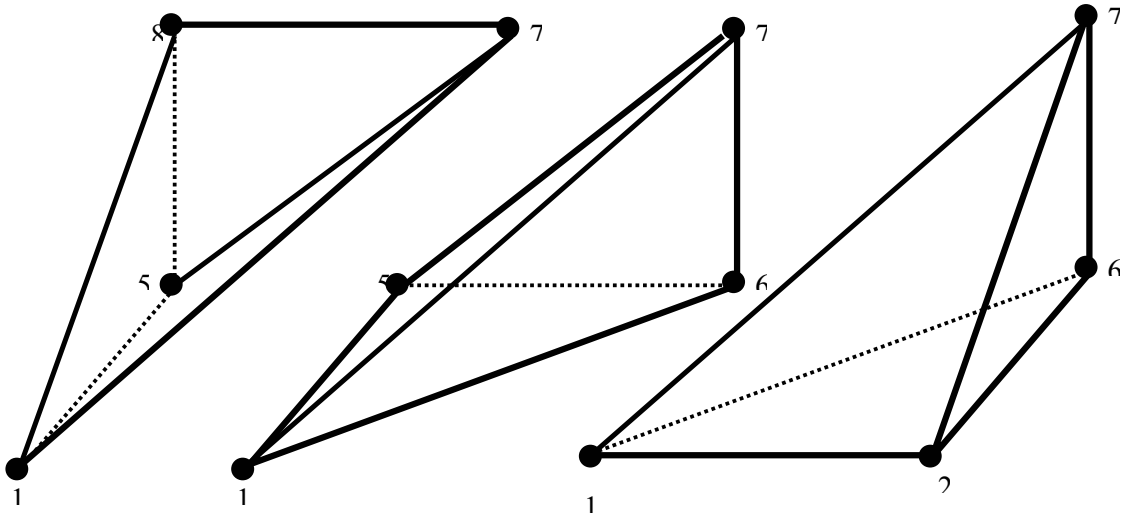

Figure A.3 Tetrahedral division of the half cell

Hence, as shown in Figure A.3, the cell is composed of six tetrahedral sub-volumes. Therefore, its volume can be expressed as follows:

$$\begin{aligned}\Delta\forall &= \frac{1}{6}\vec{r}_{71}\cdot\left\{\left(\vec{r}_{51}\times\vec{r}_{61}\right)+\left(\vec{r}_{81}\times\vec{r}_{51}\right)+\left(\vec{r}_{61}\times\vec{r}_{21}\right)+\left(\vec{r}_{21}\times\vec{r}_{31}\right)+\left(\vec{r}_{31}\times\vec{r}_{41}\right)+\left(\vec{r}_{41}+\vec{r}_{81}\right)\right\}\\ &= \frac{1}{6}\vec{r}_{71}\cdot\left\{\left(\vec{r}_{52}\times\vec{r}_{61}\right)+\left(\vec{r}_{45}\times\vec{r}_{81}\right)+\left(\vec{r}_{24}\times\vec{r}_{31}\right)\right\}\\ &= \frac{1}{3}\vec{r}_{71}\cdot\left(\vec{S}_1+\vec{S}_3+\vec{S}_5\right)\end{aligned} \tag{A.9}$$

where the displacement vector is given as:

$$\vec{r}_{71} = \left(x_1 - x_7\right)\vec{i} + \left(y_1 - y_7\right)\vec{j} + \left(z_1 - z_7\right)\vec{k} \tag{A.10}$$

where S_1, S_3, and S_5 are the previously calculated surface vectors. Substituting all these into Equation (A.9), the final form of the volume can be rearranged to give

$$\begin{aligned}\Delta\forall = \frac{1}{3}\{&\left(x_1 - x_7\right)\left(S_{1,x} + S_{3,x} + S_{5,x}\right)\\ &+\left(y_1 - y_7\right)\left(S_{1,y} + S_{3,y} + S_{5,y}\right)\\ &+\left(z_1 - z_7\right)\left(S_{1,z} + S_{3,z} + S_{5,z}\right)\end{aligned} \tag{A.11}$$

where $S_{1,x}$, $S_{1,y}$, ..., $S_{5,y}$, $S_{5,z}$ are the components of the surface vectors as calculated above.